HIGH RESOLUTION MODAL ANALYSIS USING POLES OBTAINED AT A SINGLE LOCATION

by

John Fulton Porterfield

Thesis submitted to the faculty of the
Virginia Polytechnic Institute and State University
in partial fulfillment of the requirements for the degree of

MASTER OF SCIENCE
in
Mechanical Engineering

APPROVED:

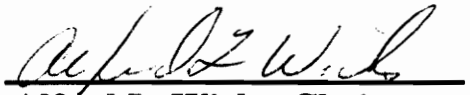

Alfred L. Wicks, Chairman

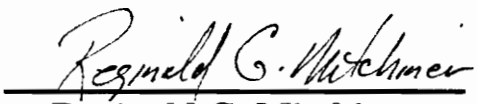

Reginald G. Mitchiner

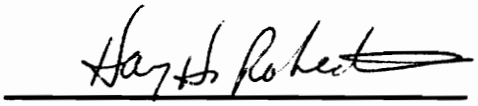

Harry H. Robertshaw

November, 1995
Blacksburg, Va

Key Words: Modal, Laser, Frequency Domain

High Resolution Modal Analysis Using Poles Obtained at a Single Location

by
John Fulton Porterfield

Alfred L. Wicks, Chairman
Mechanical Engineering
(ABSTRACT)

A method, termed the fixed-poles method, is proposed to increase the spatial resolution of experimental modal analysis results so that the resolution of the results is typical of that found in finite element modelling. The fixed-poles procedure estimates the structure's poles from a high frequency density, driving point frequency response function (FRF) measured with an accelerometer. Mode vectors are estimated from low frequency density, tightly spaced FRFs measured with a scanning laser velocimeter (SLV) using the poles estimated from the accelerometer FRF.

In experiments with a beam, the SLV was used to measure the frequency response of the beam at 31 frequencies and 472 locations. A single, 800 frequency line FRF was measured with an accelerometer, and the locations of the system's poles were estimated from the accelerometer FRF using the Rational Polynomial algorithm. Mode vectors were then estimated from the 472 SLV FRFs for the first 6 modes (1 rigid body + 5 flexible). A comparison of the results was given between the proposed method and a standard global parameter estimation technique. An investigation of the effect of the locations of the 31 measurement frequencies relative to resonances was also given.

Conclusions were that the proposed method gives comparable results to a global approach in which the system's poles were calculated only from the SLV measurements. The computational time required for the fixed-poles analysis proved to be significantly less than the global analysis, and the best results were obtained using near resonance SLV measurement frequencies.

Acknowledgments

Many people helped to make this work possible through their relentless support and patience. I would like to thank everyone but can only thank a few.

Dr. Alfred Wicks provided constant guidance and showed great patience as I learned and made mistakes. His encouragement helped me both to obtain my degree and to make the decision to pursue a graduate degree.

Thanks are due to Dr. Reginald Mitchiner and Dr. Harry Robertshaw for providing suggestions for the revision of this work and helping me to learn in their respective classes.

The Naval Surface Warfare Center of Dahlgren, VA provided generous support during my entire graduate program. Many thanks are due to the NSWC for its financial support.

I would like to thank my parents for their never-ending support and love. They provided me with a belief in the importance of education and the resources with which to pursue my education.

Thanks to the Luttrell family (Kay, Jerry, Sarah, and Greg) for the many fun evenings that helped to relieve the stress of school.

Finally, to my wife, Melissa, I would like to express my thanks for her tremendous love and support. Without her, life would not be nearly as fulfilling nor as much fun as it is.

Table of Contents

List of Figures

List of Figures (con.)

List of Tables

Chapter One

Introduction

The ways in which a linear structure can vibrate can always be described by modal superposition; combining the modes of vibration of the structure. The objective of experimental modal analysis is the estimation of the natural frequencies, damping values, and mode shapes of a structure which fully describe each mode of vibration. Various techniques can be applied to obtain estimates of these parameters, and every technique, if implemented correctly, should give similar results.

Presented here is a technique, termed the fixed-poles algorithm, for modal analysis of structures using frequency response data obtained from a scanning laser velocimeter (SLV) and an accelerometer. Frequency response functions (FRFs) are measured with the SLV and the accelerometer from a structure whose properties remained fixed during testing. Maintaining fixed structural properties allows the estimation of system poles (natural frequencies and damping) from a single driving point accelerometer FRF. With the poles of the structure known, another parameter estimation process can be applied to determine the mode vectors (mode shapes) at many closely spaced points on the structure from the FRFs measured with the scanning laser.

1.1 Background

The aim of a modal analysis is the estimation of the natural frequency, damping values, and mode shapes for modes in a certain frequency range. Typically, a modal analysis is performed by first acquiring frequency response functions (FRFs) over many points on the surface of the test subject and then applying a parameter estimation algorithm to the measured data. The parameter estimation algorithm assumes a mathematical form for the FRF and attempts to estimate the unknowns in the mathematical form.

1.1.1 Frequency Response Function Measurements

Traditional procedures of modal analysis are based upon attaching a vibration transducer to the subject and then applying a measured force. The ratio of the Fourier transform of the response to the Fourier transform of the input force is termed the frequency response function (FRF). An FRF describes the response of a structure to an input. Since the response of the structure is different for each combination of input and output locations, an FRF must be labeled so to indicate these locations.

During testing, either the location of the vibration transducer or the location of the input force moves over the structure. In the case of moving an accelerometer over the structure, the accelerometer's mass moves on the structure while testing proceeds. This moving mass causes the poles of the structure (natural frequency and damping values) to

change between measurements. That is, the modes of vibration change, only slightly if the effect of the moving mass is small, between measurements. In some cases, the effect of the mass on the structure may be so small that the changes in the structure's dynamics are unmeasurable and the presence of an accelerometer is undetectable.

In recent years, the scanning laser velocimeter (SLV) has been used as a vibration transducer. The SLV adds no mass to the structure since it measures with only a beam of light. Additionally, the SLV can be programmed to aim itself and measure automatically. Using the SLV as the moving vibration transducer and leaving the forcing location fixed during testing allows FRF measurements at different locations without moving any mass around the structure and changing the system's poles or mode vectors.

The dynamic range of the SLV is much less than that of a quality accelerometer; approximately 60 dB compared to 90 dB. The limited dynamic range of the laser limits its capability in acquiring the high quality, wide-band FRFs as are normally measured with an accelerometer.

A transducer's ability to measure a wide range of magnitudes is described by its dynamic range. Typically, when FRF measurements are made with an accelerometer, the input force contains frequency content across a wide band. By measuring the frequency content of both the input and the response, the frequency response of the structure can be calculated for all frequencies present in the input signal. Since the input spans a wide frequency range, the magnitude of the system's response spans a wide range as frequencies near resonance produce high output levels and frequencies near anti-resonance produce very low output levels. Especially for lightly damped structures,

where response magnitudes can be extreme, an accelerometer's wider dynamic range allows it to more accurately measure wide-band FRFs than could be accurately be measured with an SLV.

The limitations imposed by the SLV's dynamic range can be overcome by measuring FRFs one frequency at a time. The structure's response at a single frequency is a sinusoid with peak values that do not change with time, so the amplitude of the input force can be adjusted so that the amplitude of the response is well within the laser's dynamic range. When frequency response measurements are made at a single frequency, the operator can make adjustments to optimize the measurement process. The quality of the results can be improved by changing the magnitude of the response to make better use of the data acquisition system's analog-to-digital converter's dynamic range.

By vibrating the structure at a single frequency, the frequency response at the set frequency is obtained by determining the structure's response relative to the force input. Combination of frequency response measurements at many different frequencies yield a frequency response function.

1.1.3 Parameter Estimation Techniques

In general, there are two types of parameter estimation algorithms used to determine the poles and mode vectors of a system from frequency response function data. Frequency domain parameter estimation algorithms operate directly on the FRF as it was measured in the frequency domain. Time domain estimation techniques convert the FRF to the time domain by calculating the inverse Fourier transform of the FRF.

Time domain parameter estimation techniques operate on the time series impact response of the structure which can be obtained by calculating the inverse Fourier transform of an FRF. The impact response is not measured directly in the time domain since impacting the structure can excite non-linearities in the structure's response. Determining the impact response from an FRF obtained using a non-impulsive input lessens the chance of exciting non-linearities during testing.

Calculating the inverse transform of an FRF mathematically requires that the FRF contain equally spaced frequency lines (the frequency difference between each measurement in an FRF). This requirement means that once the frequency spacing of the FRF is chosen, it must be maintained up to the highest frequency of interest. The overall result of this requirement is that the FRFs must contain more data than is necessary to determine estimates of the modal parameters. Additionally, FRF data of poor quality must be used in the estimation in order to maintain the completeness of the FRF.

Frequency domain parameter estimation techniques operate directly on the FRF instead of the inverse transform of the FRF. Eliminating the need for taking the inverse transform eliminates any requirements on the frequency content of the FRF. As long as the FRF contains a sufficient quantity of data to determine the poles and mode vectors of the modes of interest, the FRF is sufficient.

A sufficient quantity of data exists to estimate the modal parameters if the value of the FRF is known at two frequencies for every mode desired. The mathematical definition of an FRF (equation 2.1.4.13) contains four unknowns for each mode (natural frequency, damping, and two mode vectors). FRFs are complex functions, and since a

complex value contains two pieces of independent information, a value of the FRF at a single frequency can be used to solve for two unknowns. The complex value of the FRF at two frequencies must be known to exactly determine solutions for the four modal parameters for each mode. Additional measurements of the FRF can be used to overdetermine the desired parameters and improve the quality of the estimates.

Methods of modal parameter estimation, termed global parameter estimation techniques, use many FRFs measured at different locations on the structure to determine the location of the system's poles. When measurements are made with a roving, contacting transducer, the system's poles change from FRF to FRF due to the effect of the moving mass of the transducer.

When the structure's poles are not exactly the same in all of the measured FRFs, the global parameter estimation algorithm must iteratively choose pole locations until a set of poles are determined that best fit all the measured data. Obviously, the final estimate of the poles cannot be said to be correct since there is a different set of poles at each point measured. The final set of poles can only be said to be the best available. Additionally, the computational time required grows quickly as more sets of data are added since each set must be added to the iterative process.

Localized parameter estimation techniques make use of an FRF at one location to determine the system's poles. Typically, an FRF measured at the forcing location (driving point) is used to determine the system's poles since at the driving point, the vibration transducer is not at one of the structure's nodes (points of no motion).

1.2 Motivation

In any modal analysis, there is always a desire for high spatial density in the resulting mode shapes. High density modal analyses yield high resolution mode shapes so that complicated modes are easier to visualize. Additionally, the greater number of degrees of freedom of a high density modal are much easier to compare to the many degrees of freedom of a finite element model. Comparison of high resolution results from a finite-element model to low-resolution, experimentally-obtained, modal results can only be performed by reducing the degrees of freedom of the finite element model. This process of reduction can be minimized by increasing the spatial density of the experimental results. Of course, with increasing spatial resolution comes an increase in the number of FRFs acquired since modal results can only be obtained at spatial locations where a frequency response function was measured.

The chore of acquiring a great number of tightly spaced frequency response functions requires a great deal of time, and is difficult because of the precision necessary when moving a transducer manually. The automatic scanning capability of the scanning laser is ideal for making tightly spaced response measurements.

The motivation behind the proposed fixed-poles modal analysis process is to improve the spatial density of experimental modal analysis results. Achieving this end necessitates the use of the scanning laser and a data acquisition system capable of making frequency response measurements with the scanning laser velocimeter. Additionally, a

frequency domain parameter estimation algorithm must be employed to eliminate the requirement of regular spacing on the frequency response measurements made with the SLV.

1.3 Theoretical Procedure

It has been shown that the scanning laser velocimeter can be used to measure the response of a structure at many different locations on the structure and, in doing so, not change the modal properties of the structure. By attaching an accelerometer to the point at which the structure is being forced by an electro-magnetic shaker (the driving point), an FRF measurement can be made that is not at a node of any of the excited modes. Since the accelerometer measurement is not at a node, all the excited modes are present in the measurement and so the system's poles can be estimated from the accelerometer FRF. The added mass of the accelerometer would affect the system's poles, but the accelerometer would remain fixed during all subsequent tests with the SLV in order to keep the structure's properties constant during the entire testing process.

The FRF obtained with the accelerometer would be a high frequency density driving point measurement and would reach frequencies high enough to include all the desired poles. This FRF would be used in a frequency domain curve fitter to determine the poles of the system. The accelerometer FRF would contain enough data points to greatly overdetermine all the estimated parameters, so to improve the quality of the estimates.

FRFs would be measured with the SLV at many different locations on the structure. The forcing would again be provided by the shaker that had been used to excite the structure when the accelerometer FRF was measured. The SLV FRFs would contain few data points compared to the accelerometer FRF since the measured data would be used to determine only the mode vectors at the measurement locations. With the poles estimated from the accelerometer FRF and the mode vectors calculated from the SLV data, the modal parameters for the entire structure would be known.

Compared with the FRF measurements made with the SLV, the accelerometer FRF would be of dramatically higher frequency resolution. The many times greater number of data points in the accelerometer measurements would better overdetermine the estimates of the system's poles than would the SLV data if it were employed to estimate the system's properties.

1.4 Thesis Overview

This report is separated into five sections: Introduction, Theory, Procedure, Results, Conclusions, and Recommendations. Chapter two contains theory related to modal decomposition, frequency response functions, and frequency domain parameter estimation. The several forms of the frequency response function are developed and the proposed parameter estimation process is explained.

Chapter three describes the procedures used to collect and analyze data from the experimental subject, a steel beam. The dimensions of the beam along with the modifications performed on the beam are described and illustrated.

Results of the described modal analysis are included in Chapter Four. These results include mode shapes, synthesized FRFs, and modal assurance criterion (MAC) tables. Results of an additional test of the beam data is also included. Conclusions from the results are given in Chapter Five. A comparison of the proposed fixed-poles method with a standard method is also given. Finally, chapter six includes recommendations for further study in the use of the proposed algorithm.

Chapter Two

Theory

2.1 Modal Theory

When a structure vibrates, its vibration can be described as a linear combination of the structure's modes of vibration. A mode of vibration consists of a parameter describing the frequency and damping of that mode which is termed a pole and a parameter at every point on the structure called a mode vector. Every real system has an infinite number of modes, though we are typically only interested in those in a specific frequency range.

Only proportional damping is considered in this discussion. Proportional damping occurs when the system's damping matrix is actually a linear combination of the system's mass and stiffness matrices. As will be shown, the matrix form of the system's dynamic equations can be diagonalized (decoupled) when damping is proportional. Having the system's equations decoupled greatly simplifies the calculation of the frequency response function that follows.

2.1.1 The Eigenproblem

Using Newton's laws, the dynamics of mechancial systems can be described by differential equations. The eigensolution of a system describes the system's undamped response to any forcing condition, and, for a proportionally damped system, a damped solution follows from the undamped solution.

A three degree of freedom (DOF) system as shown in figure 1 can be modeled as a series of three second order differential equations

$$\begin{aligned} m_1\ddot{x}_1 + k_1x_1 - k_1x_2 &= F_1 \\ m_2\ddot{x}_2 - k_1x_1 + k_1x_2 + k_2x_1 - k_2x_3 &= 0 \\ m_3\ddot{x}_3 - k_2x_2 + k_2x_3 + k_3x_3 &= 0 \end{aligned} \qquad (2.1.1.1)$$

This system can be represented in matrix form as a single differential equation.

$$M\{\ddot{X}\} + K\{X\} = \{F\} \qquad (2.1.1.2)$$

$$M = \begin{bmatrix} m_1 & 0 & 0 \\ 0 & m_2 & 0 \\ 0 & 0 & m_3 \end{bmatrix} \qquad K = \begin{bmatrix} k_1 & -k_1 & 0 \\ -k_1 & k_1 + k_2 & -k_2 \\ 0 & -k_2 & k_2 + k_3 \end{bmatrix}$$

$$X = \begin{Bmatrix} x_1 \\ x_2 \\ x_3 \end{Bmatrix} \qquad F = \begin{Bmatrix} F_1 \\ 0 \\ 0 \end{Bmatrix}$$

The modes of the system are inherent to the system and are not determined by the forcing function, thus, the modes can be determined from the unforced case. A harmonic solution of the form $X = Xe^{j\omega t}$ is assumed yielding

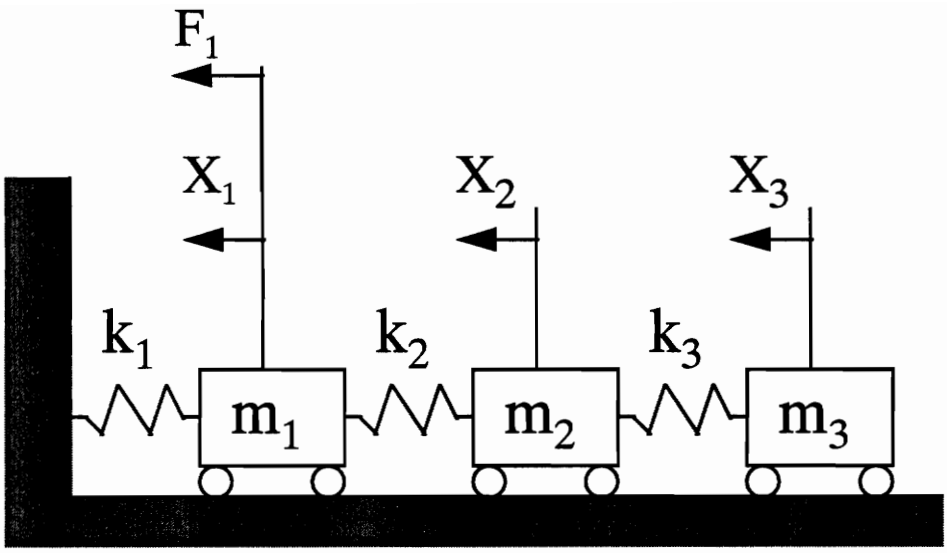

Figure 1: Three Degree of Freedom System

$$\left[-\omega^2 M + K\right]X = 0. \qquad (2.1.1.3)$$

Setting $\lambda = \frac{1}{\omega^2}$ and premultiplying by K^{-1} produces the standard form of the eigenproblem

$$\left[\lambda[I] - [K]^{-1}[M]\right]X = \{0\}$$

or

$$\lambda[I]X = [K]^{-1}[M]X. \qquad (2.1.1.4)$$

Sets of solutions to this equation consist of a scalar called the eigenvalue, λ, and a vector, X, called an eigenvector. Sets of eigenvalues and their corresponding eigenvectors are termed eigenpairs. There will be an eigenpair for each degree of freedom of the system, three eigenpairs in this example.

In a more physical sense, each eigenpair represents a different mode of vibration of the system. For an eigenpair, the square root of the inverse of an eigenvalue is the natural frequency of that mode, and the mode shape is described by the eigenvectors.

2.1.2 Diagonalization

For every eigenpair, the natural frequency (ω_i) and eigenvector (V_i) must satisfy equation 2.1.1.4 so that

$$\omega_i^2[m]V_i = [k]V_i. \qquad (2.1.2.1)$$

Premultiplying by V_i^T and considering equation 2.1.1.4 at two natural frequencies referenced by i and j yields

$$\omega_i^2 V_j^T [m] V_i = V_j^T [k] V_i = V_i^T [k] V_j \qquad (2.1.2.2)$$

$$\omega_j^2 V_i^T [m] V_j = \omega_j^2 V_j^T [k] V_i = V_i^T [k] V_j. \qquad (2.1.2.3)$$

By subtracting these equations, we obtain

$$(\omega_i^2 - \omega_j^2) V_j^T [m] V_i = 0. \qquad (2.1.2.4)$$

When $\omega_i \neq \omega_j$,

$$V_j^T [m] V_i = 0 \text{ and} \qquad (2.1.2.5)$$

$$V_j^T [k] V_i = 0. \qquad (2.1.2.6)$$

When $\omega_i = \omega_j$,

$$V_i^T [m] V_i = \hat{M}_{ii} \qquad (2.1.2.7)$$

$$\text{and } V_i^T [k] V_i = \hat{K}_{ii}. \qquad (2.1.2.8)$$

These results show how the mass and stiffness matrices of the system differential equations can be diagonalized. Diagonalization of the M and K matrices means that the differential equations have been decoupled and can be solved as a set of three second order differential equations. The diagonalization process begins with forming a matrix of eigenvectors,

$$\Phi = \begin{bmatrix} | & | & | \\ V_1 & V_2 & V_3 \\ | & | & | \end{bmatrix}$$

V_n - Eigenvector n.

Premultiplying by Φ^T and changing X to ΦY yields the diagonalized differential equation,

$$\Phi^T M \Phi \ddot{Y} + \Phi^T K \Phi Y = \Phi^T F = \hat{M}\ddot{Y} + \hat{K}Y \qquad (2.1.2.9)$$

where

$$X = \Phi Y \qquad (2.1.2.10)$$

and

$$\hat{M} = \begin{bmatrix} \hat{m}_1 & 0 & 0 \\ 0 & \hat{m}_2 & 0 \\ 0 & 0 & \hat{m}_3 \end{bmatrix} \qquad \hat{K} = \begin{bmatrix} \hat{k}_1 & 0 & 0 \\ 0 & \hat{k}_2 & 0 \\ 0 & 0 & \hat{k}_3 \end{bmatrix}.$$

(Rao 1990: 289-291).

2.1.3 Proportional Damping

Damping has not been present in the system considered up to this point since omitting it simplifies the discussion. In general, the damping matrix cannot be diagonalized by the eigenvector matrix. Without a diagonalized damping matrix, the system can no longer be decoupled.

The assumption of proportional damping means that the damping matrix is mathematically similar to the stiffness and mass matrices. Similar matrices can be diagonalized by the same matrices which, in this case, is the eigenvector matrix. The assumption of similitude means that the damping matrix is a linear combination of the mass and stiffness matrix

$$[C] = \alpha[M] + \beta[K] \qquad (2.1.3.1)$$

With the assumption of proportional damping, the entire system can be diagonalized to the form

$$\hat{M}\ddot{Y} + \hat{C}\dot{Y} + \hat{K}Y = \Phi F \qquad (2.1.3.2)$$

where $\hat{M}$, $\hat{C}$, and $\hat{K}$ are all diagonal and the transformation is performed in the same manner as in equation 2.1.2.9.

2.1.4 The Frequency Response Function

The Frequency Response Function (FRF) describes the response of a system to an input. Since the response of a system is dependent on the position of the input and measured output on the structure, an FRF is indexed with two numbers, one to indicate the location at which the response is measured and one to indicate the location at which the system is forced. The derivation of several forms of the FRF is included with a three degree of freedom system assumed throughout for illustration.

Equation 2.1.3.2 describes a system that has been diagonalized by a known eigenvector matrix. In this equation, the position vector, Y, is a vector of locations $\begin{bmatrix} y_1 \\ y_2 \\ y_3 \end{bmatrix}$ that are not necessarily available physically. The relationship between Y and the real coordinates, X, is $Y=\Phi^{-1}X$. The forcing vector has not been transformed and thus still represents physical quantities,

$$F = \begin{bmatrix} f_1 \\ f_2 \\ f_3 \end{bmatrix}$$

where f_1 is forcing at mass 1, f_2 is forcing at mass 2, and so forth.

The forcing function, F, is harmonic and the response is assumed to be harmonic, of the forms

$$F = Fe^{j\omega t} \qquad (2.1.4.1) \qquad \text{and} \qquad Y = Ye^{j\omega t}. \qquad (2.1.4.2)$$

Taking derivatives of $Ye^{j\omega t}$ and replacing Y and the derivatives of Y in equation 2.1.4.2 yields

$$-\omega^2\hat{M}Y + i\omega\hat{C}Y + \hat{K}Y = \Phi^T F. \qquad (2.1.4.3)$$

Solving the left side for Y, expanding the right side, and assuming forcing only at mass 3, yields

$$\left[\hat{K} - \omega^2\hat{M} + i\omega\hat{C}\right]Y = \begin{bmatrix} {}_1\Phi_1 & {}_1\Phi_2 & {}_1\Phi_3 \\ {}_2\Phi_1 & {}_2\Phi_2 & {}_2\Phi_3 \\ {}_3\Phi_1 & {}_3\Phi_2 & {}_3\Phi_3 \end{bmatrix}\begin{bmatrix} 0 \\ 0 \\ f_3 \end{bmatrix}. \qquad (2.1.4.4)$$

Measuring at location y1 forms an equation of scalars,

$$(\hat{k}_1 - \omega^2\hat{m}_1 + i\omega\hat{c}_1)y_1 = {}_1\Phi_3 f_3, \qquad (2.1.4.5)$$

so that the solution for y1 is

$$y_1 = \frac{{}_1\Phi_3 f_3}{\hat{k}_1 - \omega^2\hat{m}_1 + i\omega\hat{c}_1}. \qquad (2.1.4.6)$$

Solutions for y2 and y3 follow as

$$y_2 = \frac{{}_2\Phi_3 f_3}{\hat{k}_2 - \omega^2\hat{m}_2 + i\omega\hat{c}_2} \qquad y_3 = \frac{{}_3\Phi_3 f_3}{\hat{k}_3 - \omega^2\hat{m}_3 + i\omega\hat{c}_3}.$$

Equation 2.1.2.10 expanded out for clarity is

$$\begin{bmatrix} x_1 \\ x_2 \\ x_3 \end{bmatrix} = \begin{bmatrix} {}_1\Phi_1 & {}_1\Phi_2 & {}_1\Phi_3 \\ {}_2\Phi_1 & {}_2\Phi_2 & {}_2\Phi_3 \\ {}_3\Phi_1 & {}_3\Phi_2 & {}_3\Phi_3 \end{bmatrix} \begin{bmatrix} y_1 \\ y_2 \\ y_3 \end{bmatrix}, \qquad (2.1.4.9)$$

which implies that $x_1 = {}_1\Phi_1 y_1 + {}_2\Phi_1 y_2 + {}_3\Phi_1 y_3$. With y1, y2, and y3 known, a solution for x1 as a function of f3 is found to be

$$x1 = \frac{{}_1\Phi_{11}\Phi_3 f_3}{\hat{k}_1 - \omega^2\hat{m}_1 + i\omega\hat{c}_1} + \frac{{}_2\Phi_{11}\Phi_3 f_3}{\hat{k}_2 - \omega^2\hat{m}_2 + i\omega\hat{c}_2} + \frac{{}_3\Phi_{11}\Phi_3 f_3}{\hat{k}_3 - \omega^2\hat{m}_3 + i\omega\hat{c}_3}. \qquad (2.1.4.10)$$

Forming the ratio of x1 to f3 and rewriting the series as a summation yields

$$\frac{x_1}{f_3} = \sum_{n=1}^{3} \frac{{}_n\Phi_{1\,n}\Phi_3}{\hat{k}_n - \omega^2\hat{m}_n + i\omega\hat{c}_n} \qquad (2.1.4.11)$$

which is the frequency response function when point 1 is measured and a harmonic force is applied at point 3.

In general, for an N dof system, the equation for the frequency response function can be written as

$$\frac{x_a}{f_b} = \sum_{n=1}^{N} \frac{{}_n\Phi_a \, {}_n\Phi_b}{\hat{k}_n - \omega^2 \hat{m}_n + i\omega \hat{c}_n} \qquad (2.1.4.12)$$

or

$$\frac{x_a}{f_b} = \sum_{n=1}^{N} \frac{{}_n\Phi_a \, {}_n\Phi_b / \hat{m}_n}{\omega_n^2 - \omega^2 + i2\zeta_n \omega \omega_n} \qquad (2.1.4.13)$$

where $\omega_n = \sqrt{\frac{\hat{k}_n}{\hat{m}_n}}$ and $\zeta_n = \frac{\hat{c}_n}{2\sqrt{\hat{k}_n \hat{m}_n}}$.

The frequency response function can be written in several other forms that are each useful in different situations for showing different aspects of the FRF. For instance, it is clear from equation 2.1.4.13 how when the frequency at which the FRF is calculated is close to a natural frequency, the denominator of the equation approaches infinity, only limited by the damping term. Equations 2.1.4.12 and 2.1.4.13 also show that the denominator term does not change based upon the measurement location or the forcing location. Only the numerator is a function of the points of measurement and forcing.

Another form of the FRF is the partial fraction representation. The derivation of the partial fraction form of the FRF begins by rewriting equation 2.1.4.13 so that the denominator is a quadratic in ω^2,

$$\frac{x_a}{f_b} = \sum_{n=1}^{N} \frac{{}_n\Phi_a \, {}_n\Phi_b / \tilde{m}_n}{c\omega^2 + d\omega + f}, \qquad (2.1.4.14)$$

where $c = -1$, $d = 2\zeta_n\omega_n i$, and $f = \omega_n{}^2$. This quadratic can be factored into the pole-residue form of the frequency response function

$$\frac{x_a}{f_b} = \sum_{n=1}^{N} \frac{{}_nA_{ab}}{j\omega - P_n} + \frac{{}_nA_{ab}^*}{j\omega - P_n^*} \qquad (2.1.4.15)$$

where P_n is a system pole, defined as $P_n = -\xi_n\omega_n + j\omega_n\sqrt{1-\xi_n^2}$ and ${}_nA_{ab}$ is termed a residue, defined as ${}_nA_{ab} = \frac{{}_n\phi_a \, {}_n\phi_b}{2jm_n\omega_n\sqrt{1-\xi_n^2}}$. (2.1.4.16)

Finally, the form of the FRF most useful for curve fitting is the rational fraction form in which the numerator and denominator are polynomials. The rational fraction form can be calculated from the partial fraction representation by multiplying each partial fraction term so to equate the denominator terms

$$\frac{x_a}{f_b} = \frac{{}_1A_{ab}}{j\omega - P_1} \cdot \frac{\sum_{n=2}^{N} j\omega - P_n}{\sum_{n=2}^{N} j\omega - P_n} \cdot \frac{\sum_{n=1}^{N} j\omega - P_n^*}{\sum_{n=1}^{N} j\omega - P_n^*} + \frac{{}_1A_{ab}^*}{j\omega - P_1^*} \cdot \frac{\sum_{n=1}^{N} j\omega - P_n}{\sum_{n=1}^{N} j\omega - P_n} \cdot \frac{\sum_{n=2}^{N} j\omega - P_n^*}{\sum_{n=2}^{N} j\omega - P_n^*} + \cdots$$

$$\cdots + \frac{{}_{N}A_{ab}}{j\omega - P_N} \cdot \frac{\sum_{n=1}^{N-1} j\omega - P_n}{\sum_{n=1}^{N-1} j\omega - P_n} \cdot \frac{\sum_{n=1}^{N} j\omega - P_n^*}{\sum_{n=1}^{N} j\omega - P_n^*} + \frac{{}_{N}A_{ab}^*}{j\omega - P_N^*} \cdot \frac{\sum_{n=1}^{N} j\omega - P_n}{\sum_{n=1}^{N} j\omega - P_n} \cdot \frac{\sum_{n=1}^{N-1} j\omega - P_n^*}{\sum_{n=1}^{N-1} j\omega - P_n^*} \cdot$$

(2.1.4.17)

With the Laplace variable replacing jω, the equation becomes a ratio of two polynomials with the order of the numerator being one less than the order of the denominator.

$$\frac{x_a}{f_b} = \frac{\sum_{n=1}^{N-1} a_k s^k}{\sum_{n=1}^{N} b_k s^k}, \quad s=j\omega. \qquad (2.1.4.18)$$

The poles are now the roots of the denominator polynomial. This last form of the FRF is useful for curve fitting because of its simplicity.

2.2 Frequency Domain Parameter Estimation

The process of determining modal parameters from experimental data involves minimizing the difference between measured FRFs and simulated FRFs by iterating through different combinations of the modal parameters. Proposed here is a method of frequency domain curve fitting that differs from traditional methods by using a single FRF to determine the system's poles and applying these poles to the other FRFs to estimate the mode vectors. It is assumed that the system's poles do not change from measurement to measurement.

The proposed method of parameter estimation is termed the "fixed-poles" method. It is based upon the Rational Polynomial algorithm proposed by Richardson (Richardson 1982), and results using a standard technique for applying the Rational Polynomial algorithm are included for comparison. The difference between the two methods lies completely in the way in which the system's poles are calculated. The fixed-poles method curve fits a single FRF using the Rational Polynomial algorithm to determine the poles of the FRF. These poles can then be applied to all other FRFs to determine the mode vectors by solving a single equation for each FRF. Once these equations are solved, the parameter estimation is complete with the system's poles and mode vectors determined.

The traditional application of the Rational Polynomial algorithm does not initially assume that the system's poles are constant throughout all the measured FRFs. An iterative process is implemented where a set of poles that best fit all the measured FRFs is determined. These estimated poles are then assumed to be the system's poles and are then applied to all the FRFs in the same manner as the fixed-poles method in order to estimate the mode vectors.

Functionally, the fixed-poles algorithm dramatically reduces the computational resources needed by reducing the iterative process from iterating using all the measured FRFs to iterating on only one FRF. It would be foolish, therefore, to apply the fixed-poles algorithm to data where the system's poles changed during testing. This situation would typically occur when FRFs were measured by moving an accelerometer or some

other type of contacting transducer over the surface of the structure. The mass of the moving transducer would cause a shift in the subject's poles each time it was moved

2.2.1 Fixed-poles Algorithm

The fixed-poles algorithm is a technique for applying the Rational Polynomial algorithm. There are two parts to the fixed-poles analysis technique: pole identification and mode vector estimation. Pole identification consists of applying the Rational Polynomial to a single FRF in order to estimate the pole locations in that FRF. Mode vectors are estimated by setting the poles of every remaining FRF equal to those determined in the pole identification step and then solving a non-linear least squares problem. The results of the technique are the system's poles as well as a mode vector for each mode at every measurement location.

2.2.1.1 Pole Identification

Pole identification is acheived in the fixed-poles algorithm by applying the Rational Polynomial algorithm to a single driving point FRF measurement. Estimating the modal parameters of a measured FRF involves minimizing the error between the measured data and an analytical model of the FRF. In this case, the analytical model is expressed with ordinary polynomials in the rational polynomial form

$$H(j\omega_i) = \frac{\sum_{k=0}^{m} a_k (j\omega_i)^k}{\sum_{k=0}^{n} b_k (j\omega_i)^k} = \frac{N(j\omega_i)}{D(j\omega_i)} \qquad (2.2.1.1.1)$$

over the frequency indices i=1,2,...L.

Since any mth order polynomial can be represented by a sum of m+1 scaled 0 through mth order orthogonal polynomials, the ordinary polynomials of equation 2.2.1.1.1 can be replaced by orthogonal polynomials so that it becomes

$$H(j\omega) = \frac{N(j\omega_i)}{D(j\omega_i)} = \frac{\sum_{k=0}^{M} c_k \phi_{ik}}{\sum_{k=0}^{N} d_k \theta_{ik}} \qquad (2.2.1.1.2)$$

where ϕ_{ik} and θ_{ik} are kth order orthogonal polynomials evaluated at frequency ω_i. The reason for the substitution of orthogonal polynomials is not immediately apparent but becomes important later in the discussion. For an excellent discourse on the usefulness of orthogonal polynomials in this type of estimation, see Richardson (Richardson 1982).

An error criterion can be defined as the estimated FRF minus the measured FRF

$$e_i = H(\omega_i) - h_i = \frac{N(j\omega_i)}{D(j\omega_i)} - h_i. \qquad (2.2.1.1.3)$$

This equation can be simplified by multiplying through by the characteristic polynomial, $D(j\omega_i)$, and then multiplying through by the inverse of the estimated characteristic polynomial, ω_i,

$$e_i = \omega_i [N(j\omega_i) - h_i D(j\omega_i)]. \qquad (2.2.1.1.4)$$

The error at every point can be used to determine an error vector

$\mathbf{e} = \{e_1, e_2, e_3, \ldots, e_L\}^T$. The error vector then can be written out in matrix form

$$e = \begin{bmatrix} \omega_1\phi_{1,0} & \omega_1\phi_{1,1} & \cdots & \omega_1\phi_{1,m} \\ \omega_2\phi_{2,0} & \omega_2\phi_{2,1} & \cdots & \omega_2\phi_{2,m} \\ \vdots & & & \vdots \\ \omega_L\phi_{L,0} & \cdots & \cdots & \omega_L\phi_{L,m} \end{bmatrix} \begin{Bmatrix} c_0 \\ c_1 \\ \vdots \\ c_m \end{Bmatrix}$$

$$- \begin{bmatrix} \omega_1 h_1\theta_{1,0} & \omega_1 h_1\theta_{1,1} & \cdots & \omega_1 h_1\theta_{1,n-1} \\ \omega_2 h_2\theta_{2,0} & \omega_2 h_2\theta_{2,1} & \cdots & \omega_2 h_2\theta_{2,n-1} \\ \vdots & & & \vdots \\ \omega_L h_L\theta_{L,0} & \cdots & \cdots & \omega_L h_L\theta_{L,n-1} \end{bmatrix} \begin{Bmatrix} d_0 \\ d_1 \\ \vdots \\ d_{n-1} \end{Bmatrix} - \begin{Bmatrix} \omega_1 h_1\theta_{1,n} \\ \omega_2 h_2\theta_{2,n} \\ \vdots \\ \omega_L h_L\theta_{L,n} \end{Bmatrix}$$

$$= \mathbf{Pc} - \mathbf{Qd} - \mathbf{r}. \qquad (2.2.1.1.5)$$

The Forsythe polynomials ϕ and θ are used to replace the numerator, N(jω), and the denominator, D(jω), respectively. The coefficient d_n is assumed to be unity.

The real squared error is then

$$E = \mathbf{e}^H\mathbf{e} = \left[\mathbf{Pc} - \mathbf{Qd} - \mathbf{r}\right]^H\left[\mathbf{Pc} - \mathbf{Qd} - \mathbf{r}\right] \qquad (2.2.1.1.6)$$

where H represents the Hermitian transpose (conjugate transpose) which is employed to eliminate imaginary values. The minimum error condition occurs when the partial derivatives of the error function are zero with respect to the two variable vectors, **c** and **d**,

$$\frac{\partial E}{\partial \mathbf{c}} = \mathbf{0} \text{ and } \frac{\partial E}{\partial \mathbf{d}} = \mathbf{0}. \qquad (2.2.1.1.7)$$

This results in the system's normal equations

$$\begin{bmatrix} 2\,\mathrm{Re}\left[\mathbf{P}^{H}\mathbf{P}\right] & -2\,\mathrm{Re}\left[\mathbf{P}^{H}\mathbf{Q}\right] \\ -2\,\mathrm{Re}\left[\mathbf{Q}^{H}\mathbf{P}\right] & 2\,\mathrm{Re}\left[\mathbf{Q}^{H}\mathbf{Q}\right] \end{bmatrix} \begin{Bmatrix} \mathbf{c} \\ \mathbf{d} \end{Bmatrix} = \begin{Bmatrix} 2\,\mathrm{Re}\left[\mathbf{P}^{H}\mathbf{r}\right] \\ -2\,\mathrm{Re}\left[\mathbf{Q}^{H}\mathbf{r}\right] \end{Bmatrix}. \qquad (2.2.1.1.8)$$

The orthogonality of **P** and **Q** imposed by the use of the orthogonal polynomials results in the two diagonal submatrices in equation 2.2.1.1.8 becoming identity matrices

$$\begin{bmatrix} \mathbf{I}_{m+1} & \mathbf{X} \\ \mathbf{X}^{T} & \mathbf{I}_{n} \end{bmatrix} \begin{Bmatrix} \mathbf{c} \\ \mathbf{d} \end{Bmatrix} = \begin{Bmatrix} \mathbf{g} \\ \mathbf{0} \end{Bmatrix} \qquad (2.2.1.1.9)$$

where

$$\mathbf{X} = -2\,\mathrm{Re}\left[\mathbf{P}^{H}\mathbf{Q}\right]$$

$$\mathbf{g} = 2\,\mathrm{Re}\left[\mathbf{P}^{H}\mathbf{r}\right]$$

I = identity matrix.

The system described by equation 2.2.1.1.5 is decoupled so that vectors **c** and **d** can be solved for independently according to the equations

$$[\mathbf{I} - \mathbf{X}^{T}\mathbf{X}]\mathbf{d} = -\mathbf{X}^{T}\mathbf{g}, \text{ and} \qquad (2.2.1.1.10)$$

$$\mathbf{c} = \mathbf{g} - \mathbf{X}\mathbf{d}. \qquad (2.2.1.1.11)$$

The problem becomes iterative since the ω_x terms were initially guesses and can be updated with new estimates of the characteristic polynomial. The process of solving for new estimates of **c** and **d** and updating ω_x continues until the error condition, E, reduces to an acceptable level. At that point, the best estimates of **c** and **d** are accepted as the final values (Han 1991: 45-50).

With the coefficients of the orthogonal polynomial solution for the FRF known, the normal polynomial denominator terms can be calculated by setting the normal and orthogonal denominator polynomials equal to each other and then equating coefficients on the powers of x. The normal polynomial numerator coefficients can be solved for in a like manner. Though not needed, the normal polynomial numerator coefficients are necessary to synthesize the fitted FRF in order to check estimate quality. The poles of the system can be determined by solving for the roots of the now fully known normal polynomial denominator.

2.2.1.2 Mode Vector Estimation

With the poles of the system set, the denominator of the FRF equation is determined. The parameter estimation problem is thus reduced to determining the numerator coefficients for each measurement point. The problem can be formulated for each FRF in the same way as the estimation of the parameters of the pole FRF but with the values of vector **d** known. The iterative nature of the problem is eliminated since the estimate of the denominator, ω_x, is now exactly known. The estimate of the numerator coefficients simply involves solving the equation $\mathbf{c = g - Xd}$ for every point at which a measurement was taken.

The normal polynomial numerator coefficients can be determined as previously described and then the FRF for each point is completely known in rational fractional

form. Through algebraic manipulation, the FRF can be converted into pole-residue form, equation 2.1.4.15,

$$H_{ik}(j\omega) = \sum_{r=1}^{n}\left[\frac{{}_rA_{ik}}{s - P_r} + \frac{{}_rA_{ik}^*}{s - P_r^*}\right] \qquad (2.2.1.2.1)$$

where s=jω and ${}_rA_{ik} = \dfrac{{}_r\phi_i\,{}_r\phi_k}{2jm_r\omega_{dr}}$ is a residue. Finally, scaled mode vectors can be determined from the residues by dividing each residue for a given mode by the square root of the driving point residue for that mode. With the system's poles determined and the mode vectors known at each point on the structure, the parameter estimation is complete.

2.2.2 Global Parameter Estimation Algorithm

Global parameter estimation techniques formulate the estimation problem differently than the fixed-poles algorithm. The global estimation algorithm is formed by rewriting equation 2.2.1.1.10 so that all measured FRFs are included in the estimation of the system's poles, hence the term "global." Including the extra data results in a set of overspecified equations to be solved simultaneously

$$\begin{bmatrix} U_1 \\ U_2 \\ \vdots \\ U_p \end{bmatrix}\{D\} = \begin{Bmatrix} V_1 \\ V_2 \\ \vdots \\ V_p \end{Bmatrix} \qquad (2.2.2.1)$$

$$\text{where } [U_k] = \left[I - [X_k]^t [X_k] \right] \text{ and}$$

$$\{V_k\} = -[X_k]^t \{H_k\}.$$

This set of equations can be solved by a least squares method for the orthogonal polynomial denominator coefficients. The orthogonal polynomial numerator coefficients can then be solved for each FRF by solving equation 2.2.1.1.11. The FRF can then be simulated and the error between simulated and measured FRFs calculated. The estimate of the denominator term, ω_i , in equation 2.2.1.1.4 is updated with the new denominator coefficients and the process is repeated. This looping continues until the error condition is met.

2.3. Scanning Laser Velocimeter

The principle of laser vibrometry is based upon the Doppler shift and is made practical through homodyning. The Doppler shift is a well known phenomenon familiar to anyone who has been passed by a train blowing its whistle or a police car with its siren sounding. A Doppler shift occurs when there is relative motion between the subject and source of a wave. The relative motion causes the emanated waves to reach the subject in a shorter period of time if the relative motion brings the source and subject together, thus the effect is an apparent increase in frequency of the wave. An apparent reduction in the frequency of the wave occurs if the relative motion separates the source and subject.

2.3.1 The Doppler Shift

When a moving surface is subject to a wave, the wave is reflected off the surface. The motion of the surface causes a shift in the reflected wave since the time between waves bouncing off the surface is changed due to the motion of the surface.

The basic equation for the Doppler shift when a planar wave strikes a subject moving at a velocity, V, with an angle of θ between the velocity vector and a line normal to the wavefront is

$$\Delta\nu = \frac{V\cos\theta}{\lambda} \qquad (2.3.1.1)$$

where $\Delta\nu$ is the shift in frequency apparent to the moving subject and the wavelength of the emitted wave is λ. Obviously, if the angle θ is 90 degrees then the frequency shift is zero. Physically, this means that the Doppler shift can only be used to measure relative velocity along the axis normal to the wave front. Therefore, an SLV can only measure the true velocity of a point on a surface if the velocity vector of that point is exactly parallel to the laser beam (Drain 1980: 36).

2.3.2 Homodyning

Laser vibrometry uses a light beam as the source wave. The frequency of the source laser light is approximately $4.7\text{x}10^{14}$ Hz and the shift due to the Doppler effect is generally in the range 10kHz-10 Mhz. The resulting shifted wave is in the range of 10^8 to 10^{11} Hz, still too high to directly measure.

The most effective way to measure the shifted frequency, and thus estimate the velocity of the subject, is to add the shifted and unshifted signals in a process known as heterodyning. Consider, for example, two sinusoidal signals, E and E'

$$E = E_1 \cos(2\pi\nu_1 t + \phi_1) \qquad (2.3.2.1)$$

$$E' = E_2 \cos(2\pi\nu_2 t + \phi_2) \qquad (2.3.2.2)$$

where E is the original signal and E' is the Doppler shifted signal. An optical detector responds to the square of the optical electrical field. Adding the signals results in the output of the detector being

$$i(t) = B(E_1 \cos(2\pi\nu_1 t + \phi_1) + E_2 \cos(2\pi\nu_2 + \phi_2))^2. \qquad (2.3.2.3)$$

Multiplying out the terms in equation 2.3.2.3 yields

$$i(t) = B(E_1^2 \cos^2 u + 2E_1E_2 \cos u \cos v + E_2^2 \cos^2 v) \qquad (2.3.2.4)$$

where $u = 2\pi\nu_1 t + \phi_1$ and $v = 2\pi\nu_2 t + \phi_2$.

Applying trigonometric identities to the equation 2.3.2.4 results in a form showing the various frequencies present in the output of the optical detector,

$$i(t) = B[\tfrac{1}{2}(E_1 + E_2) + E_1E_2 \cos(u - v) + E_1E_2 \cos(u + v) + \cdots$$

$$\cdots + \frac{E_1^2}{2}\cos(2u) + \frac{E_2^2}{2}\cos(2v)]. \qquad (2.3.2.5)$$

The frequencies of E1 and E2 started out too high to measure, and so the terms containing the frequencies 2u, 2v and u+v could be filtered out of the signal. The remaining signal,

therefore, contains an offset and a sinusoid whose frequency is the difference between the two initial signals

$$i(t) = B[\tfrac{1}{2}(E_1 + E_2) + E_1E_2 \cos(2\pi(\nu_1 - \nu_2)t + (\phi_1 - \phi_2)). \qquad (2.3.2.6)$$

The resulting frequency output of the optical detector is the Doppler shift in the original laser beam (Drain 1980: 54-55).

The process of homodyning is invisible to the laser operator as homodyning occurs within the laser unit. The Doppler signal can be monitored by the operator, but the final output of the laser unit is simply a voltage signal proportional to the velocity of the target.

2.3.3 Data Acquisition Software

The Galactic Class Interface (GCI) is a program created in the Labview graphical programming environment to acquire and analyze force transducer and laser response time series data and to control the movement of the laser during testing. Force transducer response and laser response are acquired simultaneously so to fix the phase relationship between the two signals. The GCI not only acquires the data, but processes the data to determine the magnitude and phase of the force and velocity signals.

Velocity and force measurements are performed in the time domain using single frequency excitation. Frequency response functions measured using the SLV are acquired one frequency at a time by fitting a sinusoid to both the input (force) and output (velocity) channels. The estimates of the magnitude and phase of the output signal are divided by

the estimates for the input signal to determine the frequency response at the driving frequency. The response at multiple frequencies is estimated to form a frequency response function.

2.3.3.1 Force Transducer Response Estimation

The force transducer response is a single frequency signal of known frequency (set by the operator). The real and imaginary components are unknown as is the DC offset of the signal. For each sample, the model of the response is

$$f(t_i) = F_o + F_A \sin(\omega_s t_i) + F_B \cos(\omega_s t_i) + \eta_i \qquad (2.3.3.1.1)$$

where F_A is the real component, F_B is the imaginary component, F_o is the DC offset, and η_i is the error term. With this model, a Multiple Least Squares (MLS) problem can be formulated using every data point. Solving the MLS problem results in the determination of the real and imaginary components, the DC offset, and the error terms (Dominguez 1994: 34-36).

Only the phase of the force signal relative to the response signal is of significance during analysis. It would be convenient for the force signal to be considered zero phase, so that the phase of the velocity is relative to the input force. Zero phase implies that the representation of the force signal is composed of only a real component. An entirely real representation of the force signal can be obtained by multiplying the complex representation of the force signal by its complex conjugate. In order to maintain the phase relationship between the force and response signals, the complex representation of

the response signal must also be multiplied by the complex conjugate of the original force signal. The final effect of these calculations is the elimination of the imaginary part of the force signal while still maintaining the important phase relationship between the two signals.

2.3.3.2 Laser Response Estimation

The model of the response of the laser velocity output parallels that of the force signal,

$$u(t_i) = U_o + U_A \sin(\omega_s t_i) + U_B \cos(\omega_s t_i) + \varepsilon_i \qquad (2.3.3.2.1)$$

where U_o is the DC offset, U_A is the real component, U_B is the imaginary component, and ε_i is the error term. Again, the frequency of the response is known since it equals the frequency set by the operator.

The response of the laser is much more subject to sudden and severe losses in data quality in comparison to the force transducer. To deal with these poor data points, a more robust regression strategy than MLS, M-estimation, was implemented using the Iterated Reweighted Least Squares (IRLS) algorithm. This method down-weights data that poorly follows the other data so that the effects of dropouts on the final solution is minimized. After the scaling process mentioned in section 2.3.3.1, the final result of this estimation is real and imaginary values of the velocity as measured by the scanning laser (Dominguez 1994: 61-62).

The error term in equation 2.3.3.2.1 is useful as a measure of signal quality much in the same way a coherence term is useful for weighting the quality of data in a frequency response function. The magnitude of the error term relative to the magnitude of the velocity estimates indicates the degree to which the sinusoidal model fits the actual data.

2.3.3.3 Scanning

The process of scanning involves the GCI commanding the laser unit to move the laser beam over the surface of the subject and acquiring data once the laser has moved. The laser source remains fixed during scanning and motion of the beam is produced by reflecting the beam off a pair of mirrors inside the laser unit. Two mirrors are used to angle the laser beam in horizontal and vertical planes. Analog inputs are supplied from the GCI to galvanometers inside the laser unit that are attached to the aiming mirrors. When a voltage is applied to one of these galvanometers, the galvanometer moves and the attached mirror moves with it to aim the beam at a particular location. Combinations of inputs to the horizontal and vertical mirrors are used to target off axis locations.

Chapter Three

Procedures

The following outlines the procedures used to acquire and analyze data used to formulate the results of section four. Frequency response data was acquired from a steel beam using the scanning laser velocimeter as well as an accelerometer. Natural frequencies, damping values, and mode shapes were obtained from this data by curve fitting the data.

A beam was chosen as the subject on which to perform a modal analysis using the fixed-poles method. The simple geometry of a beam made angle corrections to the laser measurements, as described in section 3.1.2.3, straightforward. Additionally, the modes of vibration of a beam can be determined from beam dynamic theory for comparison to experimental results.

3.1 Experimental Procedure

The procedures relating to acquiring data relating to the steel beam test specimen are described below. Four types of data were acquired in the quantities indicated below:

- 5 accelerometer based frequency response functions,

- 5 accelerometer coherence functions for the FRFs,
- 31 velocity magnitude and phase estimates from the SLV at 472 locations, and
- 31 estimates of the force magnitude during the measurement of the velocity with the SLV at each of the 472 locations.

3.1.1 Steel Beam

A slender stainless steel beam was used as the subject on which to perform a modal analysis. The beam was excited by an electro-magnetic shaker. A series of measurements of the velocity field of the beam were performed with the SLV, each at a different excitation frequency. In addition to the laser measurements, several measurements of a frequency response function of the beam were taken with an accelerometer.

3.1.1.1 Subject Preparation

The modal analysis subject was a 55x3x1/4 inch beam made of 302 stainless steel. The specimen was prepared for testing by having three holes drilled and tapped into one end (hereafter referred to as the "top" end of the beam). The holes were drilled through the beam and tapped with #4-40 threads. The holes were lined up along the top edge of the beam and are illustrated in figure 2.

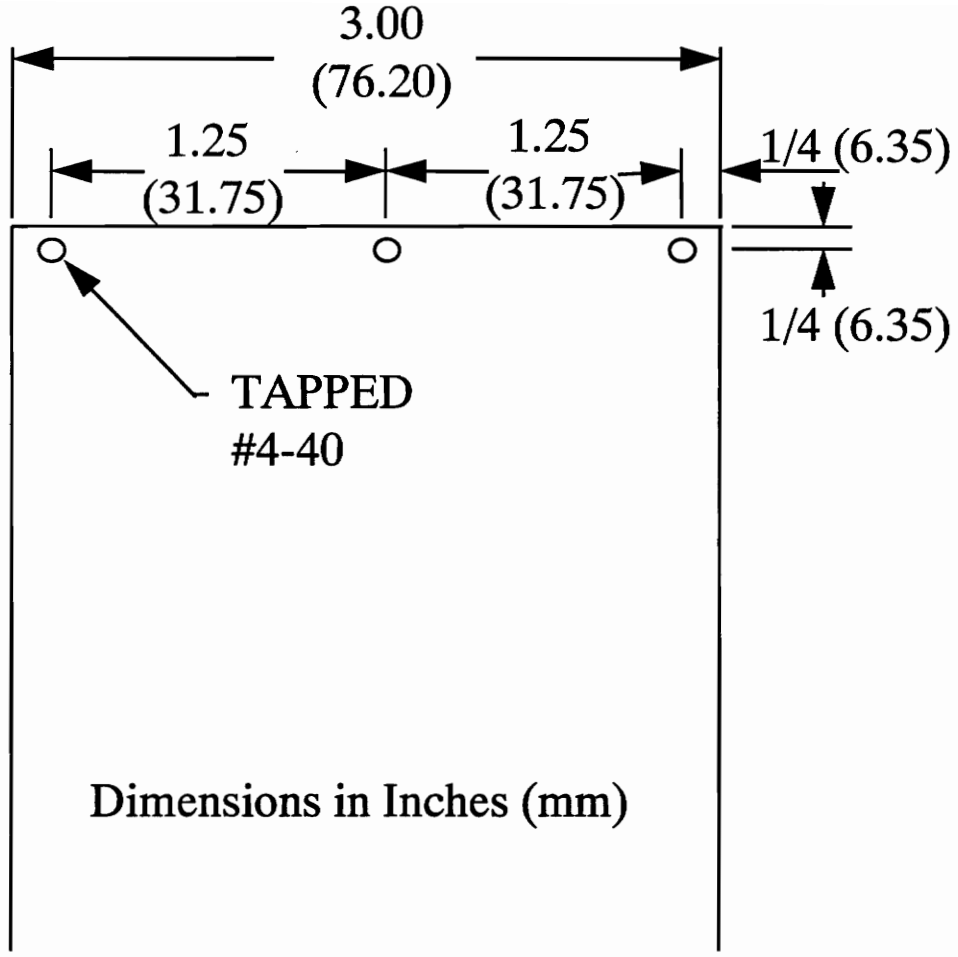

Figure 2: Beam Detail Dimensions

3.1.1.2 Subject Support

The beam was supported by several strands of thin line wrapped around a stud threaded into the center hole in the top of the beam so to simulate a free-free end condition. A free-free configuration is preferable to other boundary conditions since it is easily repeated. The support line was attached to an overhead hook and the weight of the specimen was fully supported by the line. A flat section of foam was placed under the beam to prevent it from swaying excessively while supported.

3.1.2 Frequency Response Measurements

Frequency response measurements were acquired from the beam with two vibration transducers; a scanning laser velocimeter (SLV) and an accelerometer. The setup of the beam and anything touching it remained the same during all tests so that the characteristics of the beam remained fixed during testing. This requirement of the fixed qualities of the beam meant that the accelerometer had to remain affixed in the same location on the beam during both accelerometer measurements and SLV measurements. An electromagnetic shaker was used to input force into the beam during both SLV and accelerometer testing. Additionally, the same force transducer was used to measure the input force during both types of testing so, by necessity, the force transducer and shaker remained in a constant arrangement during all testing.

The source of excitation for the beam was an electromagnetic shaker attached through a ball jointed rod and a force transducer. The connection of the shaker to the beam is illustrated in figure 3. The connection between the shaker and the beam was a

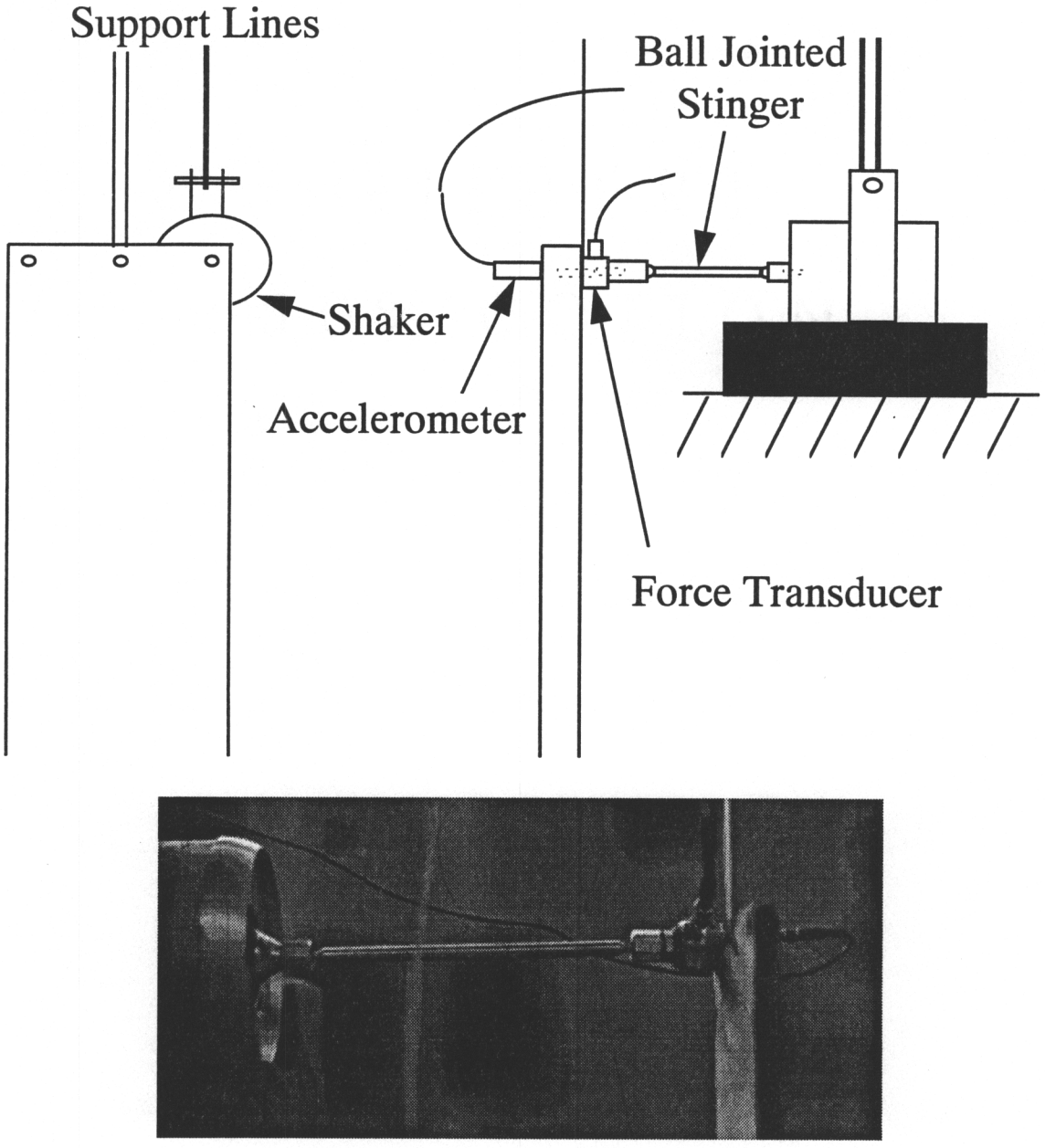

Figure 3: Shaker/Beam Connections

long, thin rod with a ball joint at each end. The ball joints prevented the rod from placing a torque or a bending load on the beam.

The input signal to the shaker was a sine wave with the frequency manually set by the operator on a Hewlett Packard 3324A signal generator. A Harmon Kardon amplifier was used to amplify the signal. The excitation frequency was input to the measurement software during each test. A schematic of the test assembly is shown in figure 4.

3.1.2.1 Input Force Measurement

The force input into the beam was measured with a Kistler force transducer (S/N 025820) located between the shaker and the specimen. The force transducer was screwed to a stud that was screwed into a tapped hole on the outer edge of the beam. This setup is shown in detail in figure 3.

The signal generated by the force transducer was amplified and filtered through an eight-pole Butterworth low-pass filter. The filter settings (except for gain) were all set to be the same as those operating on the velocity signal. Phase shifts and amplitude changes caused by the filters were canceled when the frequency response function was calculated since both the filters on both the velocity and force channels were matched.

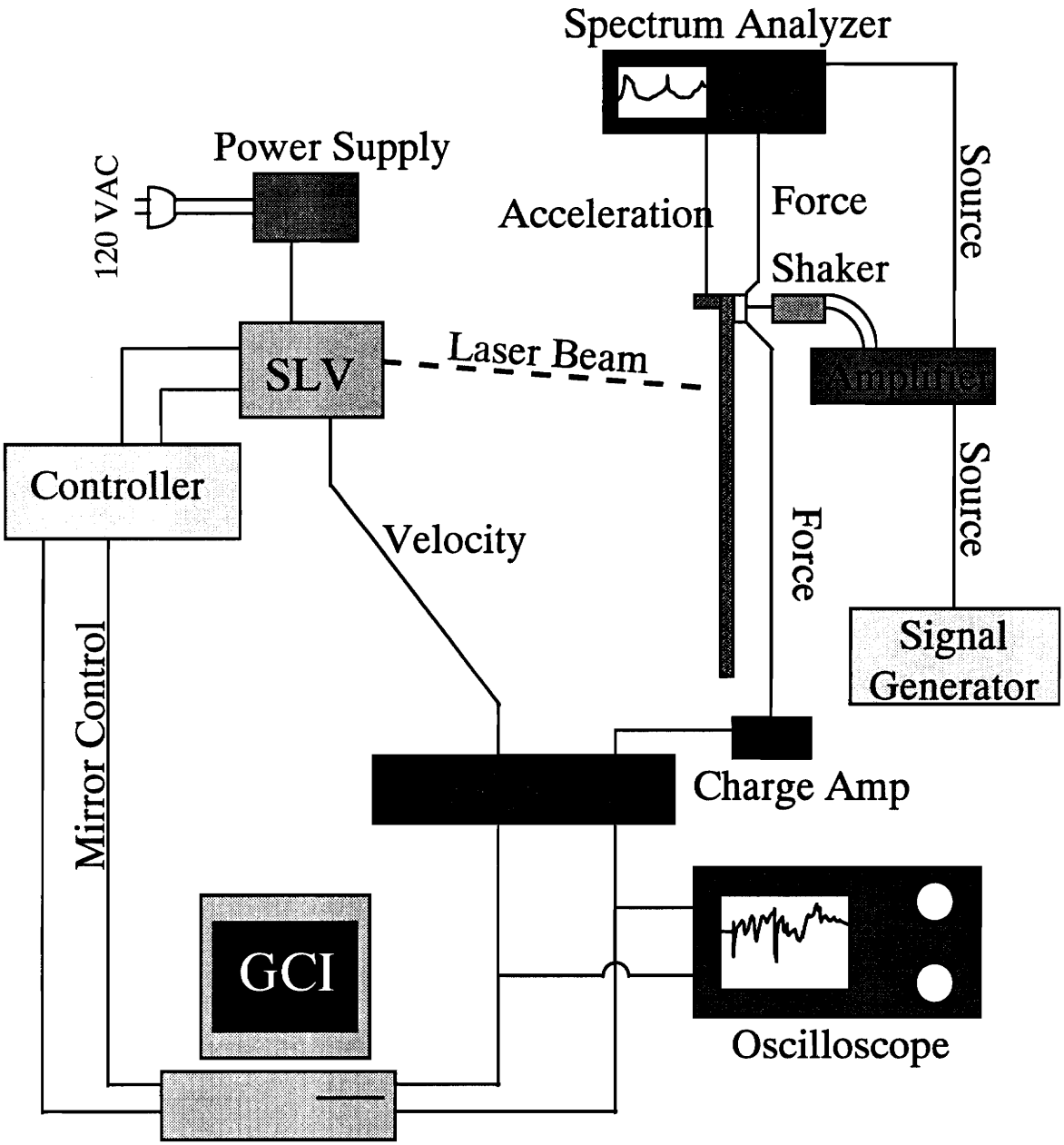

Figure 4: Schematic of Test Setup

3.1.2.2. Scanning Laser Velocimeter Measurements

The response of the steel beam was measured at 472 points on the surface of the beam. The force input was a single frequency sinusoid and the response was measured with a scanning laser velocimeter (SLV) programmed to return to each of the 472 locations during subsequent tests. The task of moving the laser and acquiring data was performed by the Galactic Class Interface (GCI) as described in section 2.3.3. Measurements were performed 31 different times with the beam being shaken at a different frequency each time. Figure 5 shows an FRF with SLV measurement frequency locations marked with an "x" and the location of resonances indicated by magnitude peaks and phase changes.

3.1.2.2.1 Aiming

The SLV was aligned so that it would be approximately centered and square with the beam, as shown in figure 6. Aligning the SLV and beam resulted in simplifying post processing of the data and allowed the measurement grid to be aligned with the beam.

The GCI was used to control the aiming of the laser. A grid of 472 (8 by 59) measurement locations was programmed and the GCI aimed the laser during testing.

3.1.2.2.2 Data Acquisition

The GCI was used to measure the force and velocity signals and also to estimate the magnitude and phase of these signals through data fitting algorithms. Each signal was fit to a sinusoid using a least squares approach. Details of the data fitting algorithms

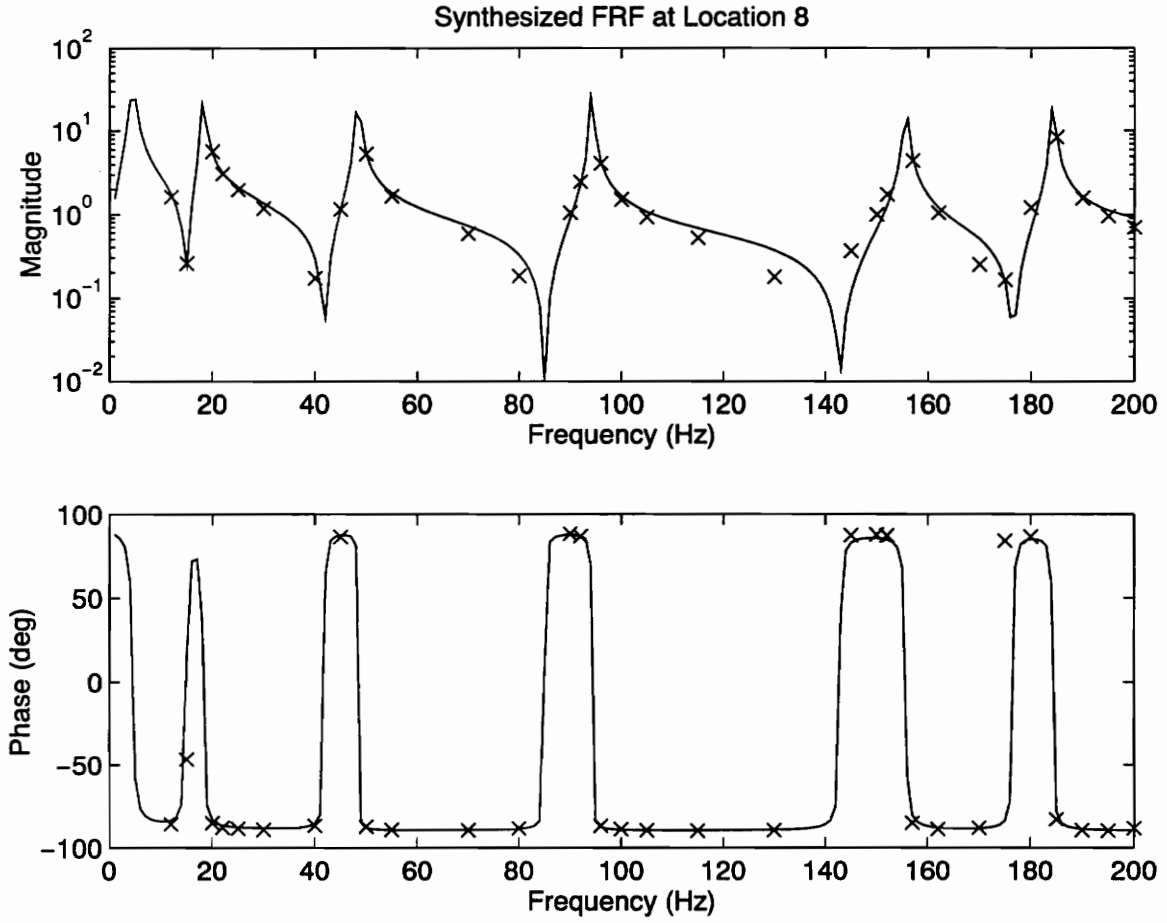

Figure 5: Scanning Laser Measurement Frequencies (x) Relative to Resonances

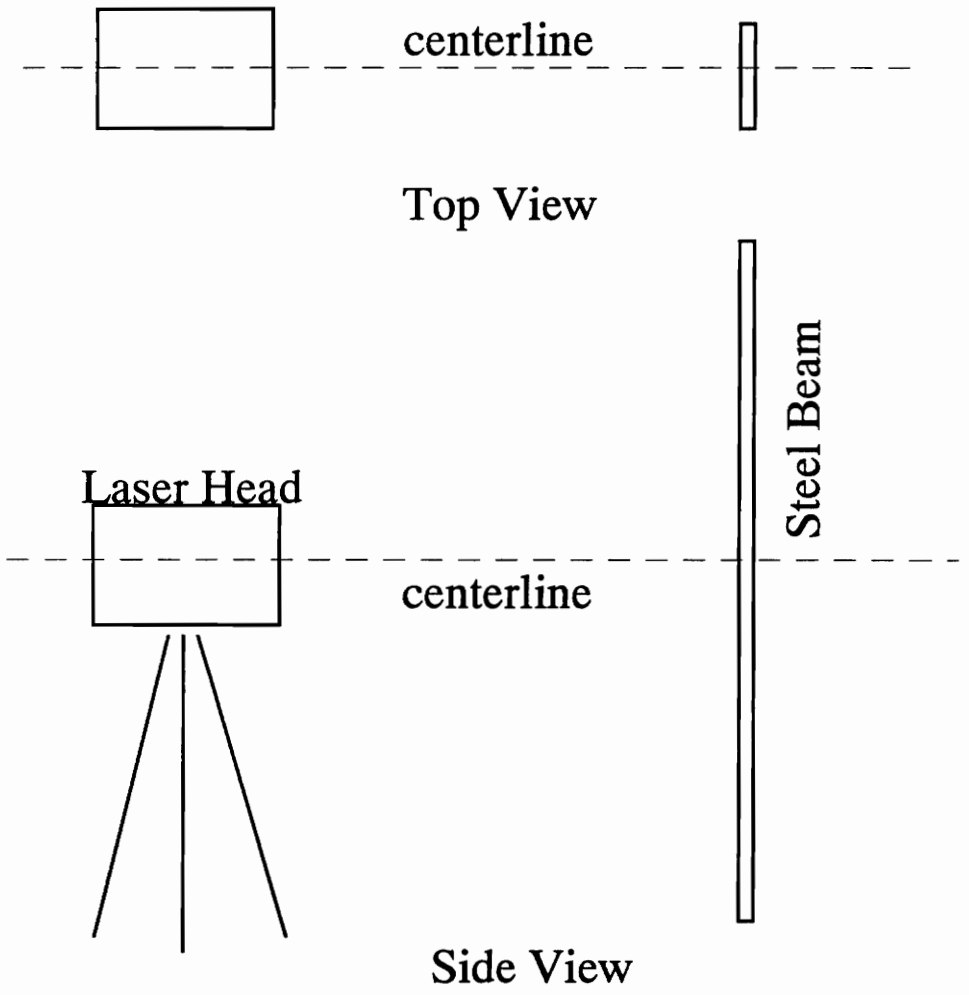

Figure 6: Approximate Orientation of SLV and Subject

employed by the GCI are described in section 2.2.1 and the referenced literature. As described, the GCI fit a sinusoid of the frequency at which the structure was shaking to the force transducer response. The real and imaginary response of the force transducer were estimated, and the real and imaginary components of the response were calculated relative to the input . The imaginary component of the force signal was eliminated by multiplying the complex representation of the force signal by its complex conjugate. An equal scaling factor was applied to the complex representation of the velocity response so to maintain the phase relationship between the force and velocity signals. The final output of the GCI was, therefore, a complex representation of the velocity and a real representation of the input force for each measurement location at each frequency. Additionally, the GCI output a standard deviation of the error between the analytical model of the response and the measured data.

3.1.2.2.3 Filtering

Velocity signals contained high frequency content that was eliminated through the use of an eight pole butterworth low pass filter in a Frequency Devices model 9016 filter. The force signal was also filtered in order to eliminate the effects of the filter on the frequency response function. Additionally, the gain of the filter was varied in order to maintain the signal amplitude since the analog to digital converter dynamic range was fixed during testing. The effects of all gains were accounted for in post-processing of the data.

3.1.2.3 Accelerometer Measurements

Five measurements of the frequency response function at the driving point were made with the accelerometer. These five measurements varied by the time in which they were made, the input used, and the frequency measured. The chart below indicates how the measurements differed.

Test #	Time	Input Force	Frequency Span
1	Before SLV Test	Periodic Chirp	5-205 Hz
2	After SLV Test	Periodic Chirp	5-205 Hz
3	After SLV Test	Periodic Chirp	0-200 Hz
4	After SLV Test	Burst Chirp	5-205 Hz
5	After SLV Test	Burst Random	0-200 Hz

3.1.2.3.1 Input Forces

Three input forces were used to measure the driving point FRF with an accelerometer: Periodic Chirp, Burst Chirp, and Burst Random. Each input is illustrated in figure 7. The Periodic Chirp produces a fast sine sweep across the frequency span in which frequency content exists only at frequencies that are measured. For example, if a Periodic Chirp from 0-100 Hz were chosen and the spectrum analyzer acquired frequency response data at 0.5 Hz intervals, then the sine sweep would include only the frequencies

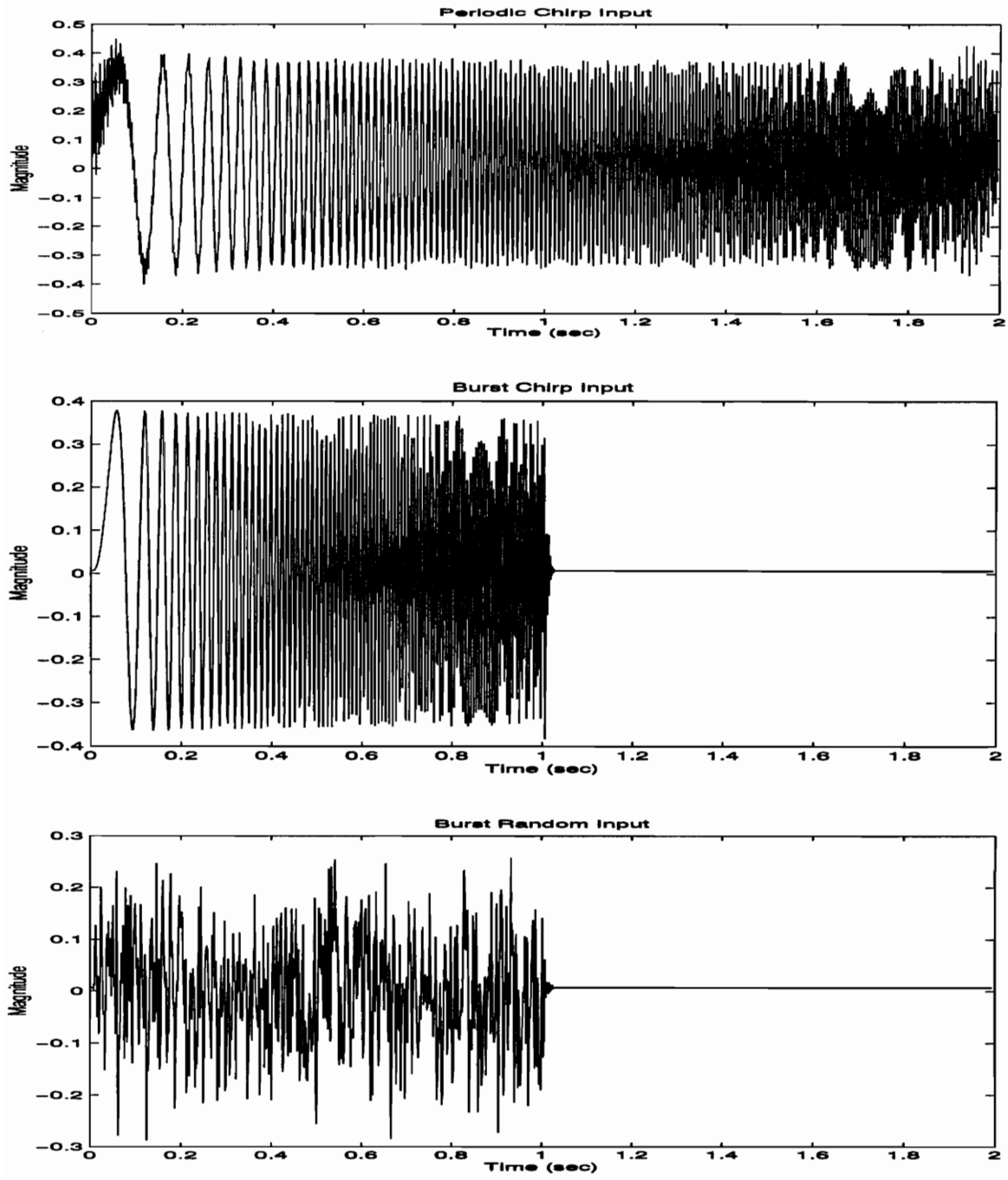

Figure 7: Periodic Chirp, Burst Chirp, and Burst Random Signals

0.5, 1.0, 1.5,...,99.0, 99.5, 100 Hz. Inputting frequencies only at the measured frequencies eliminates leakage from the response data.

Spectral leakage is the result of content in the time signal that is not periodic within the time block when the signal is being sampled. A signal whose magnitude is different at the end and beginning of a time block is not periodic in the time block. The greater the difference between the beginning and end conditions, the greater the amount of leakage in the Fourier transform of that signal.

The result of leakage is an apparent increase in the amount of damping in an FRF. Figure 8 shows an example of the Fourier transform of a non-periodic signal and a periodic signal, where both signals are of the same amplitude in the time domain. The Fourier transform of the non-periodic signal drops off slower than the periodic signal and the magnitude of the non-periodic signal is lower at its fundamental frequency. These factors combine to produce results with higher damping when modal parameters are estimated from an FRF corrupted with leakage. Minimizing leakage is always desirable when measuring frequency response functions.

A Burst Chirp is simply a Periodic Chirp with a period of zero force input after the input force has ceased. The system's response begins decaying after the force ceases and thus when the time block ends, the response will be approaching zero. With the final response measurement being close to zero, the effect of leakage due to a non-zero end condition in the response data helps to reduces leakage.

A Burst Random input, like a Burst Chirp, contains a period of force input followed by a period of inactivity. The reason for this pause in the input force is the same

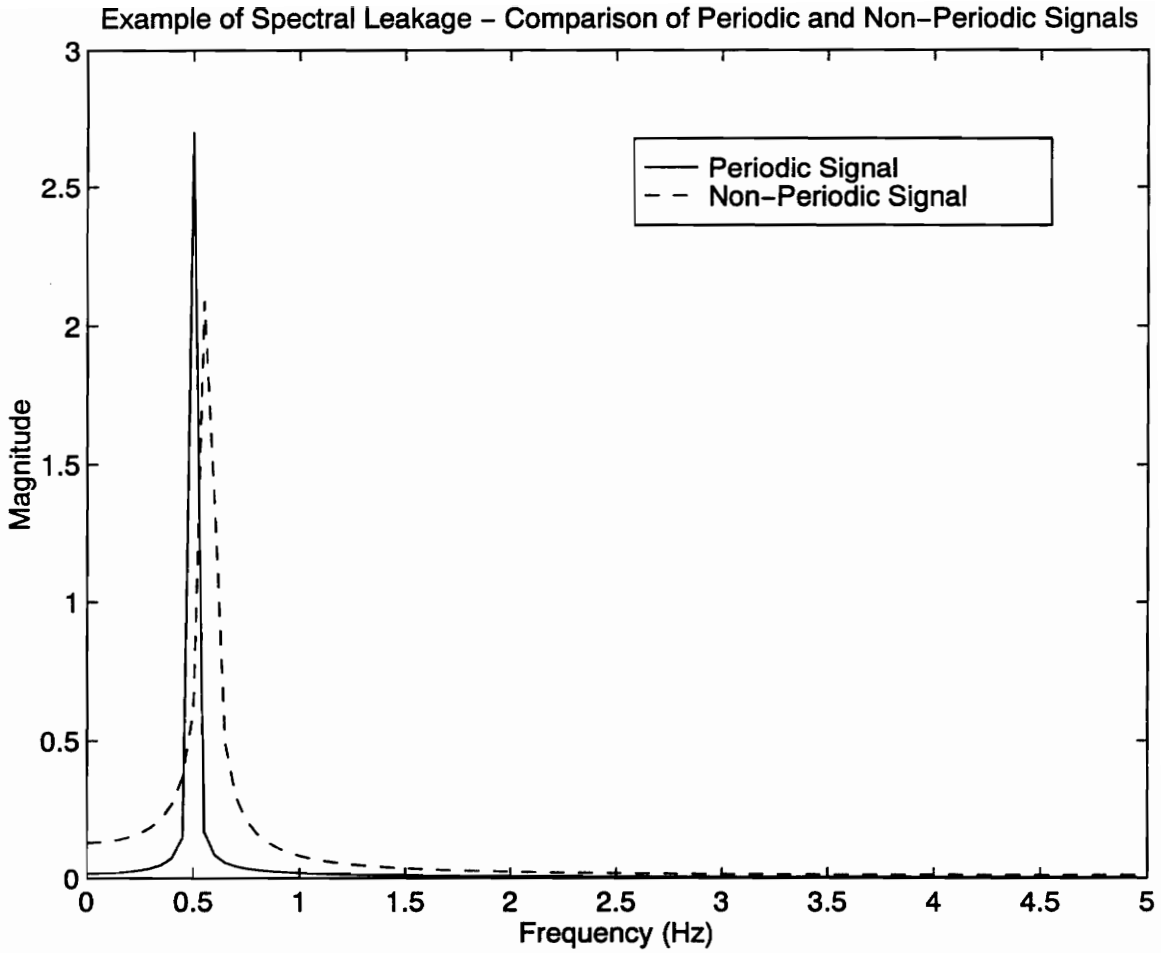

Figure 8: Example of Spectral Leakage

as that for a Burst Chirp, reduction of leakage. The difference between the two inputs is that the period of force input consists of a random force level and thus, the input frequencies are random. Random input frequencies mean that some of the frequency content of the input is not equal to the frequencies measured. This results in leakage that distorts the frequency response function.

3.1.2.3.2 Frequency Span

The frequency span varied during testing between 0-200 Hz and 5-205 Hz. The chirp inputs consisted of fast sine sweeps and this resulted in some troubles at low frequency. At very low frequency, shaking the beam resulted in high amplitude motions at the bottom end of the beam. Undesirably large oscillations are to be expected since the impedance of the beam is very high at low frequency. The unfortunate result of this high amplitude was that the beam tended to shake itself off the anti-sway foam. Preventing the input frequency from dropping below 5 Hz helped reduce this problem. The 0-200 Hz test with a Periodic Chirp input was performed after other 5-205 Hz tests in order to determine if the 0-5 Hz region could add significantly to the results.

3.1.2.3.3 Data Acquisition

Accelerometer based FRFs were measured using a HP 35665A spectrum analyzer. The analyzer provided the force inputs to the shaker during accelerometer testing. Windows were not used on the acquired data.

3.2. Data Analysis

Frequency response functions were measured from two sources, the scanning laser velocimeter (SLV) and an accelerometer. The SLV FRFs were measured at 472 locations but contained frequency information at only 31 frequencies. The five accelerometer FRFs were all measured at the driving point and consisted of the frequency response at 800 different frequencies. Since the accelerometer FRFs were measured at the driving point, all excited modes are included in this FRF.

The five accelerometer FRFs each were measured using a different procedure in order to test the effect of the measurement process on the final results of the curve fit. Each accelerometer FRF was curve fit in order to determine the locations of the poles present. These poles were then applied individually to the scanning laser FRFs to calculate the mode vectors at each location.

An accelerometer FRF was used to estimate the system's poles because of the quality and high frequency density of the accelerometer FRFs. Because of its wide dynamic range in comparison to the SLV, an accelerometer is better able to measure a wide frequency FRF with high quality results (high coherence). The many lines of resolution in an accelerometer FRF allows the problem of estimating poles from the FRF to be greatly overspecified so to improve the quality of the estimation.

3.2.1 Pre-Processing

Before curve fitting, experimental data had to be prepared so to account for test methods and formatting. Frequency response data obtained from the scanning laser were

processed into frequency response functions. Additionally, gain values that changed during testing were accounted for and velocity measurement errors due the angle between the laser beam and the steel beam were corrected. Accelerometer data was fully processed within the spectrum analyzer and only required format changes before being curve fitted.

3.2.1.1 Calculation of the Frequency Response Function

Output from the GCI consisted of the force magnitude and real and imaginary components of the velocity. In order to calculate the frequency response at a single location, the real and imaginary parts of the velocity magnitude were divided by the force signal magnitude. The result of this calculation were the real and imaginary parts of the frequency response at the point in consideration. This calculation was performed for all 472 locations in each of the 31 data sets.

The frequency response data was output from the GCI in groups organized according to frequency. Normally, frequency response functions are organized according to the location; i.e., the data set consists of the response of a single point at many frequencies. Since the curve fitter required FRFs to be organized according to location, the original 31 sets of 472 measurements were reorganized into 472 FRFs each consisting of 31 data points.

3.2.1.2 Gain Adjustments

During testing, as previously mentioned, filter gains were changed to make the velocity signal better fit the dynamic range of the A/D converter within the acquisition system. These changes were accounted for in post-processing by multiplying the frequency response functions by appropriate scaling values.

3.2.1.3 Laser Angles

As described in Section 2.3, the scanning laser measures velocity only along the line of the laser beam. This means that the true velocity is measured by the laser only when there is no angle between a vector defined by the motion of the point being measured on the structure and the laser beam. When the vector of motion is perpendicular to the laser beam, none of the true velocity is measured.

The vectors of motion of the points on the surface of the steel beam were assumed normal to the surface of the beam. The laser source remained fixed while the beam was aimed with mirrors towards points all over the surface of the beam. The laser beam, therefore, was measuring the surface velocity of the beam at an angle at every point on the beam except that point directly in front of the laser. The angle between the velocity vector and the laser beam was at its greatest extreme when the laser was pointed at the end of the long edge of the beam. This condition is illustrated in figure 9.

Accounting for the errors imposed by laser angles was reasonably simple since the laser source was aligned with the beam and the angles of the laser beam were stored in

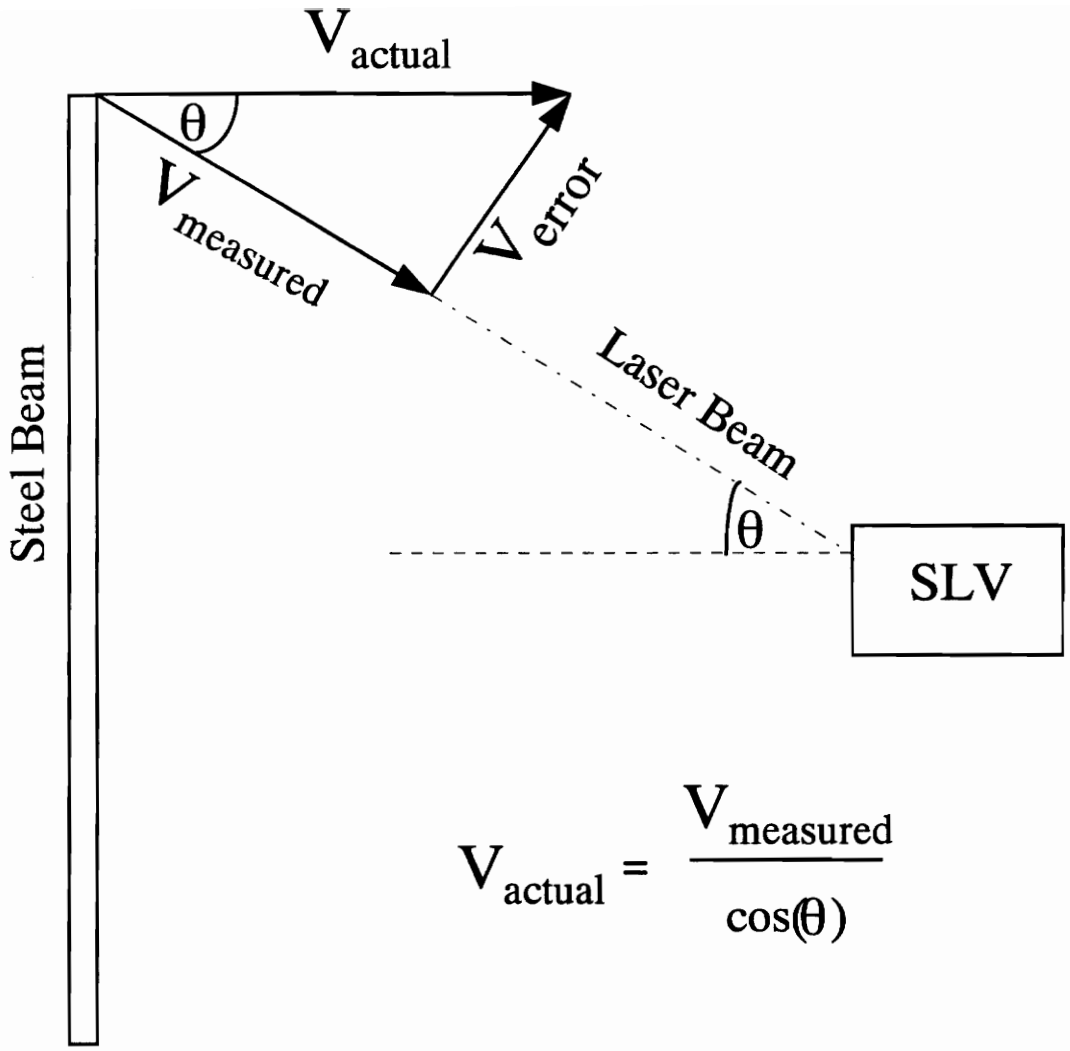

Figure 9: Laser Measurement Errors

the data acquisition system. The equation of the actual velocity from the measurement angle and the measured velocity is simply the geometric relationship

$$V_{actual} = \frac{V_{measured}}{\cos(\theta)} \qquad (3.2.1.3.1)$$

where θ is the angle between the velocity vector and the laser beam.

The short edge of the beam was 3 inches long and the laser was approximately 140 inches from the beam. The laser angle required to reach each end of this edge was approximately 1.2 degrees. The cosine of 1.2 degrees is 0.99978 which changes the measured velocity by 0.02%. Additionally, this would be the maximum error imposed by measuring in this direction. Since the measured and actual velocities differed by such an insignificant amount, measurement errors were not accounted for in this direction. Only measurements along the long edge of the beam were adjusted for angle errors. Errors along the long edge of the beam were still small, being at most 1.9% errant.

3.2.1.4 Laser Phase Correction

Signal processing within the laser unit takes a finite amount of time and so produces a time lag of the velocity response of the laser relative to the input force. In the measured frequency response data, this time lag produces a phase deviation that grows with increasing response frequency. A measurement of the laser frequency response relative to an accelerometer's response was measured to determine the severity of the laser lag. A plot of the frequency response of the laser relative to a PCB 307A accelerometer (S/N 996) is shown in figure 10.

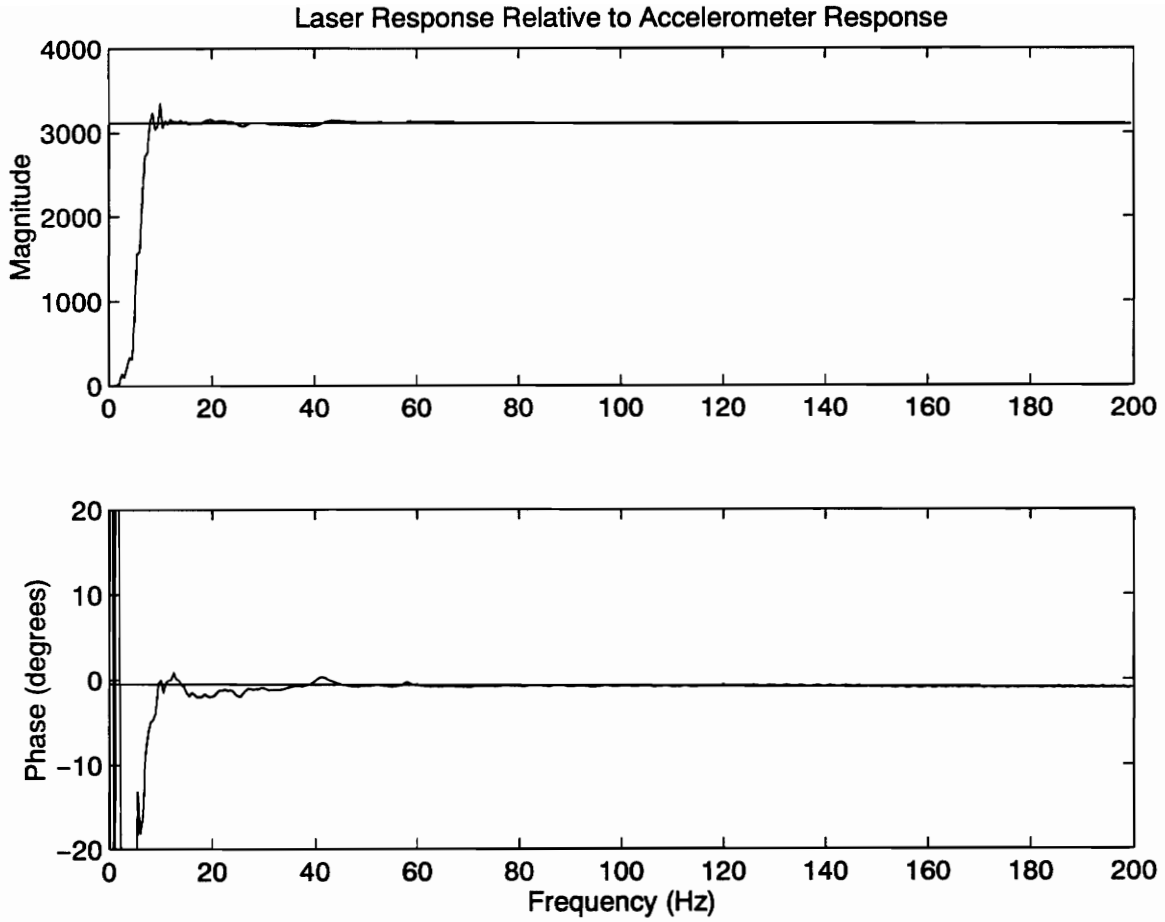

Figure 10: Laser Frequency Response Relative to an Accelerometer (measured and analytical)

Using a least squares approach, a first order response was fit to the measured FRF data from 100 Hz to 200 Hz. Lower frequency data was of low quality (low coherence) and was not included in the fit. The fit equation was of the form

$$\frac{V}{A} = a_1 j\omega + a_2 \qquad (3.2.1.4)$$

with the resulting coefficient values being a_1=-0.0214+0.01477j and a_2=3116.453-26.994j. The fit of equation 3.2.1.4 to the actual data is shown in figure 10.

Multiplying the laser frequency response data by the inverse of equation 3.2.1.4 eliminated the phase lag imposed by the laser. The multiplying factors were also scaled to unity so to affect only the phase of the frequency response data.

3.2.2 Parameter Estimation

A Matlab-based, parameter-estimation algorithm named "Modhan" was used to analyze the frequency response data. The program had been modified by its co-creator, Julien Maillard, to allow fixed pole and traditional analyses of the data as described in sections 2.2.1 and 2.2.2, respectively. Format changes were required on both scanning laser FRFs and accelerometer FRFs in order to load the data into the estimation program.

3.2.2.1 Pole Identification - Accelerometer Data

Poles were determined by curve fitting the accelerometer based FRFs. Five FRFs were acquired and the poles of each was individually determined with the curve fitting using the Rational Polynomial algorithm. Coherence plots were included with each FRF,

so data points with a coherence of less than 0.95 were not used in the parameter estimation. Eliminating low coherence data allows the curve fitting program to fit only high quality data, thereby eliminating any bias in the estimation that may be a result of fitting data that is corrupted with noise.

3.2.2.2 Residue Estimation - Laser Data

Scanning laser data was analyzed six times as described:

1. Fixed-poles algorithm using poles from accelerometer FRF #1
2. Fixed-poles algorithm using poles from accelerometer FRF #2
3. Fixed-poles algorithm using poles from accelerometer FRF #3
4. Fixed-poles algorithm using poles from accelerometer FRF #4
5. Fixed-poles algorithm using poles from accelerometer FRF #5
6. Global parameter estimation approach using only SLV data.

The first five of these analyses were exactly the same except for the numerical values of the poles used, so these are described as a whole in section 3.2.2.2.1. The sixth analysis was an analysis of the data using the global parameter estimation algorithm as described in section 3.2.2.2.2.

3.2.2.2.1 Fixed-poles Algorithm

Five sets of poles were determined each from a different accelerometer FRF. Using each set of poles, residues were fit across the entire 200 Hz frequency band to each of the 472 SLV FRFs using the fixed-poles option in the parameter estimation program.

The process of estimating residues given pole locations involves solving equation 2.2.1.1.11 as described in section 2.2.1.1.

3.2.2.2.2 Global Parameter Estimation Algorithm

When the global parameter estimation algorithm (section 2.2.2) is applied to fit poles and residues simultaneously to the laser data, an iterative procedure develops where the computer continuously changes its pole and mode vector estimates until an error criterion is met or the end of iterations is reached.

Initial values of the poles were input into the estimation program to help minimize computation time by reducing the number of iterations required to find a solution. Initial pole values were determined by first estimating the poles present in a small set of laser FRFs. Afterward, the entire set of 472 FRFs were used to fit poles and residues across the entire frequency span.

3.2.2.3 Varying Frequency Locations

It would be of interest to the experimentalist to know at which frequencies to acquire data with the SLV when using the fixed-poles method. Beam response data was acquired at 31 frequencies over a range from 0 to 200 Hz. In general, of course, the frequencies should be spaced out to span the entire region of interest. Covering the entire span assures content from all modes so that all modes appear in at least some data at a level that is well above the noise floor. Knowing that the entire frequency range should

be spanned, the question then becomes whether to measure at frequencies near resonance or frequencies away from resonance.

An experiment was performed with the beam response data to indicate the preferable location of measurement frequencies relative to resonances. The 31 data points were broken up into two sets of 18 data points. Some of the very low frequency data points (<12 Hz) were shared by the two sets since all very low frequency data points were significantly away from the rigid body mode at approx. 5 Hz. This was done to eliminate any bias resulting from the lack of proximity to the rigid body mode that the set of data with response near resonance would have had. Essentially, this should eliminate the rigid body mode from having any effect on the fit quality of the flexible modes in the two tests.

The two sets of 472 FRFs with 18 data points each were analyzed using Modhan. The fixed-poles used came from the fourth accelerometer test (Burst Chirp) and the residues were calculated. Figure 11 shows the location of the near resonance frequencies and off resonance frequencies used in each analysis.

3.2.3 Post-Processing

The residues output from the curve fitting software were modified in two ways after curve fitting. First, mode vectors were calculated from the mode vectors. Secondly, the real part of the residues were eliminated.

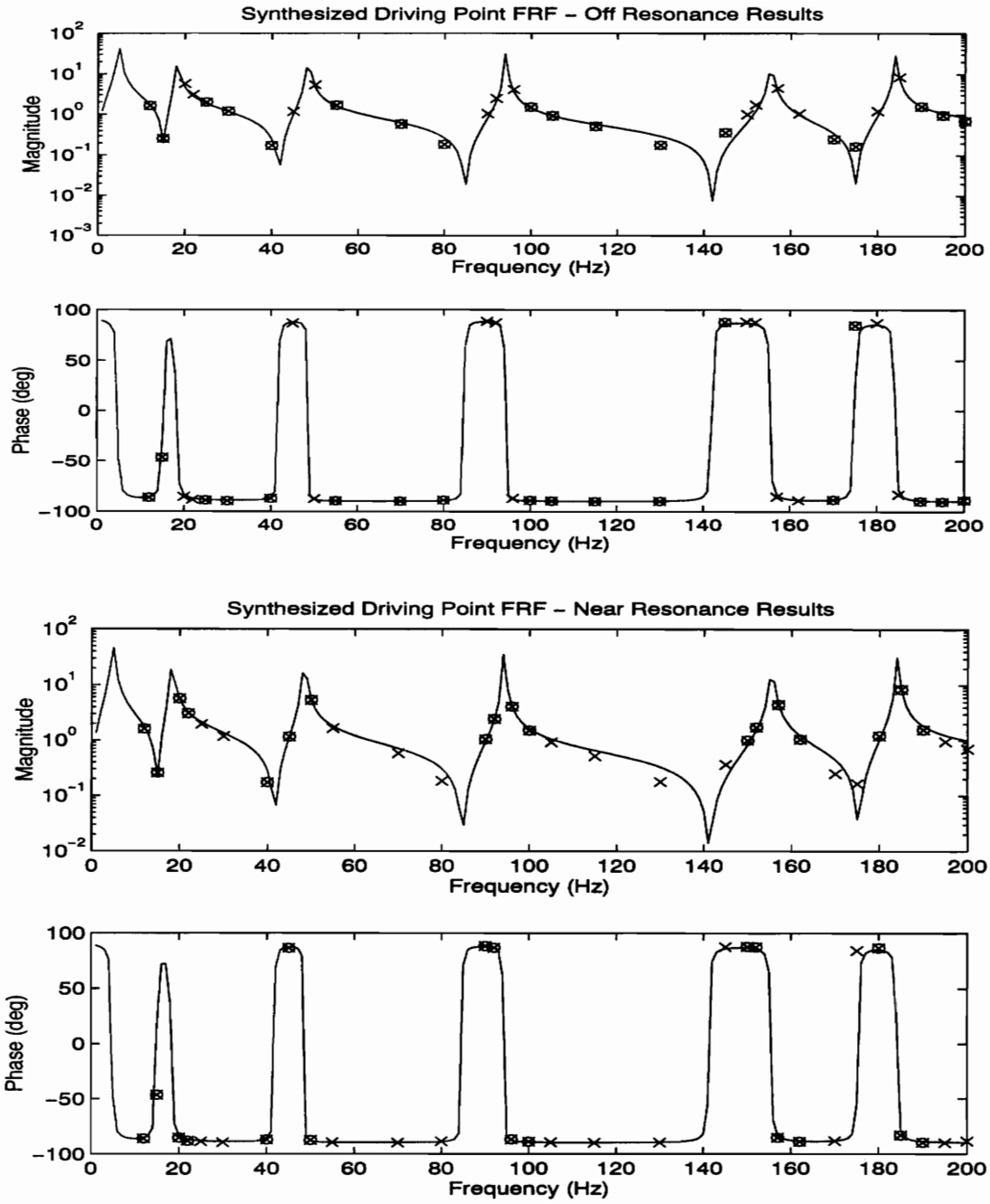

Figure 11: Off Resonance (top) and Near Resonance (bottom) Measurement Frequencies
x - Laser Measurement Frequency
o - Measurement Frequency Used in the Analysis

3.2.3.1 Calculation of Mode Vectors

Residues are the product of mode vectors and other variables as defined in equation 2.1.4.15. The output of Modhan is a residue for each mode at every measurement location and the natural frequencies and damping values for each mode. Individual mode vectors for each mode were calculated by dividing every residue by the square root of the driving point residue for that mode, which results in a mode vector scaled by the modal mass.

As an example of calculating mode vectors from residues, where the driving point is location 1, the driving point residue for mode 3 is defined as

$$ {}_3A_{11} = \frac{{}_3\phi_1 \, {}_3\phi_1}{2jm_3\omega_3\sqrt{1-\xi_3^2}} = \frac{{}_3\phi_1}{\sqrt{2jm_3\omega_3\sqrt{1-\xi_3^2}}} \cdot \frac{{}_3\phi_1}{\sqrt{2jm_3\omega_3\sqrt{1-\xi_3^2}}}. \quad (3.2.3.1.1) $$

The residue at a location m for mode 3 is

$$ {}_3A_{m1} = \frac{{}_3\phi_m \, {}_3\phi_1}{2jm_3\omega_3\sqrt{1-\xi_3^2}}. \quad (3.2.3.1.2) $$

Dividing equation 3.2.3.1.2 by the square root of equation 3.2.3.1.1 cancels the driving point mode vector, ${}_3\phi_1$, from equation 3.2.3.1.2 and results in a scaled mode vector at location m

$$ {}_3A_{m1} \Big/ {}_3A_{11} = \frac{{}_3\phi_m}{\sqrt{2jm_3\omega_3\sqrt{1-\xi_3^2}}} \quad (3.2.3.1.3). $$

A mode vector at each point on the structure for each mode was calculated in the same manner as illustrated in the example. The mode vectors were used to calculate the modal assurance criterion (MAC) tables shown in chapter 4.

3.2.3.2 Residue Modification

A problem arose when FRFs were simulated using the residues output from Modhan. When an FRF was simulated using the unmodified residues and plotted as magnitude and phase (figure 12), the magnitude of the fit was excellent but the phase showed significant difference between real and analytical data. Especially near anti-resonance, the phase difference between analytical and actual data was disturbing. The problem was partly solved by eliminating the real part of the residues.

The cause of some of the errors between actual and analytical data can be traced to small errors in the curve fitting process. The phase of an FRF at any frequency is the inverse tangent of the ratio of the imaginary and real parts of the FRF at that frequency. Near anti-resonance, the magnitude of the FRF is very small, and in most cases, the real and imaginary contributions from each mode are very small. In order to obtain a good fit, the very small complex numbers from each mode must sum together in a very precise way. If, for instance, one residue was estimated to be larger than it should be, then that mode will have too great an influence. Near anti-resonance, that small error in calculating the residue can have enough effect to switch the sign of the real or imaginary part of the FRF when the contributions of all modes are summed. Of course, changing the sign in one of the terms in a ratio has a great effect on the inverse tangent of that ratio, especially when plotted.

The assumption of normal modes is typically used to help eliminate phase problems. Making the normal mode assumption forces the mode vectors for each mode

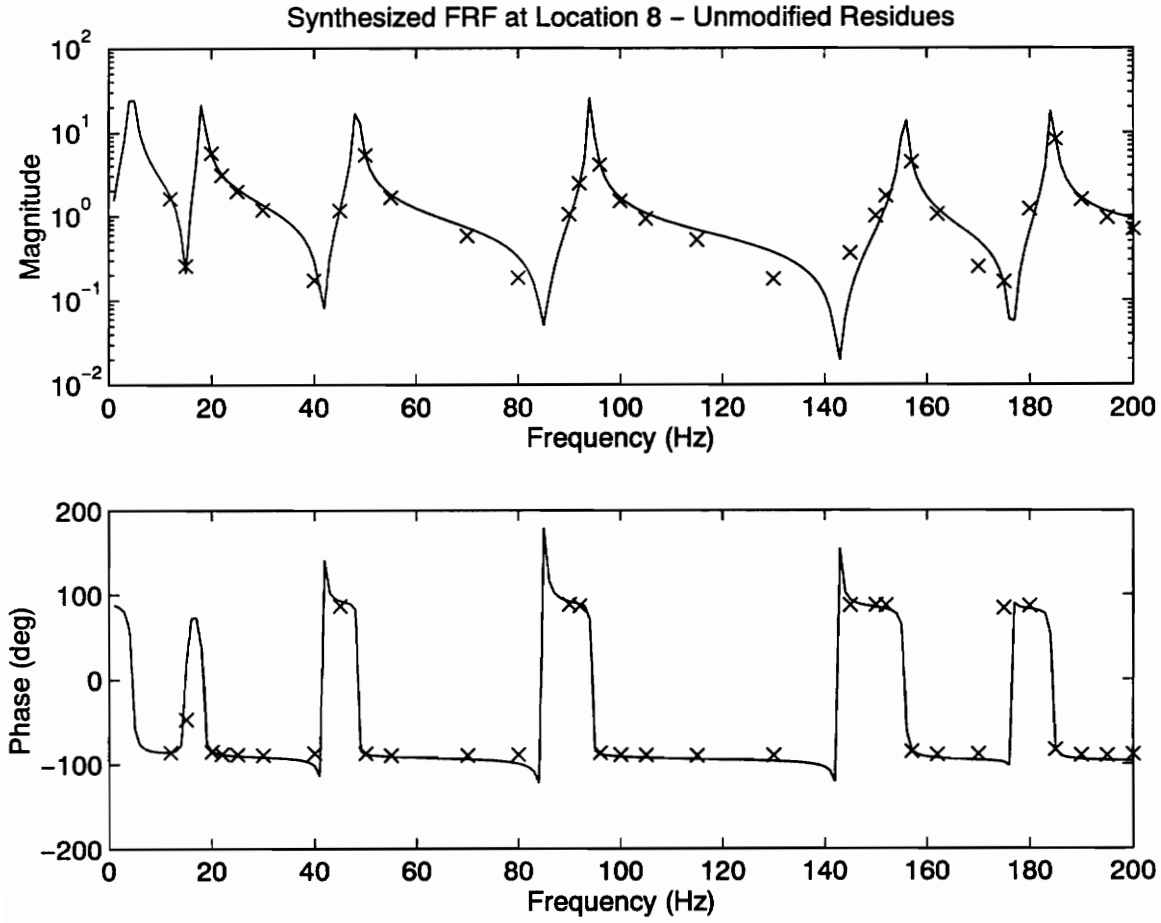

Figure 12: Synthesized FRF Calculated Using Unmodified Residues

of a system, when plotted on a real vs. imaginary plot, to all form a line. The estimated mode vectors for the beam created a "thick" line where the thickness was formed by the distribution of points that did not lie exactly on the line. This thick line indicated that the distribution of points around the line was caused by slight curve fitting errors. It would be desirable to reduce the thickness of the line so to eliminate the distribution that, by the normal mode assumption, should not be present.

The residues are simply the mode vectors multiplied by the driving point mode vector and should also, by the normal mode assumption, form a line. The complex residues were dominated by the imaginary components and, as shown in figure 13, formed a "thick" line along the imaginary axis. Since the real parts of the residues could not be eliminated by rotating all the residues, the real part was essentially eliminated by scaling it by a factor of 0.001. Recalculating the mode vectors from the modified residues and plotting the mode vectors shows that the mode vectors form a much less distributed (thinner) line, as shown in figure 14. Reducing the real part of the residues, therefore, had the effect of rotating the mode vectors so the modes are normal.

The final effect of reducing the magnitude of the real part of the residues is to improve the agreement of the actual and analytical results when shown as magnitude and phase as in figure 15. As illustrated in figures 16 and 17, when real and imaginary plots are used, the agreement between actual and analytical results is good even without removing the real part of the residues. This illustrates how the disagreement between the sets of results is greatly magnified by plotting the phase of the data.

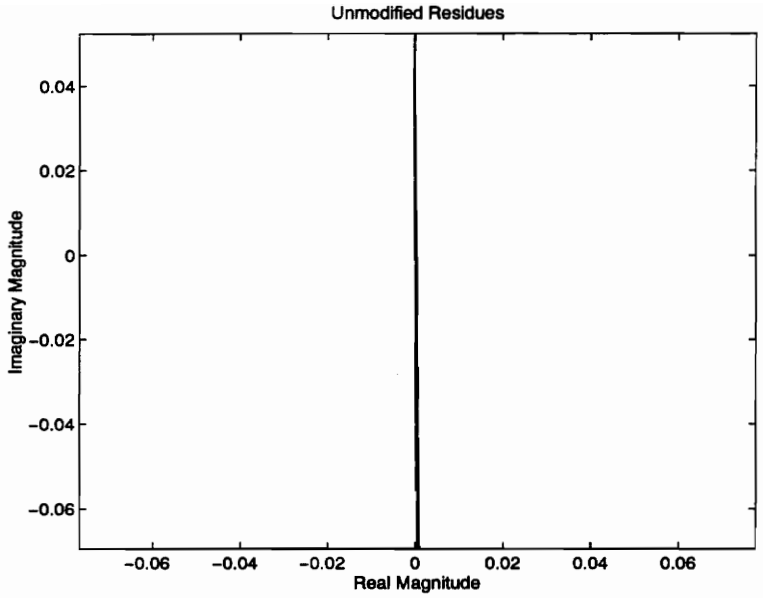

Figure 13: Unmodified Residues Showing Dispersion Around the Imaginary Axis

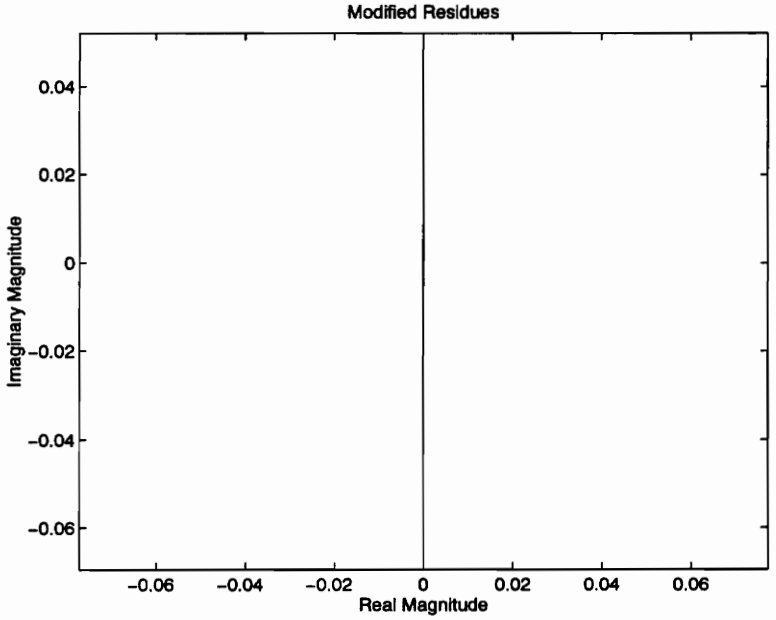

Figure 14: Modified Residues Showing Lack of Dispersion Around Imaginary Axis

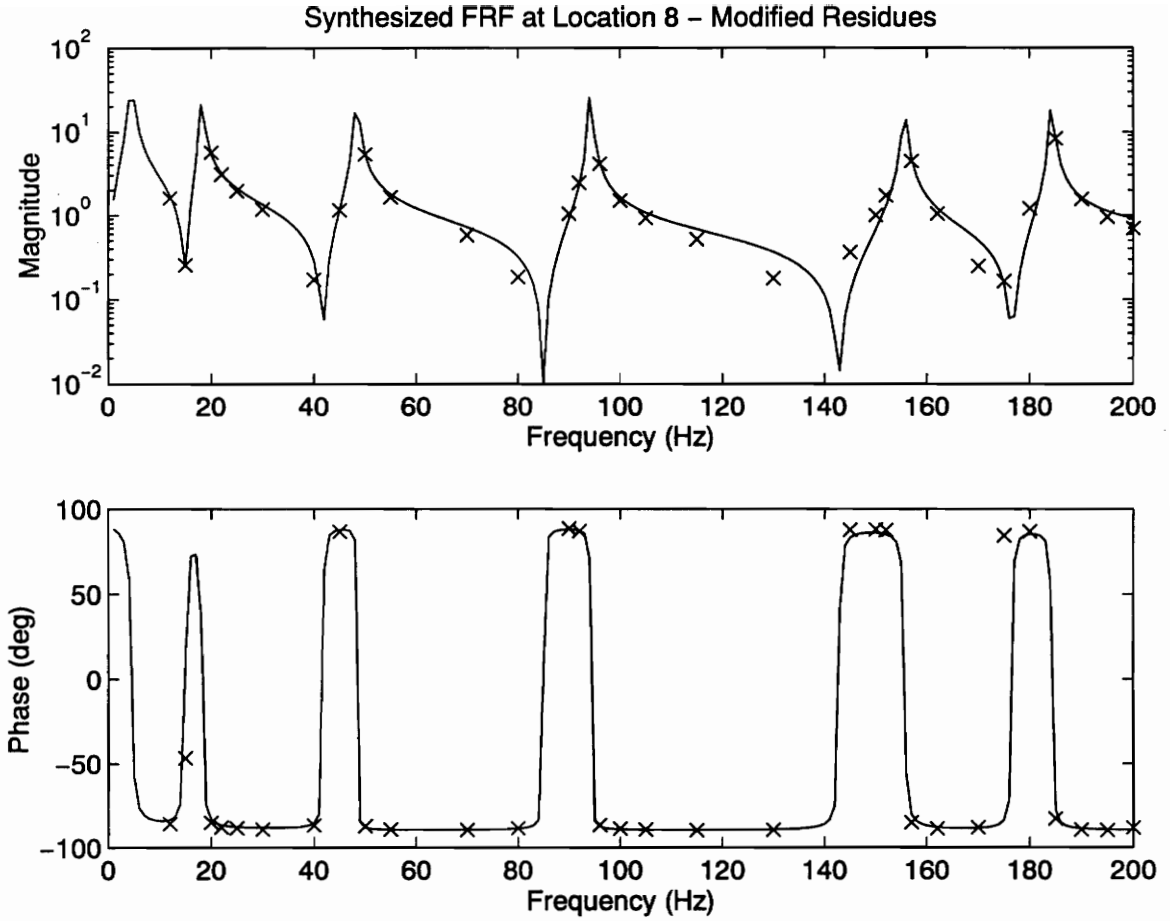

Figure 15: Synthesized FRF Calculated Using Modified Residues

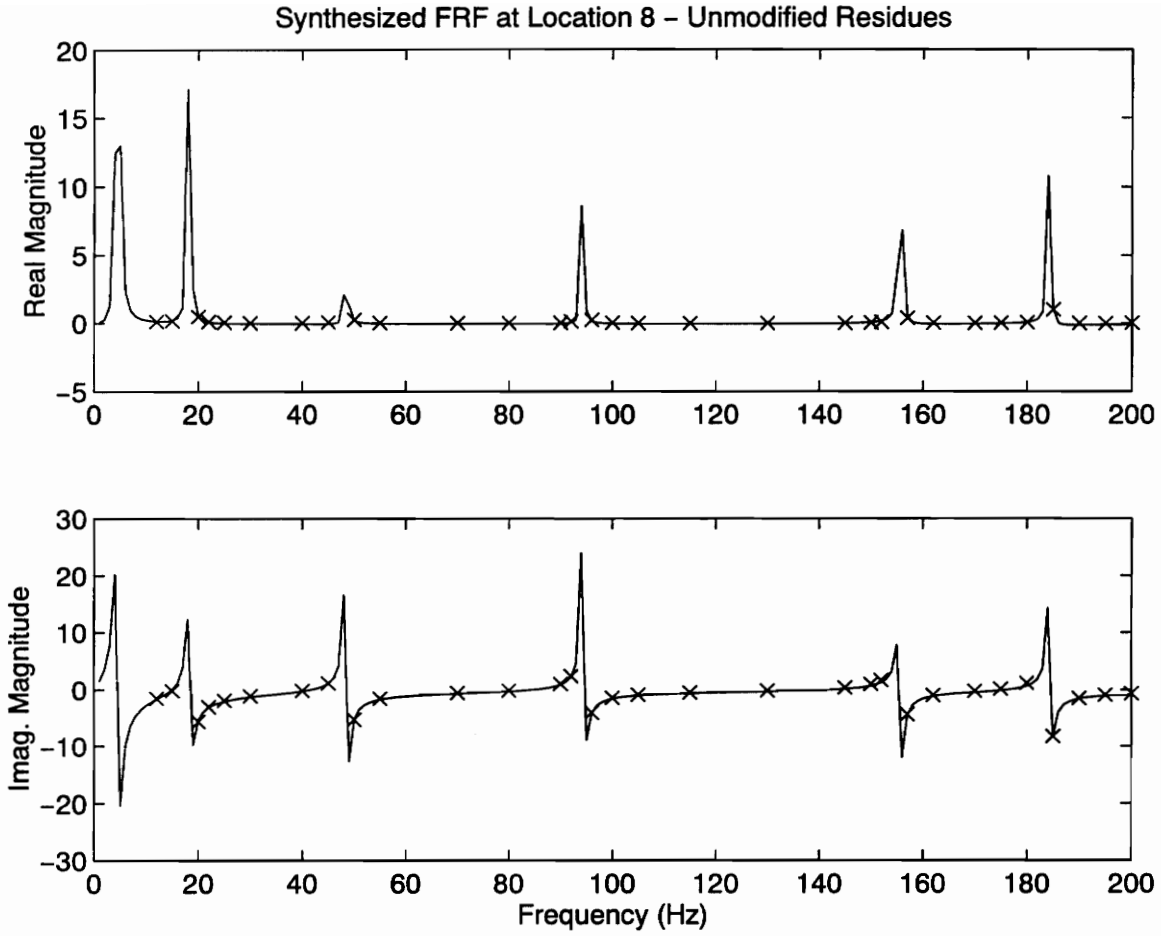

Figure 16: Synthesized FRF Calculated Using Unmodified Residues

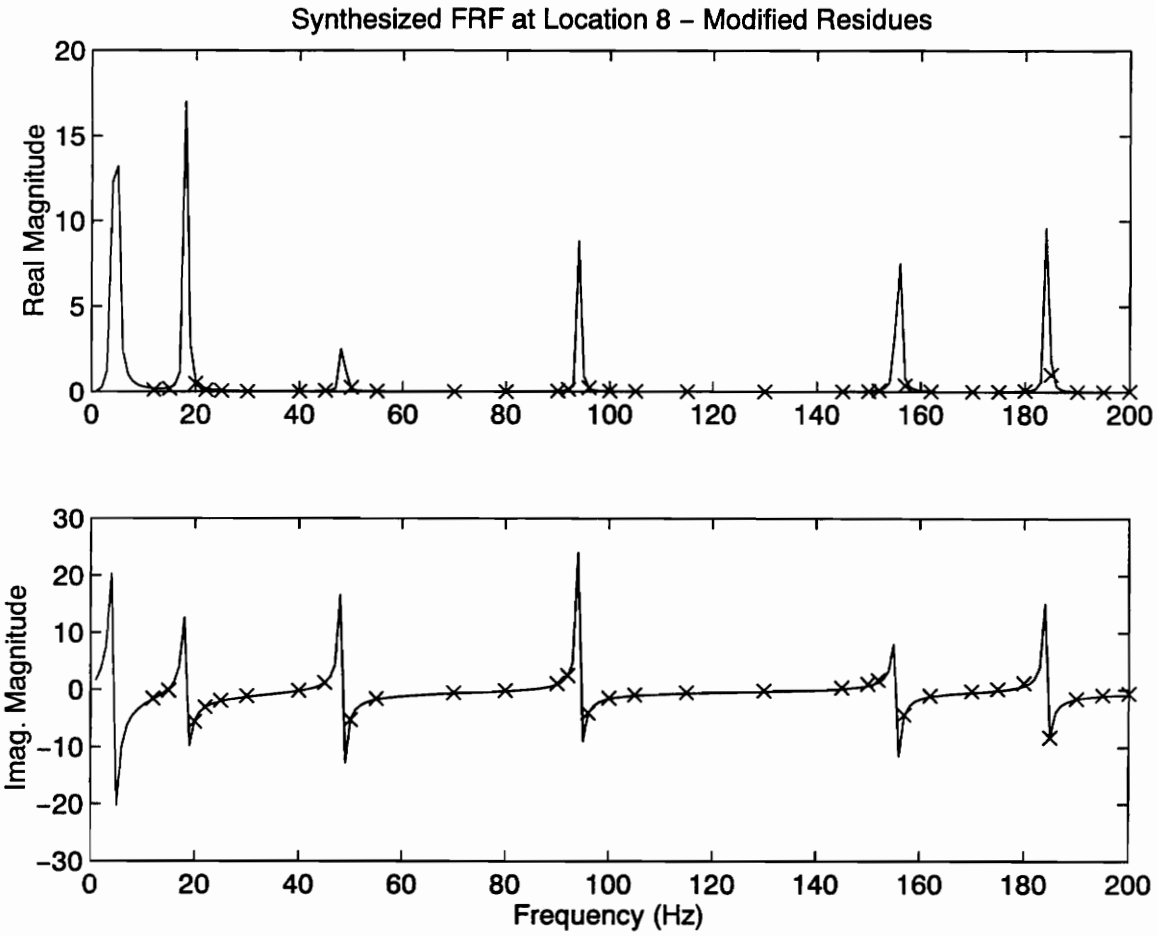

Figure 17: Synthesized FRF Calculated Using Modified Residues

Chapter Four

Results

The accuracy of modal parameter estimates can be determined in several ways. Often, the mode shapes of a structure are intuitively known from the basic geometry of the structure. In this case, the bending and torsional modes of a beam are familiar, and estimated mode shapes must agree with the intuitively known beam modes. Additionally, measured data can be used as a comparison to analytical results. With the modes of a structure known, the measured FRFs can be synthesized. Comparison of actual to analytical results indicates the quality of the parameter estimates. Finally, in this case where a beam is the subject, the orthogonality of the mode shapes of a beam can be used to determine if modes are fully decoupled from each other. With these three tools, analytical results can be compared to intuition and measured data to indicate the quality of the estimation.

4.1 Definitions

Synthesized FRFs and modal assurance criterion (MAC) tables are defined in the following sections. Both synthesized FRFs and MAC tables are included as results.

4.1.1. Synthesized FRFs

Synthesized FRFs are obtained by calculating a frequency response function from the poles and residues that the parameter estimator outputs. FRFs as functions of poles and residues are given in section 2.1.4. The synthesized FRF is calculated for an FRF that was actually measured and the results are overlaid. A good fit will result in good agreement between the synthesized FRF and the actual FRF.

4.1.2. Modal Assurance Criterion

Modal assurance criterion (MAC) tables indicate the degree of orthogonality between the sets of mode vectors. The mode vectors of a beam are orthogonal so that the following integral holds true (Rao 1990: 400)

$$\int_0^1 \Phi_i \Psi_j dx = 0. \qquad (4.1.2.1)$$

In the discrete case, the following relationship indicates the degree of orthogonality between two sets of mode vectors, where Φ and Ψ are sets of mode vectors,

$$MAC_{\Phi}^{\Psi} = \frac{\sum \Phi^* \Psi \sum \Phi \Psi^*}{\sum \Phi \Phi^* \sum \Psi \Psi^*} \qquad \begin{array}{l} = 1 \text{ when } \Phi = \Psi \\ = 0 \text{ when } \Phi \neq \Psi. \end{array}$$

A MAC table is formed by determining the MAC for every combination of modes, so for a system with N degrees of freedom, the MAC table with have N^2 entries. Since each combination will fit one of the possibilities, $\Phi = \Psi$ or $\Phi \neq \Psi$, every entry

in the MAC table should be zero or one. The degree to which the entries vary from zero indicates the degree to which the mode shapes lack orthogonality. A MAC table with non-unity entries that vary a great deal from zero indicate poor parameter estimation quality.

4.2 Mode Shapes

The estimated mode shapes of the test beam are shown along with theoretical mode shapes from Euler beam theory (Rao 1990: 398) in figures 18-23. Only the bending modes could be calculated from Euler beam theory, so theoretical mode shapes are shown only for the four bending modes. Results from a plate (two dimensional) theory would predict the torsional modes of the structure as well as the bending modes, but since the torsional mode is the highest experimentally determined mode of the subject, it is not invalid to compare the experimental bending modes to one dimensional theoretical results. No comparison is given between the torsional mode and theoretical predictions.

The first mode estimated from the measured data is a rigid body mode. The presence of the support constraints cause the beam to oscillate as a rigid body instead of translating or rotating continuously in one direction, as one would expect from a true (0 Hz) rigid body mode. Some flexure is present in the estimate of the rigid body mode, as shown in figure 18. The flexure is due to poor estimation quality resulting from a lack of measurement frequencies near the rigid body mode's natural frequency (approx. 5 Hz).

The mode shapes obtained using the pole estimates from any of the accelerometer driving point FRFs are visibly the same, so results from other estimations are not included. Additionally, the mode shapes obtained using the global estimation algorithm are not visibly different from those obtained using the fixed-poles algorithm. The MAC tables shown in sections 4.5 and 4.6 quantify the comparison of the mode shapes obtained from each analysis.

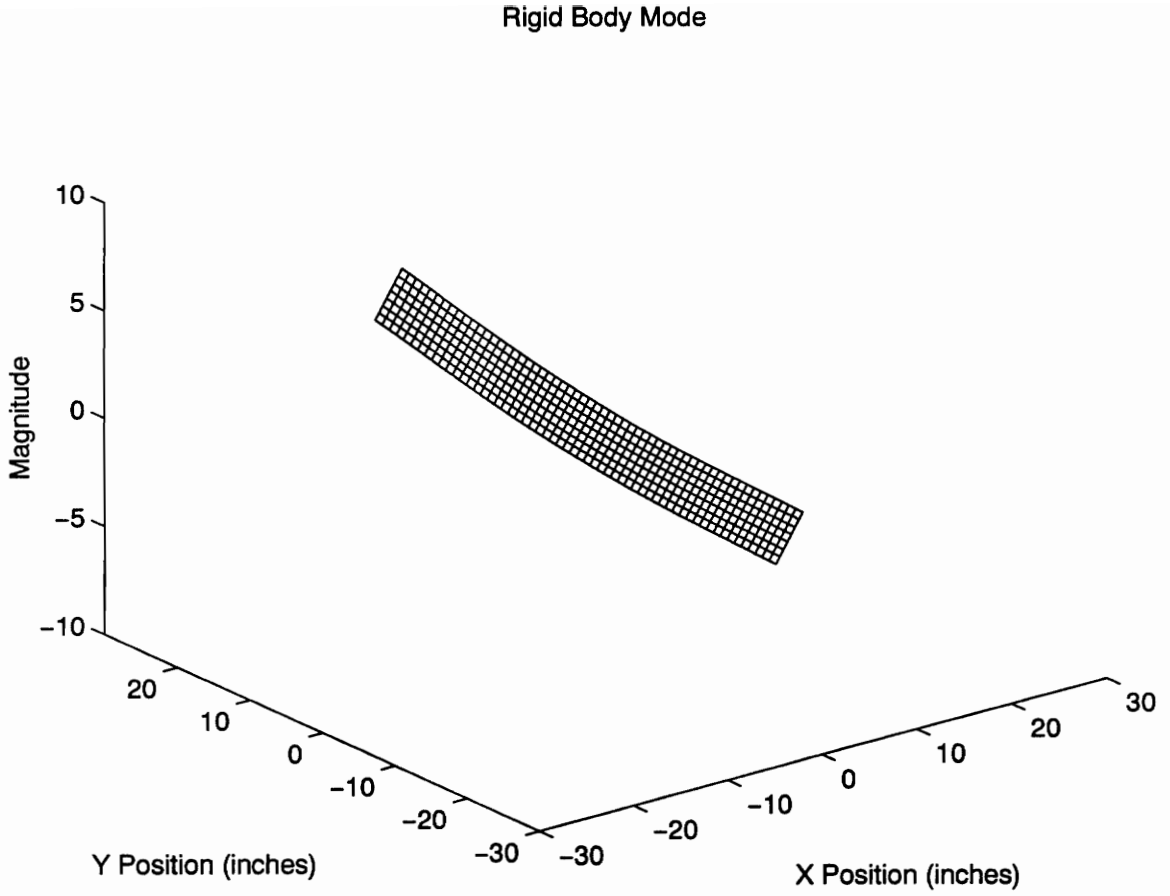

Figure 18: Rigid Body Mode

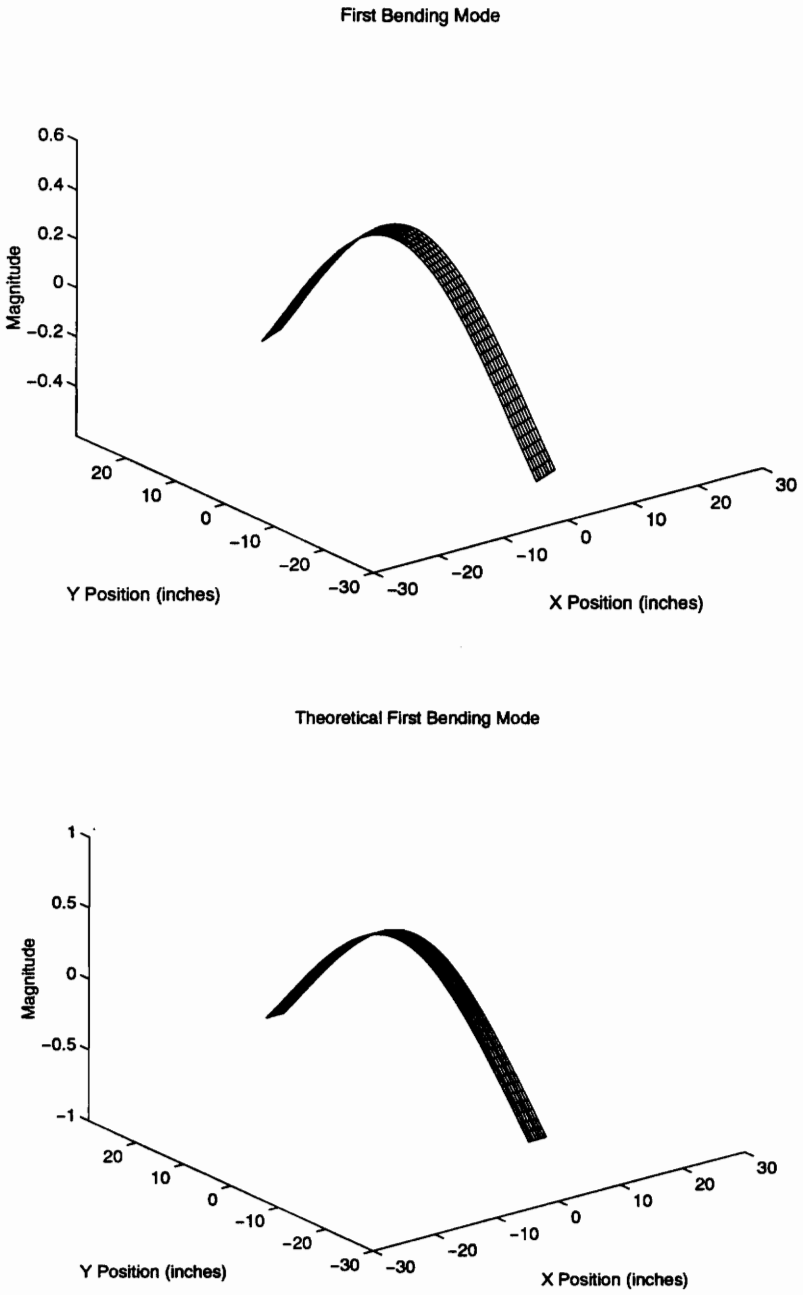

Figure 19: First Bending Mode - Experimental (Top) & Theoretical (Bottom)

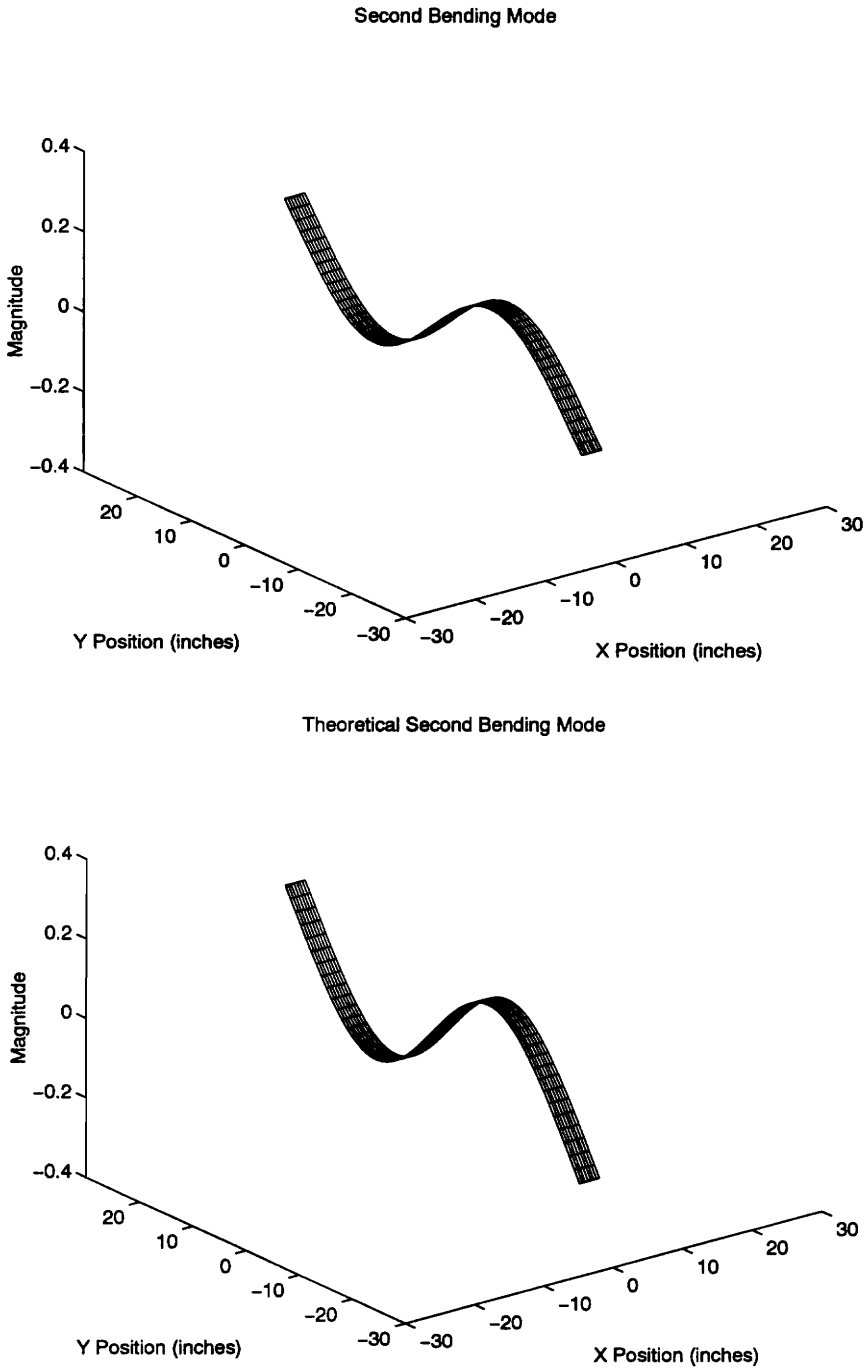

Figure 20: Second Bending Mode - Experimental (Top) & Theoretical (Bottom)

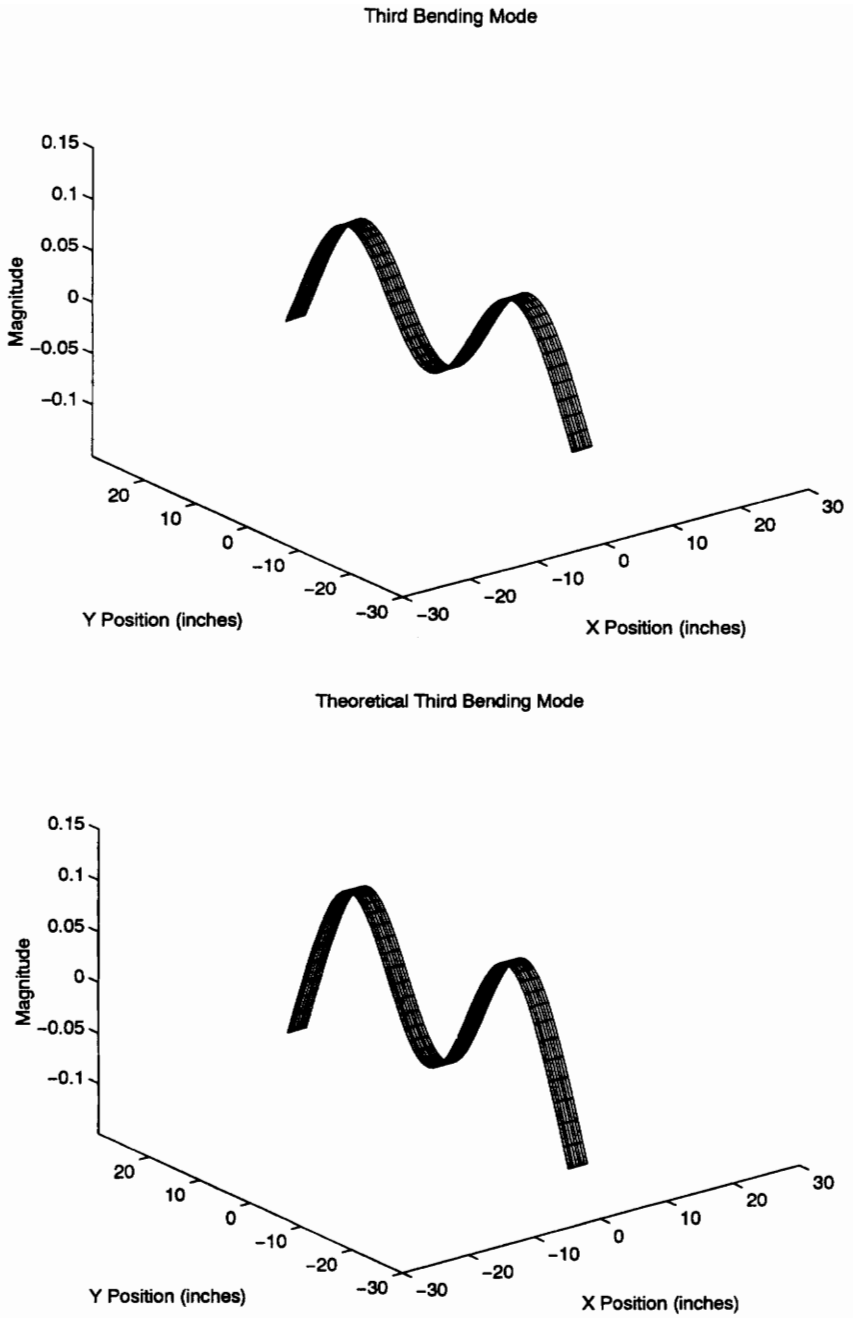

Figure 21: Third Bending Mode - Experimental (Top) & Theoretical (Bottom)

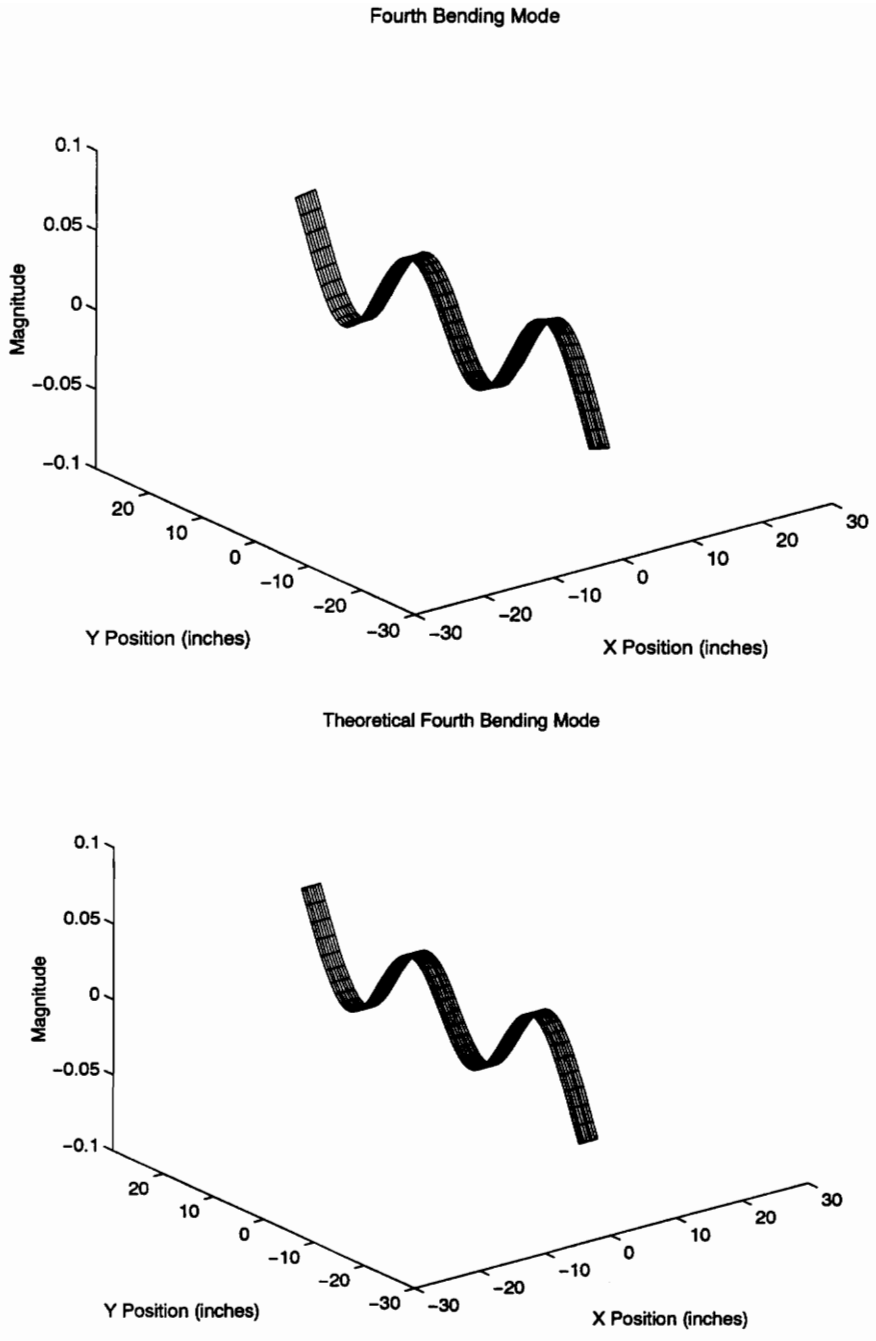

Figure 22: Fourth Bending Mode - Experimental (Top) & Theoretical (Bottom)

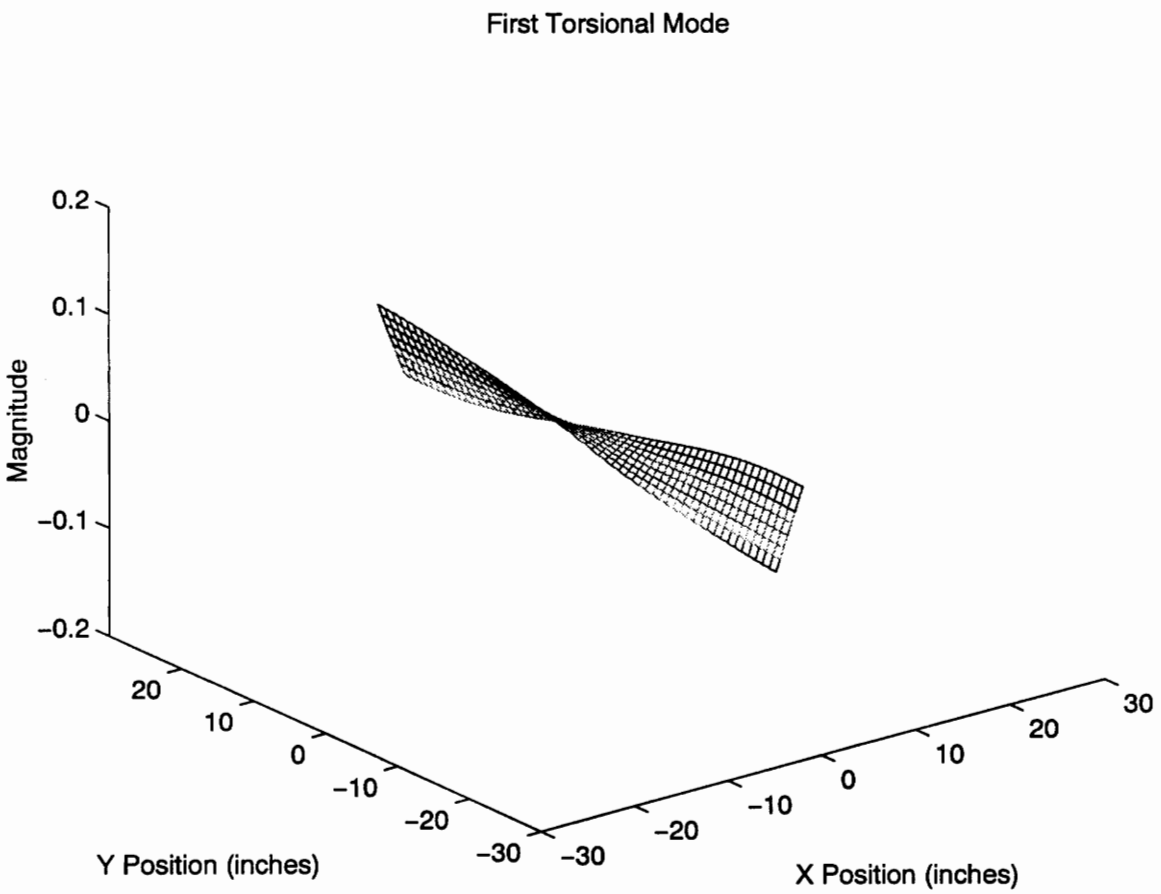

Figure 23: First Torsional Mode

4.3 Synthesized Driving Point FRFs

The five driving point FRFs measured with the accelerometer are shown in figures 24-28. FRFs synthesized from the estimated parameters are overlaid on the measured FRFs for comparison. The measured FRFs are shown as solid lines and the synthesized FRFs are shown as dashed lines.

Table 1 lists the natural frequencies and damping values for the poles estimated from each of the five driving point accelerometer FRFs and the pole values estimated in the global parameter estimation analysis.

Table 1: Natural Frequencies and Damping Estimates

	Rigid Body Mode		First Bending Mode		Second Bending Mode	
Pole FRF	freq (Hz)	damp. ratio	freq (Hz)	damping ratio	freq (Hz)	damp. ratio
1	4.45	0.0702	18.21	0.0137	48.40	0.0012
2	4.77	0.0418	18.24	0.0152	48.41	0.0015
3	5.58	0.0214	18.28	0.0177	48.41	0.0015
4	5.04	0.0927	18.37	0.0130	48.42	0.0015
5	4.72	0.0970	18.53	0.0088	48.43	0.0017
Global Estimation	4.11	0.0491	18.55	0.0084	48.51	0.0018

	Third Bending Mode		Fourth Bending Mode		First Torsional Mode	
Pole FRF	freq (Hz)	damp. ratio	freq (Hz)	damp. ratio	freq (Hz)	damp. ratio
1	94.24	0.0009	155.63	0.0016	184.27	0.0009
2	94.16	0.0009	155.46	0.0013	184.10	0.0011
3	94.16	0.0009	155.45	0.0014	184.10	0.0011
4	94.18	0.0013	155.45	0.0010	184.07	0.0011
5	94.15	0.0009	155.45	0.0013	184.08	0.0010
Global Estimation	94.22	0.0011	155.36	0.0009	183.99	0.0008

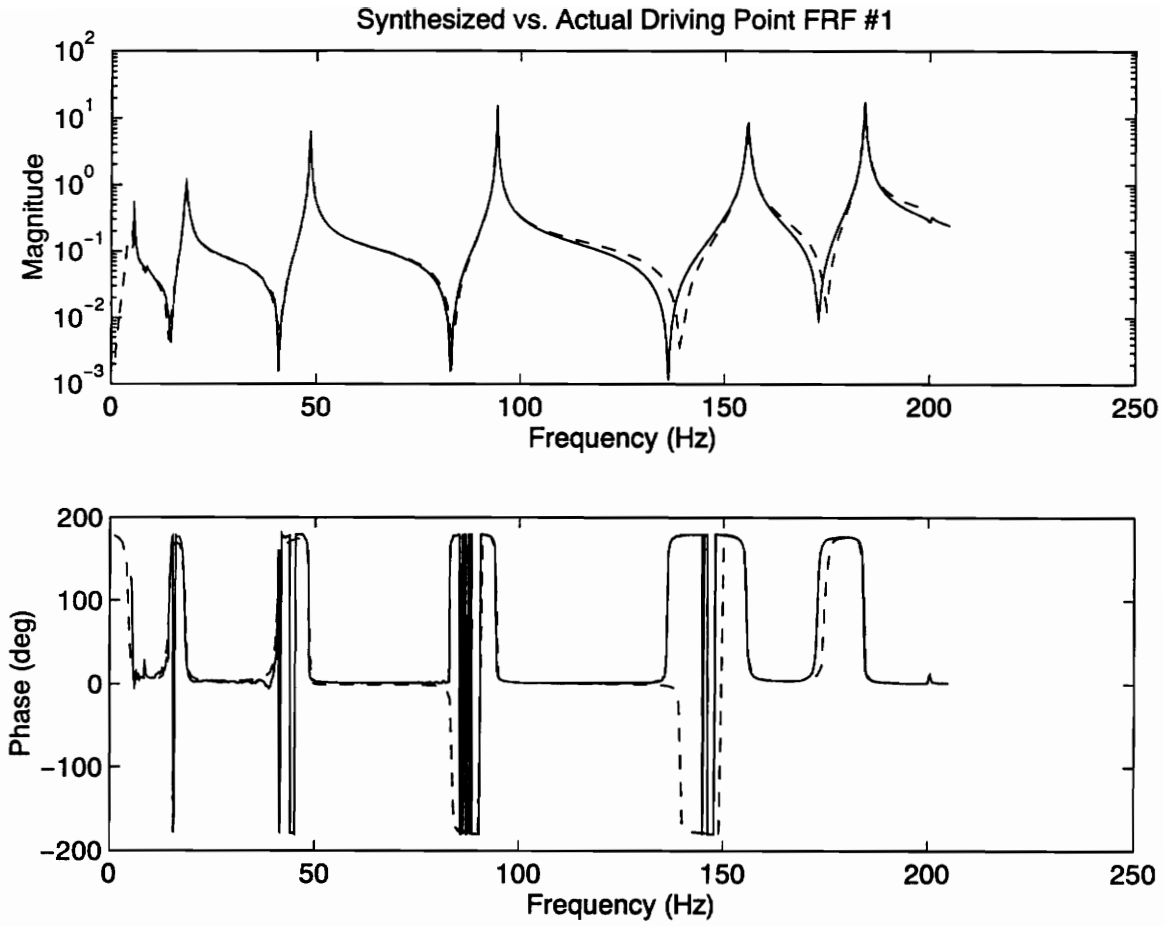

Figure 24: Accelerometer Driving Point FRF #1
Solid Line - Actual Data
Dashed Line - Analytical Model

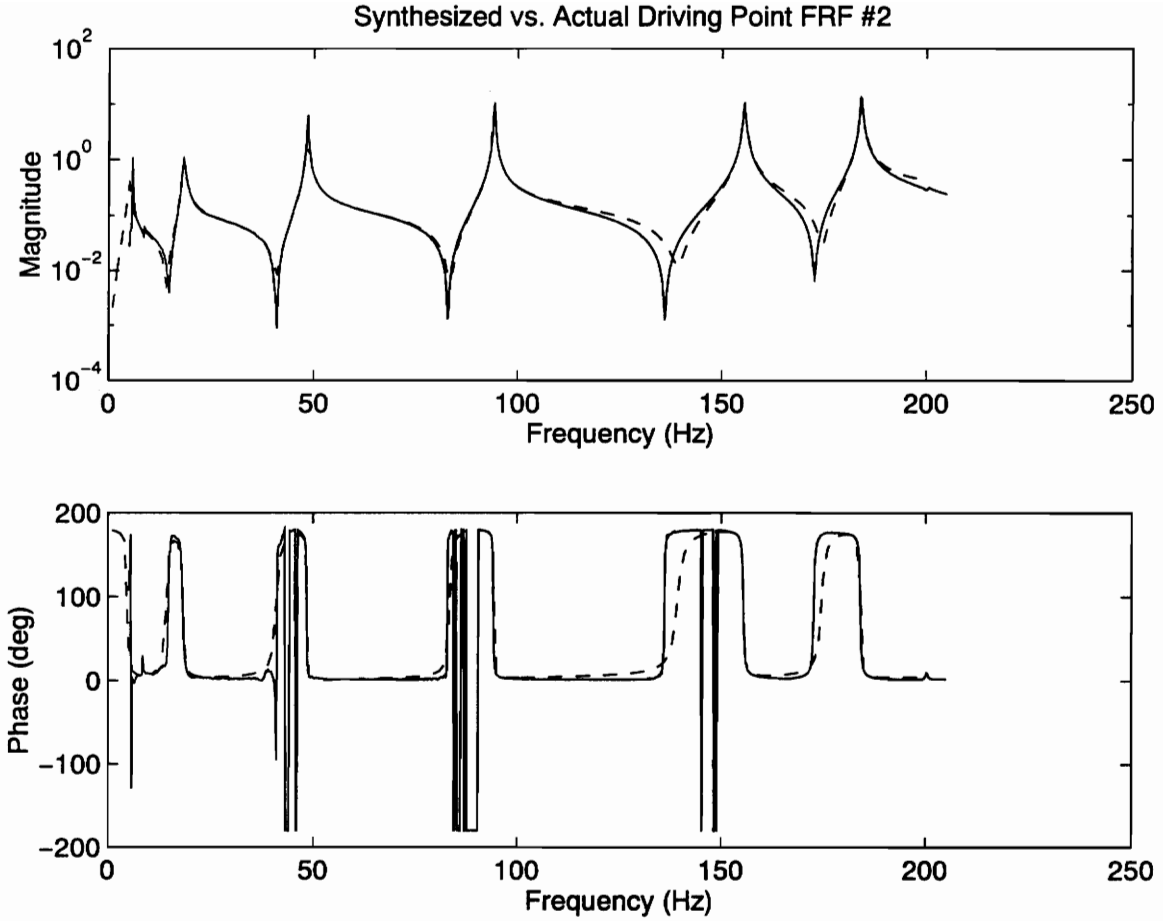

Figure 25: Accelerometer Driving Point FRF #2
Solid Line - Actual Data
Dashed Line - Analytical Model

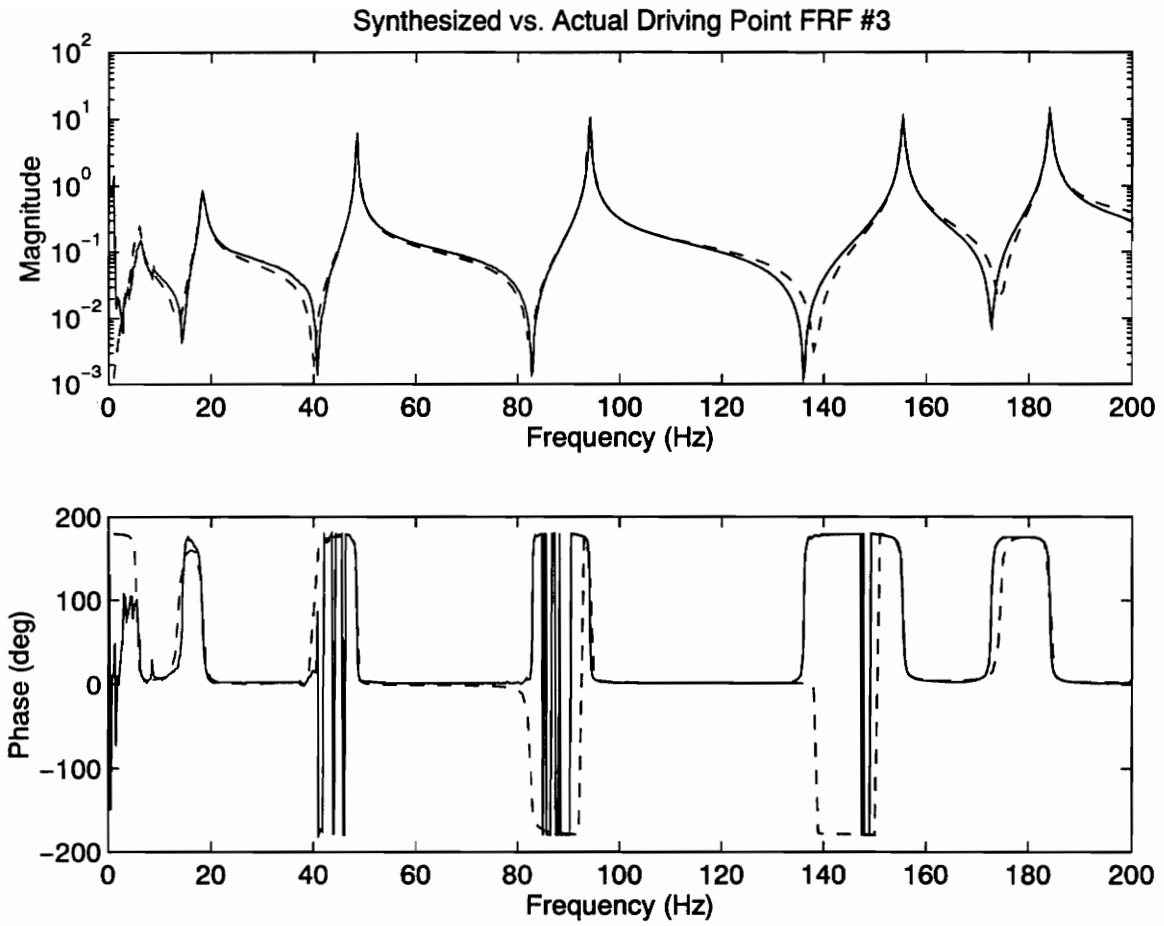

Figure 26: Accelerometer Driving Point FRF #3
Solid Line - Actual Data
Dashed Line - Analytical Model

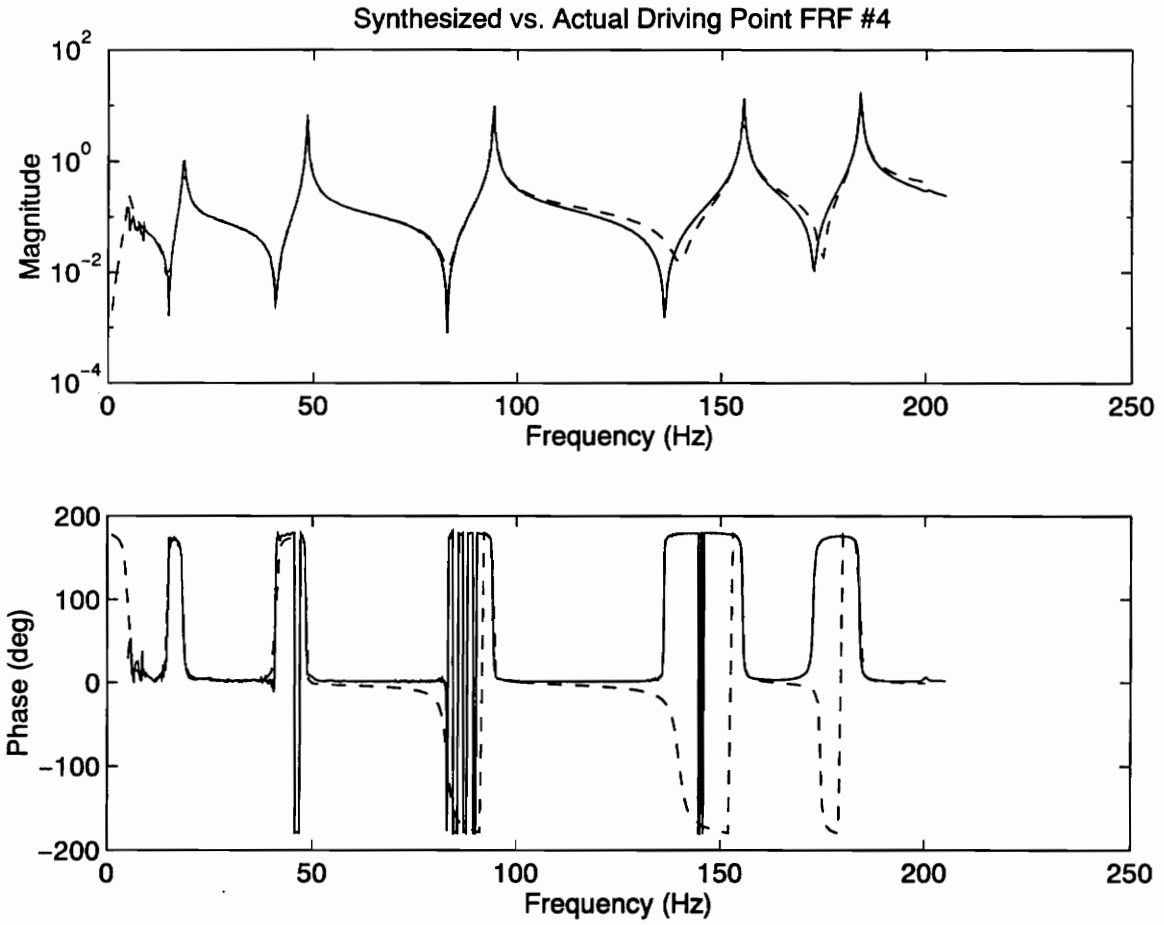

Figure 27: Accelerometer Driving Point FRF #4
Solid Line - Actual Data
Dashed Line - Analytical Model

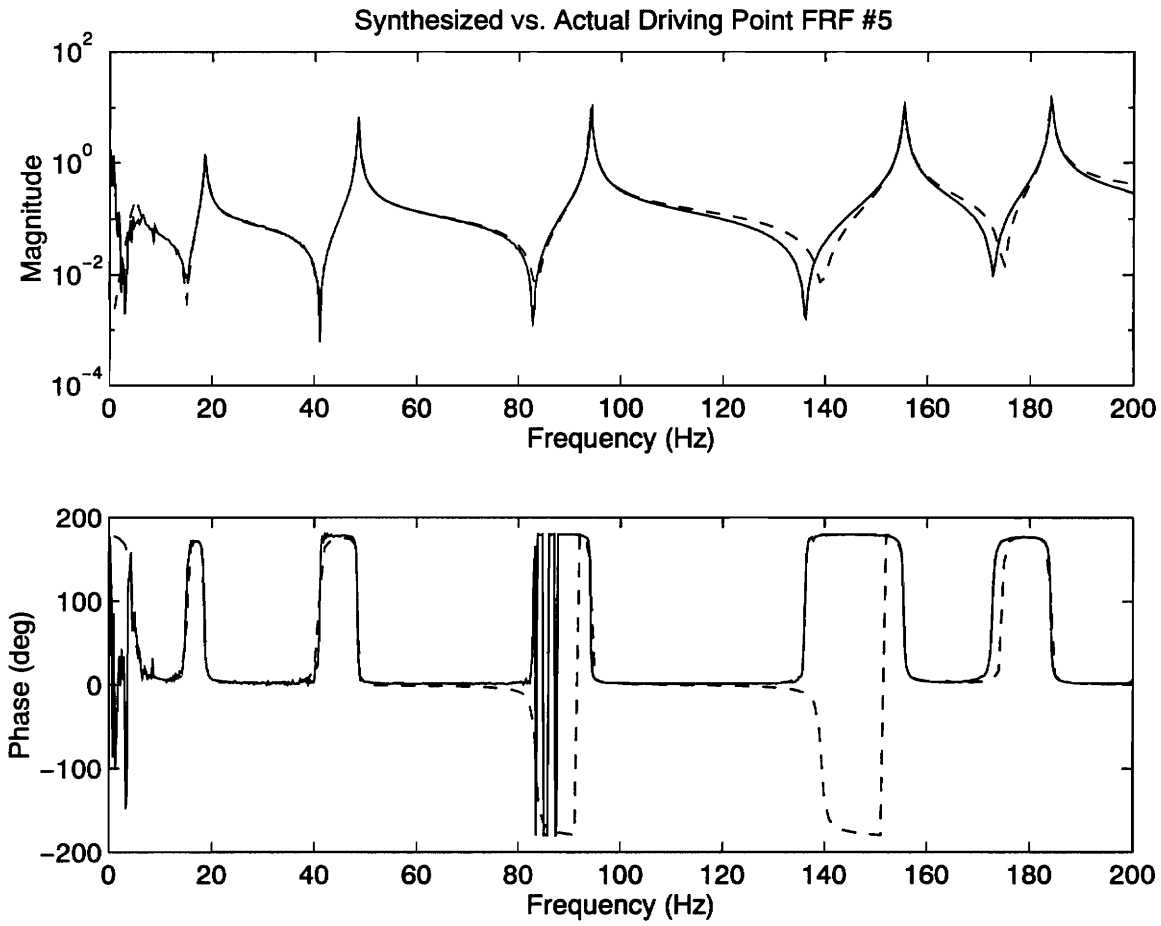

Figure 28: Accelerometer Driving Point FRF #5
Solid Line - Actual Data
Dashed Line - Analytical Model

4.4 Scanning Laser Velocimeter FRFs

The laser measured FRFs at eight locations on the beam are shown in figures 29-53 along with FRFs synthesized from estimated parameters. Measured values of the FRF are indicated by an 'x', and the estimated fit is shown as a solid line.

For comparison, three synthesized FRFs are shown for each of the eight measured FRFs shown: two synthesized FRFs resulting from fixed-poles analysis and one synthesized FRF from the global parameter analysis. Poles obtained from accelerometer FRFs numbers four and five provided the best fit to the measured data, and FRFs synthesized from the results of fixed-poles analysis with these sets of poles are included.

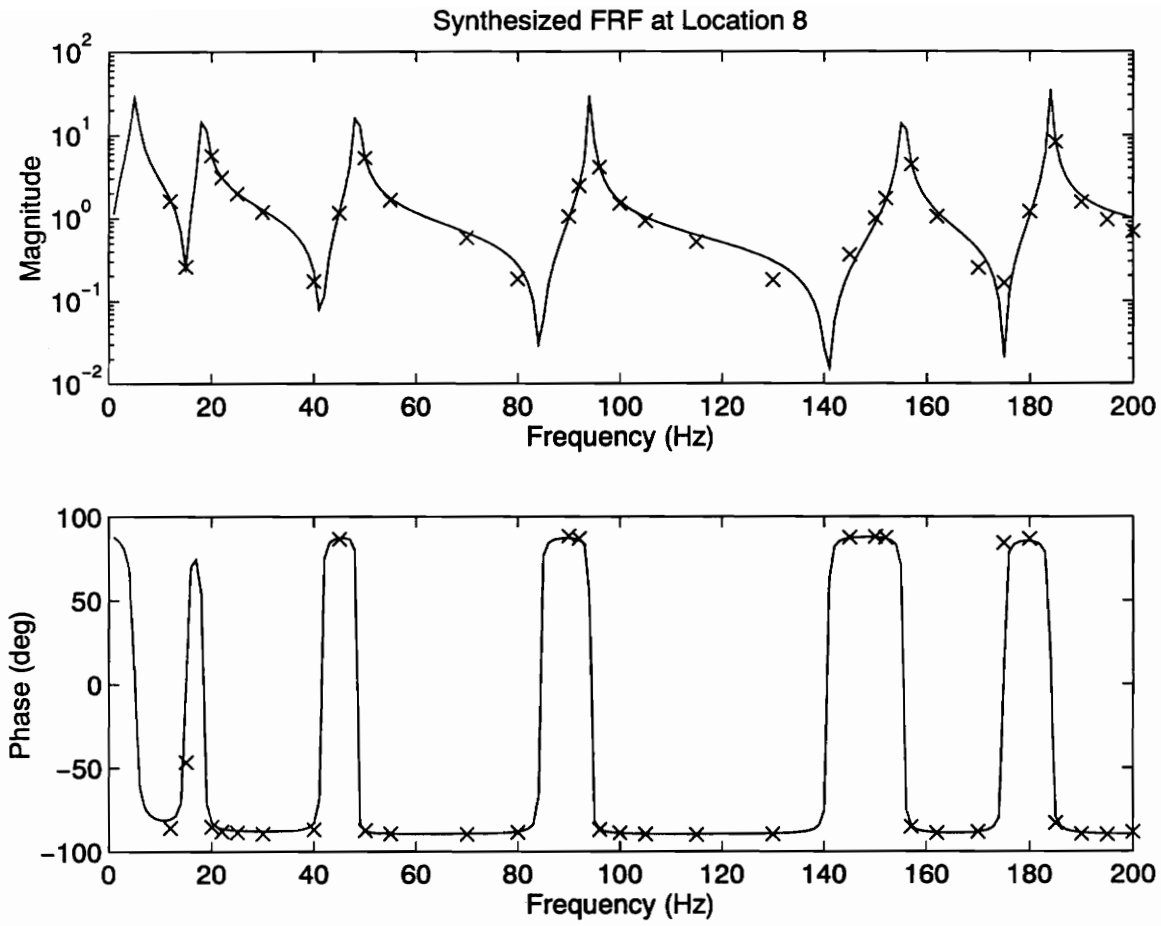

Figure 29: Synthesized FRF at Driving Point Using Poles from FRF #4

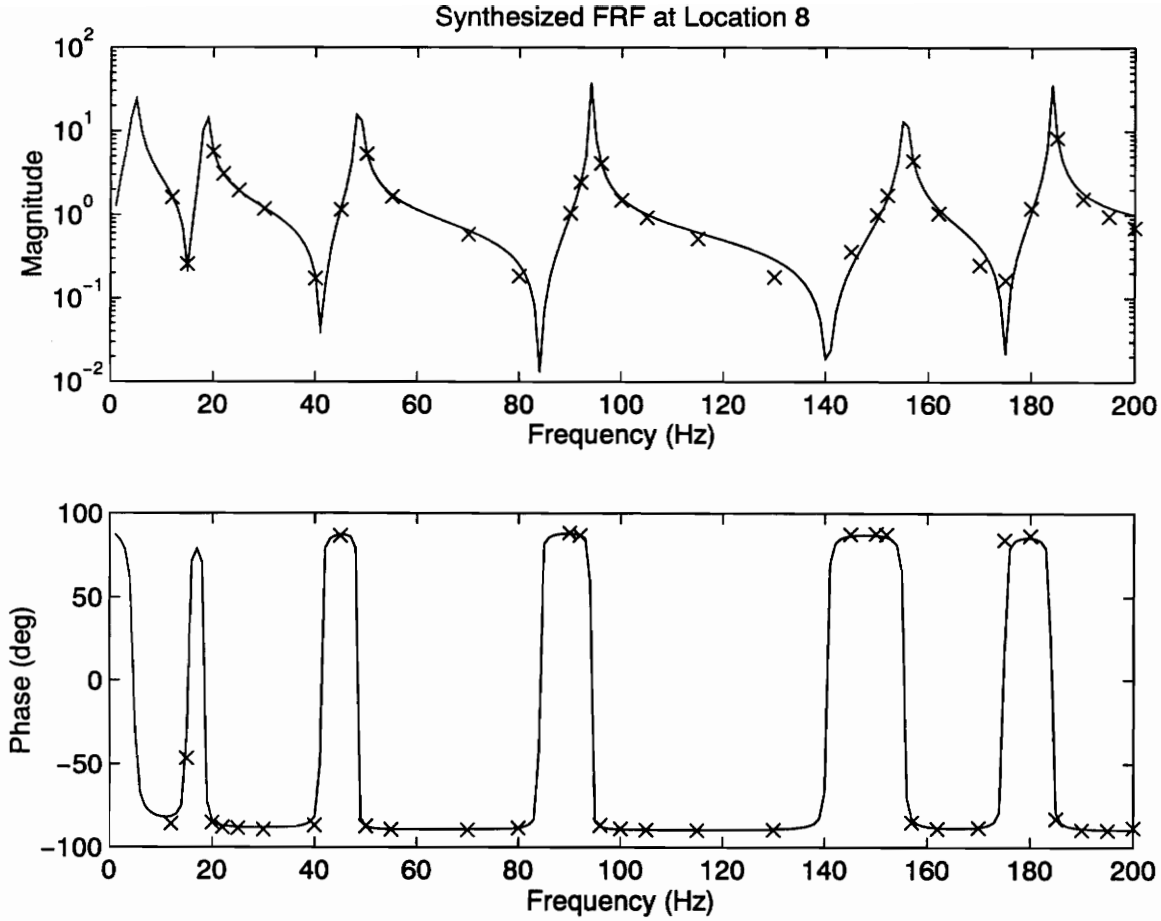

Figure 30: Synthesized FRF at Driving Point Using Poles from FRF #5

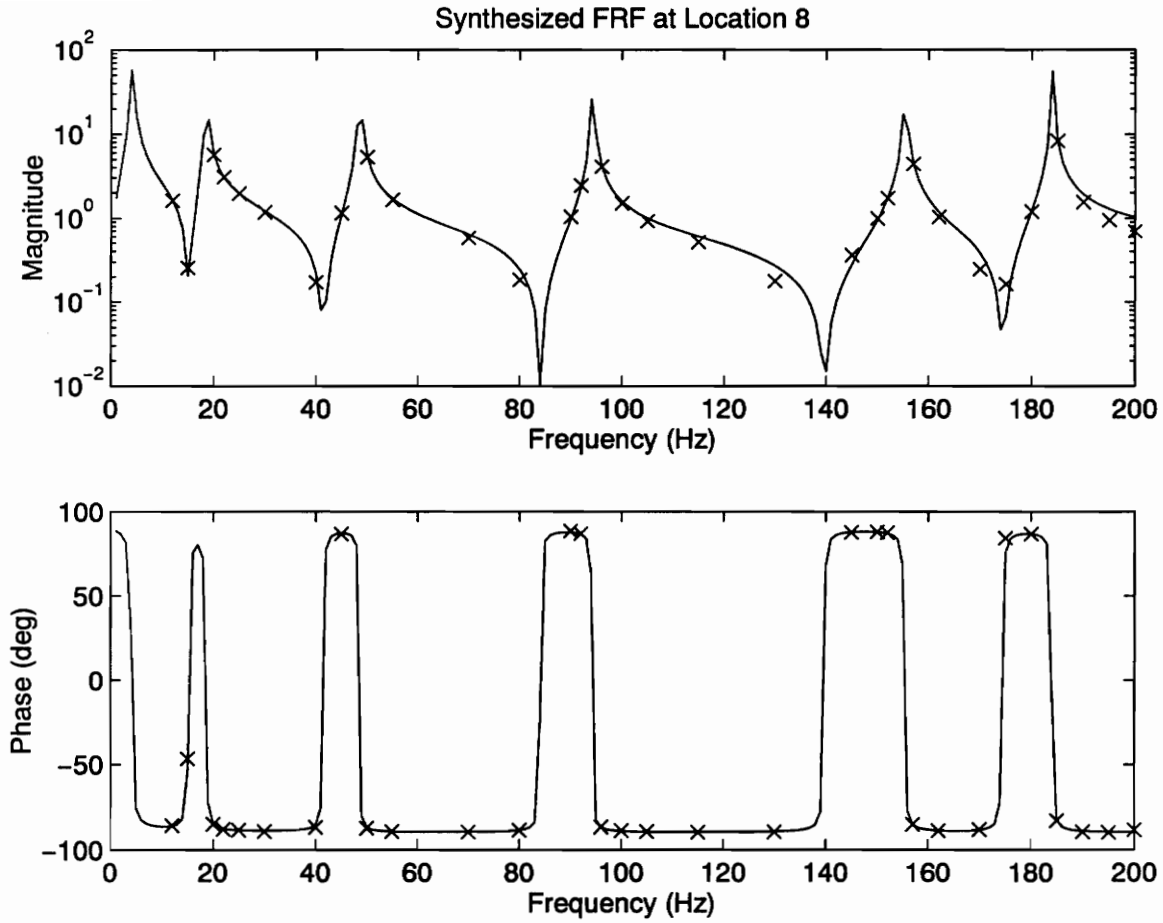

Figure 31: Synthesized FRF at Driving Point Using the Global Parameter Estimation Technique

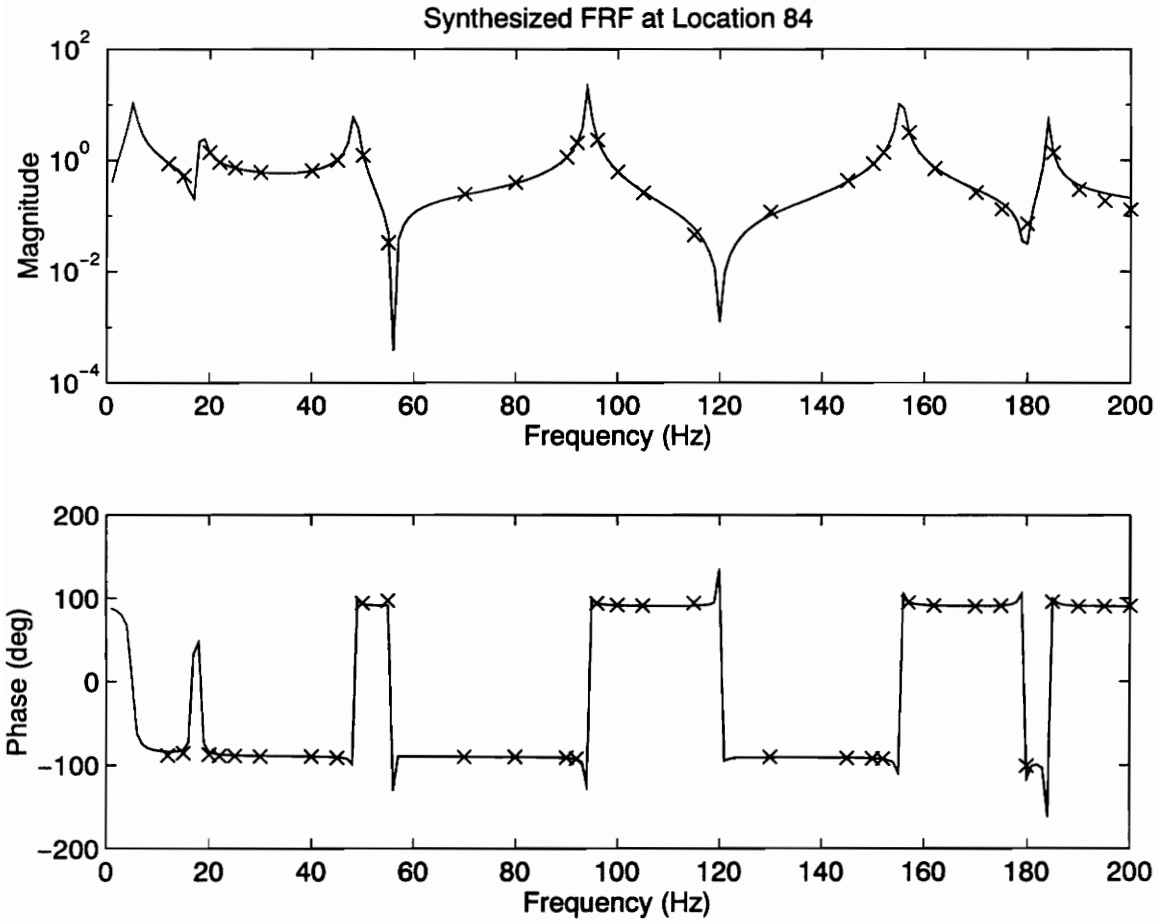

Figure 32: Synthesized FRF at Location 84 Using Poles Obtained from FRF #4

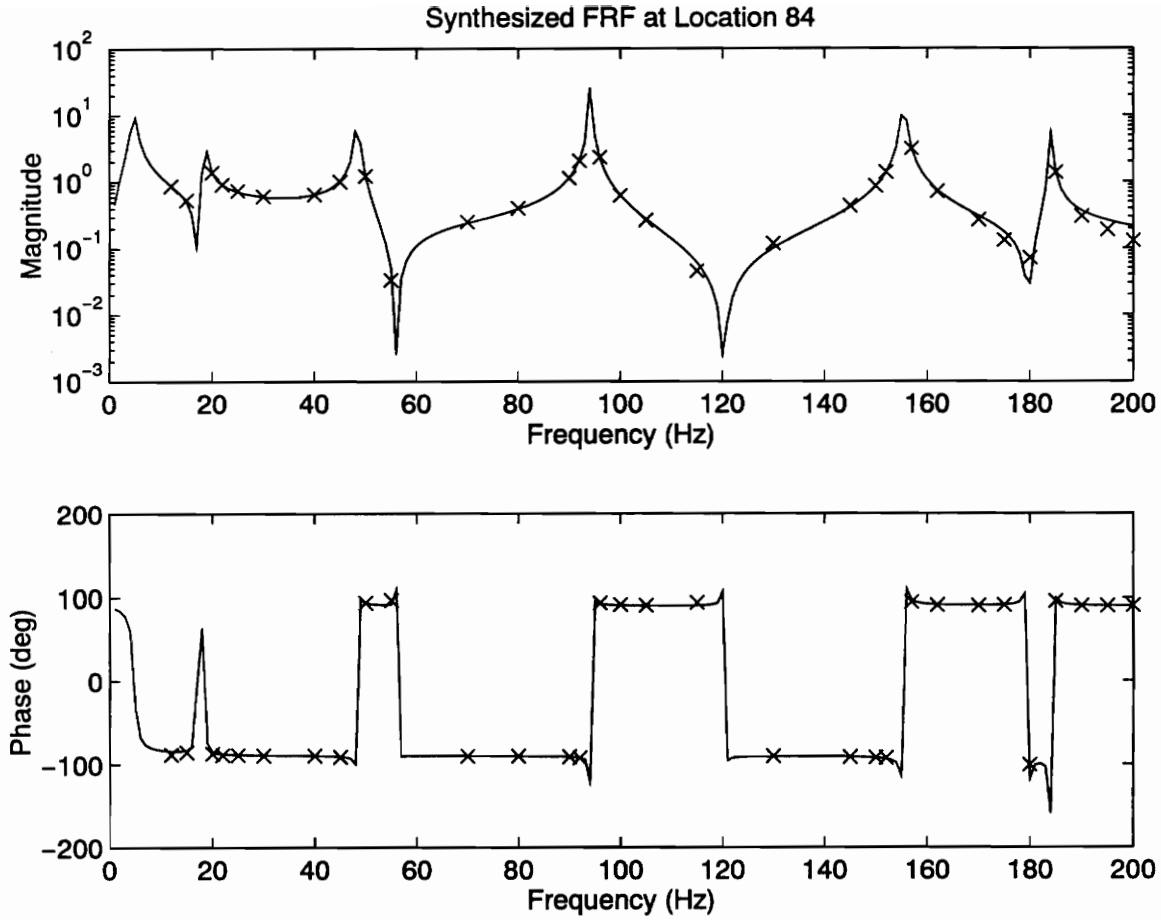

Figure 33: Synthesized FRF at Location 84 Using Poles Obtained from FRF #5

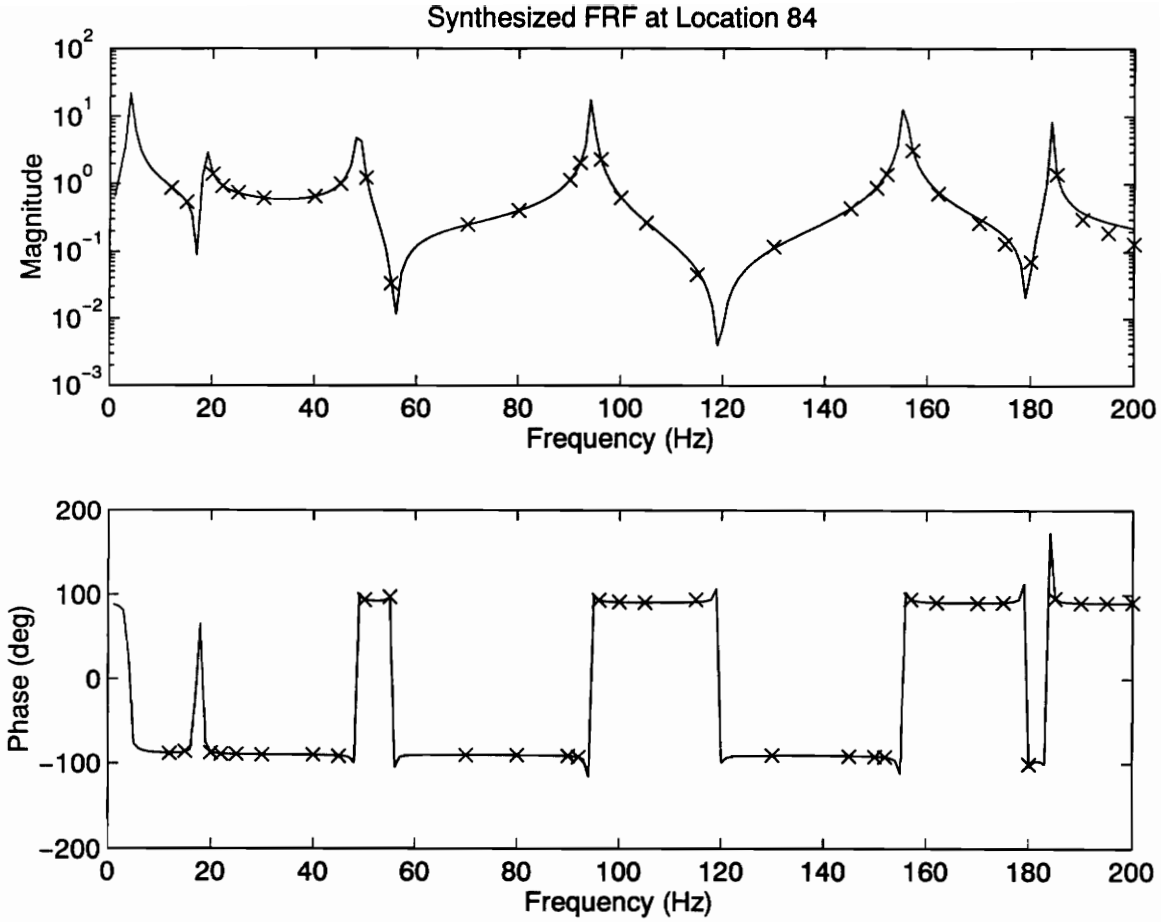

Figure 34: Synthesized FRF at Location 84 Using the Global Parameter Estimation Technique

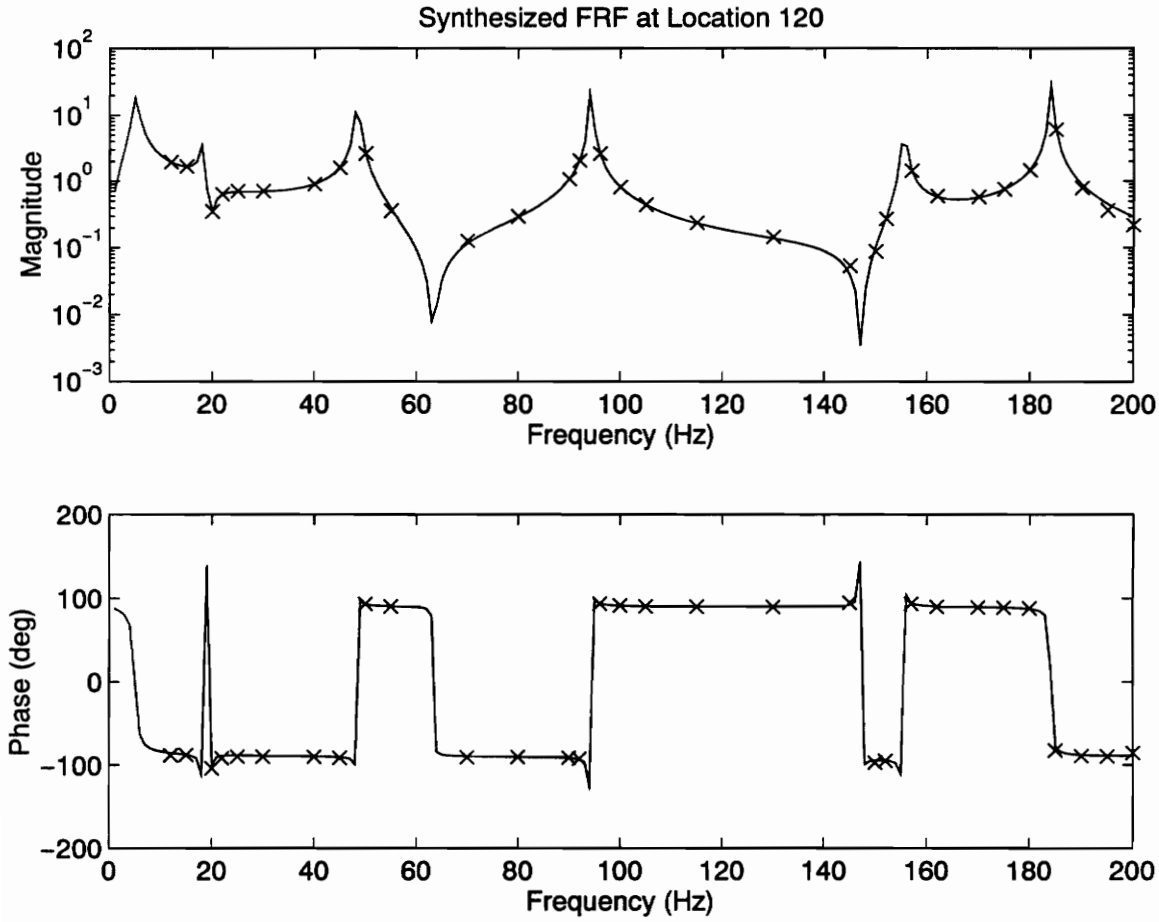

Figure 35: Synthesized FRF at location 120 using poles from FRF 4

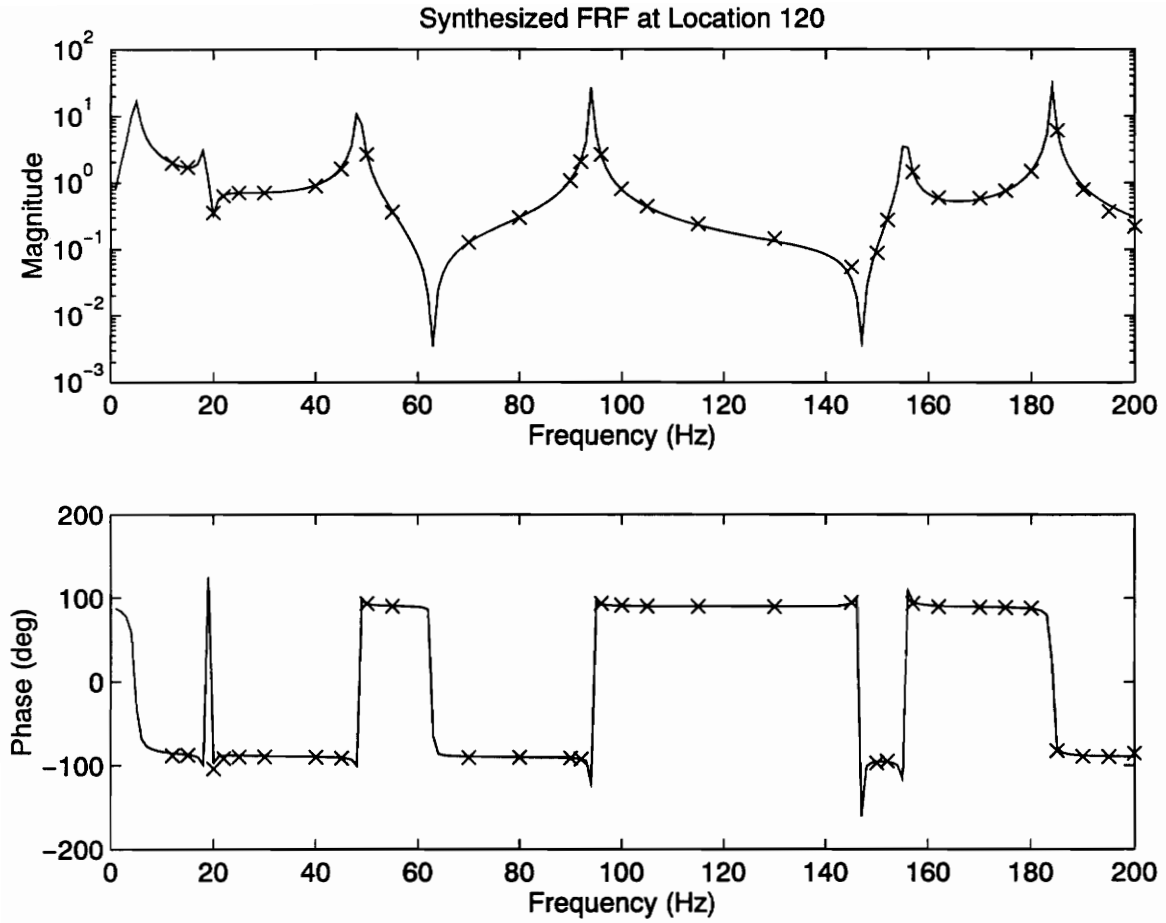

Figure 36: Synthesized FRF at location 120 using poles from FRF 5

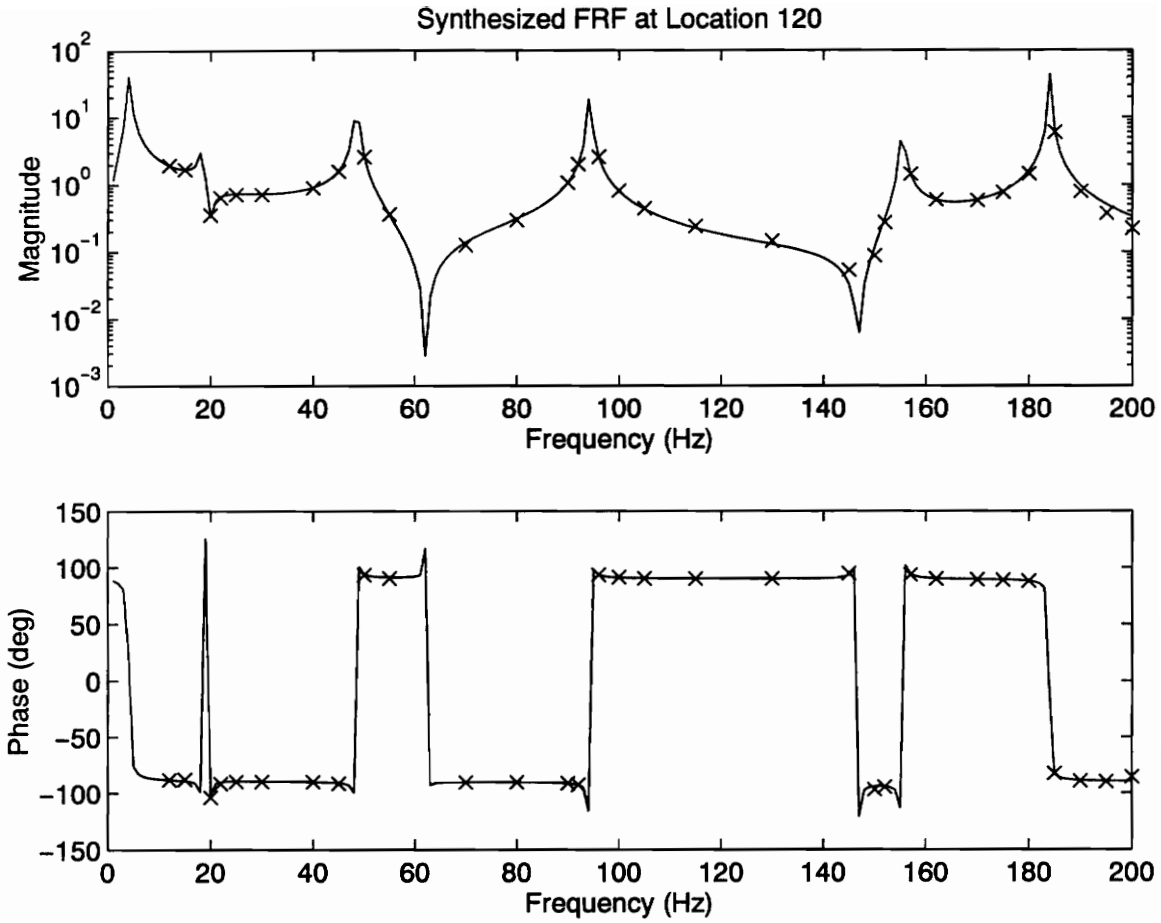

Figure 37: Synthesized FRF at location 120 using the Global Parameter Estimation Technique

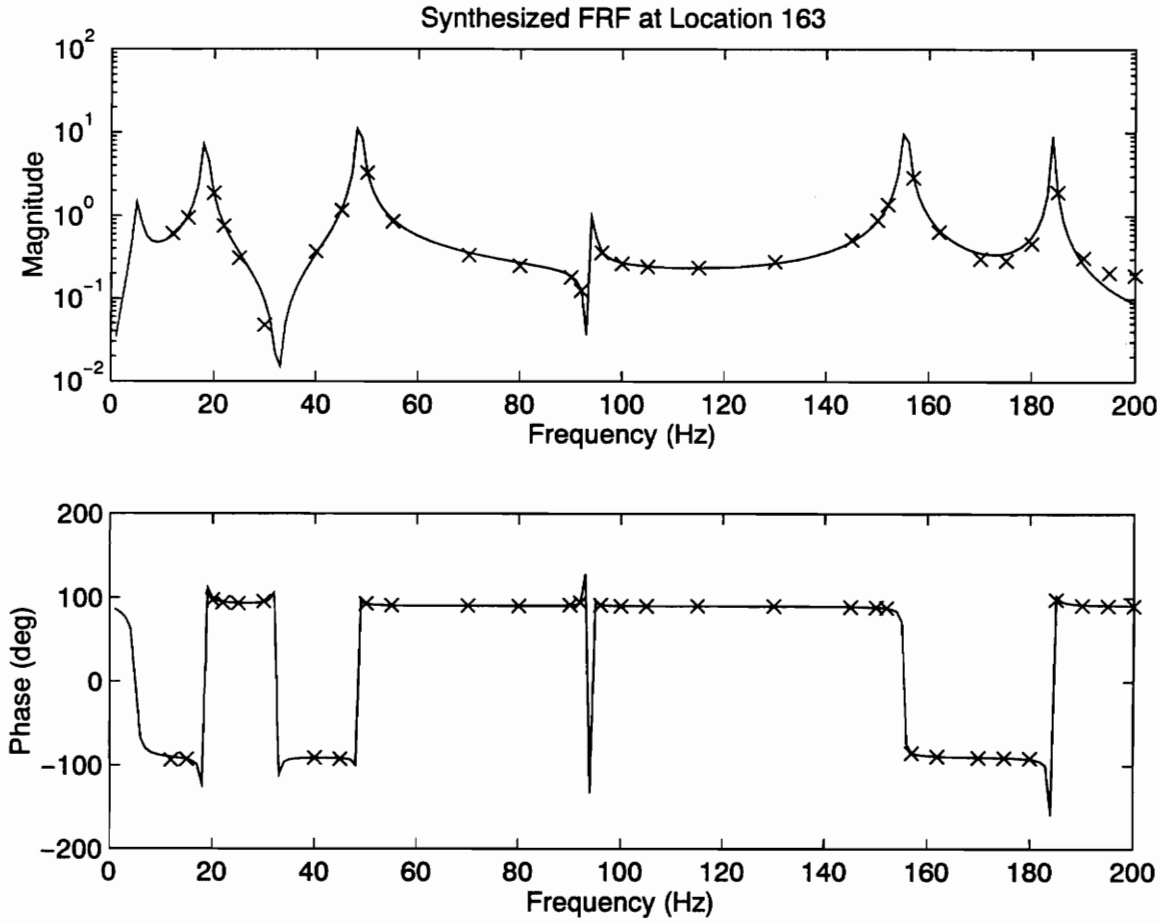

Figure 38: Syntheisized FRF at location 163 using poles from FRF #4

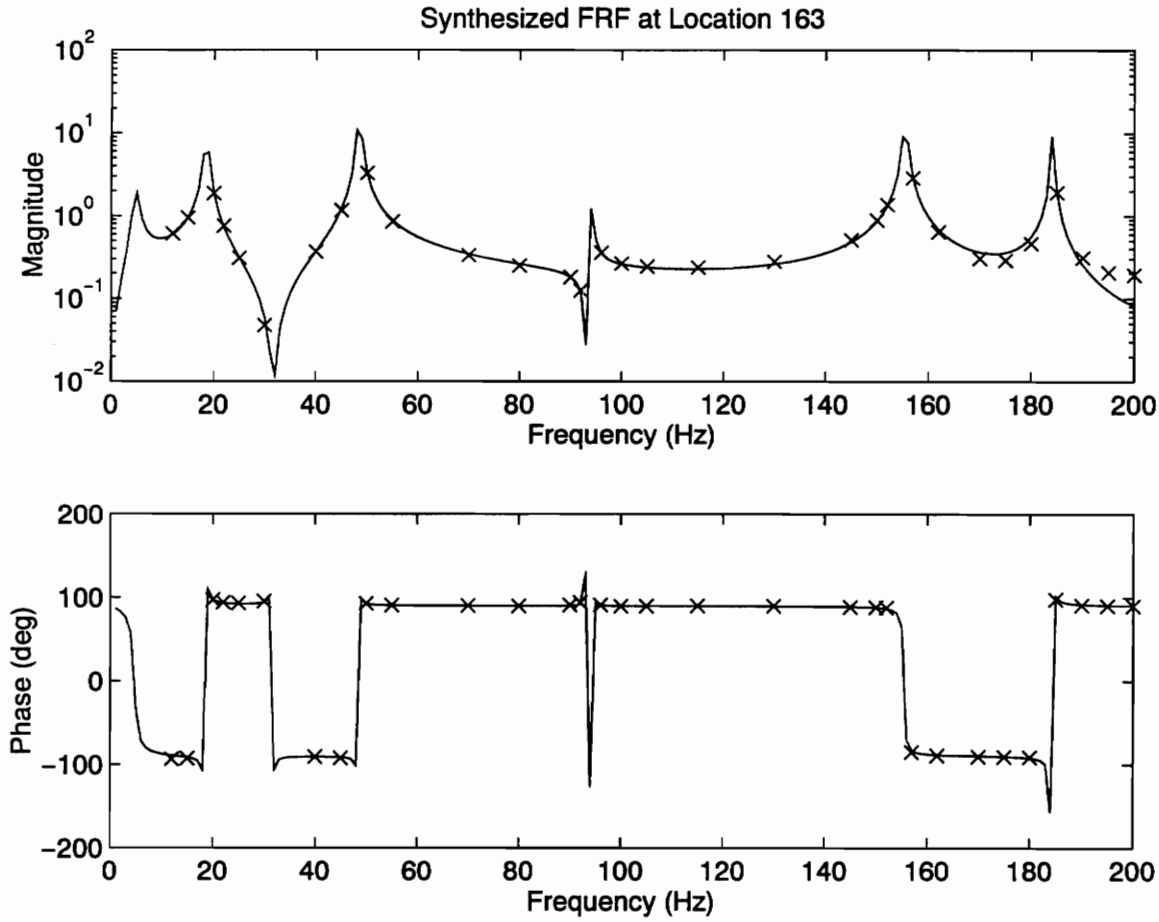

Figure 39: Syntheisized FRF at location 163 using poles from FRF #5

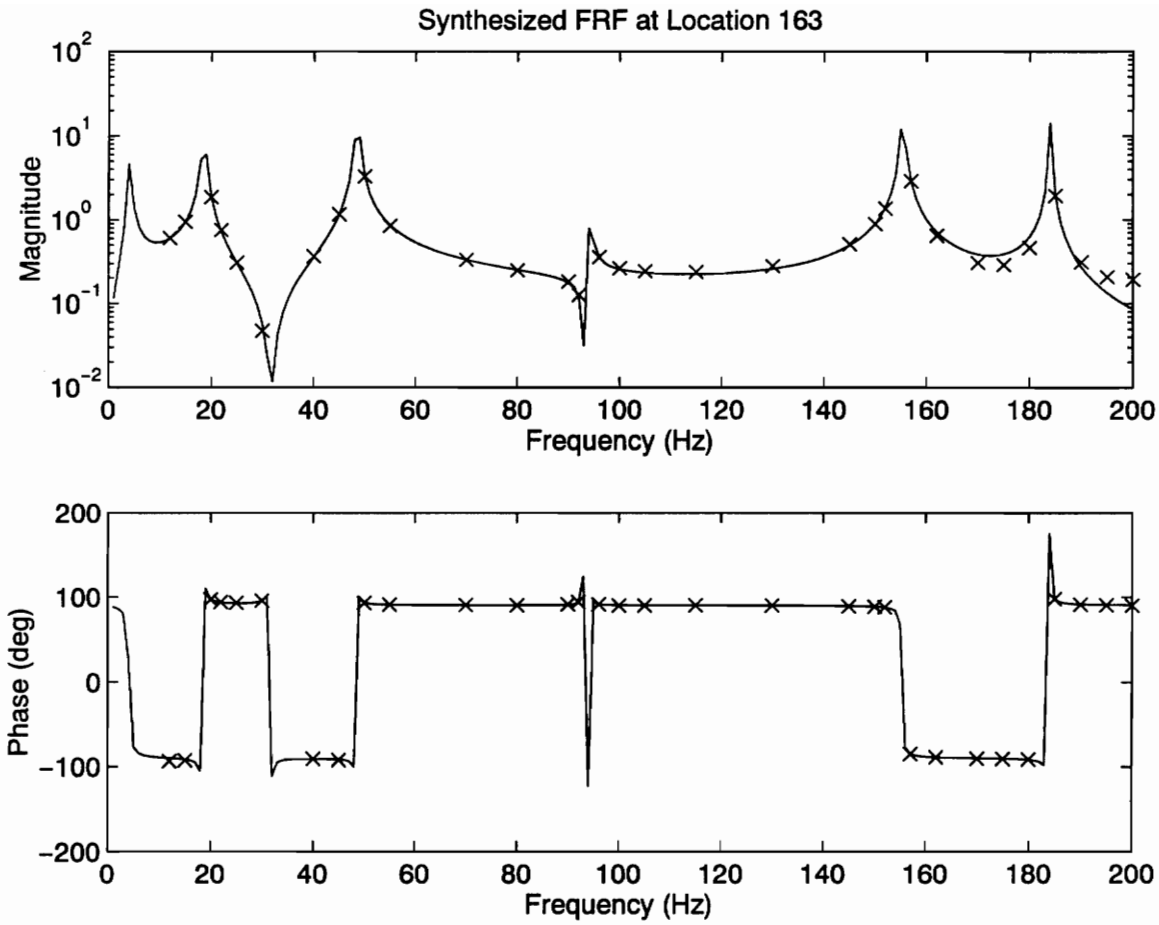

Figure 40: Synthesized FRF at location 163 using the Global Parameter Estimation Technique

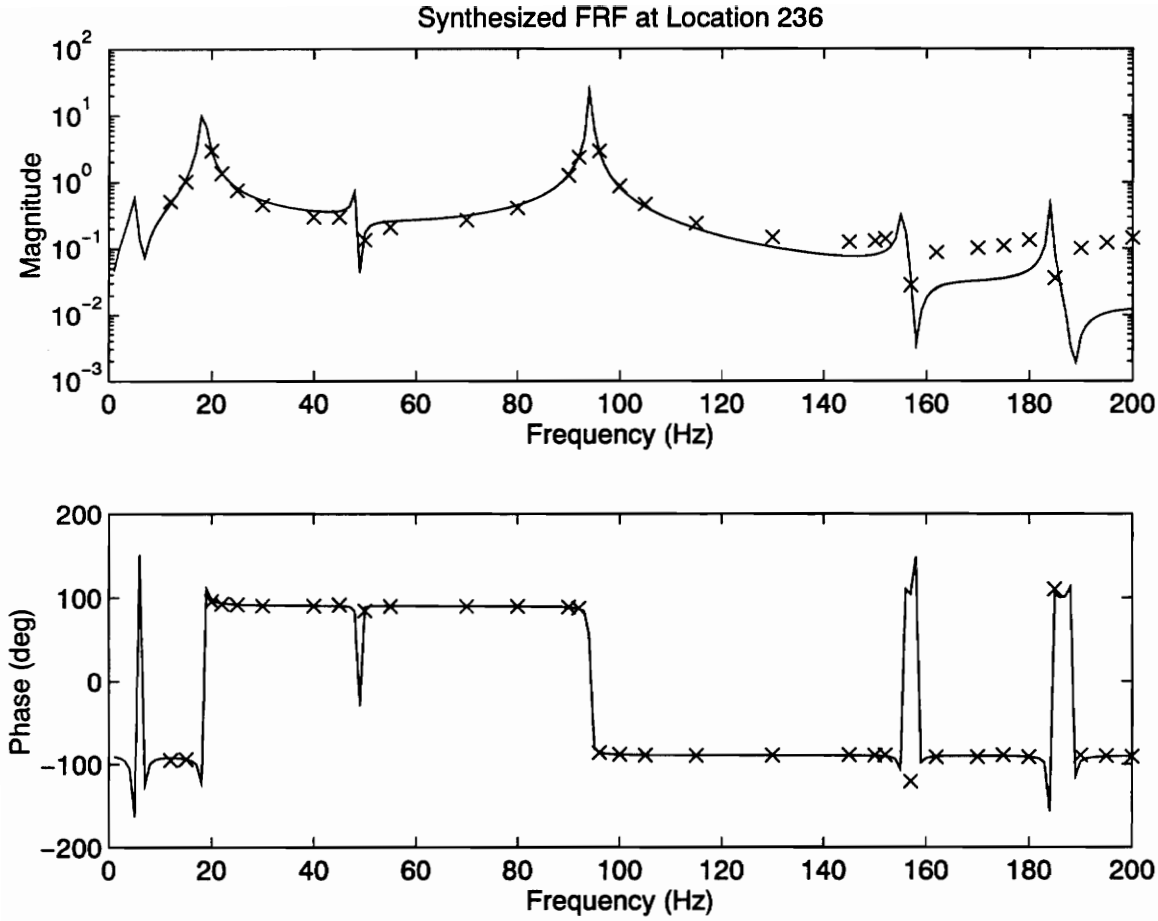

Figure 41: Synthesized FRF at location 236 using poles from FRF #4

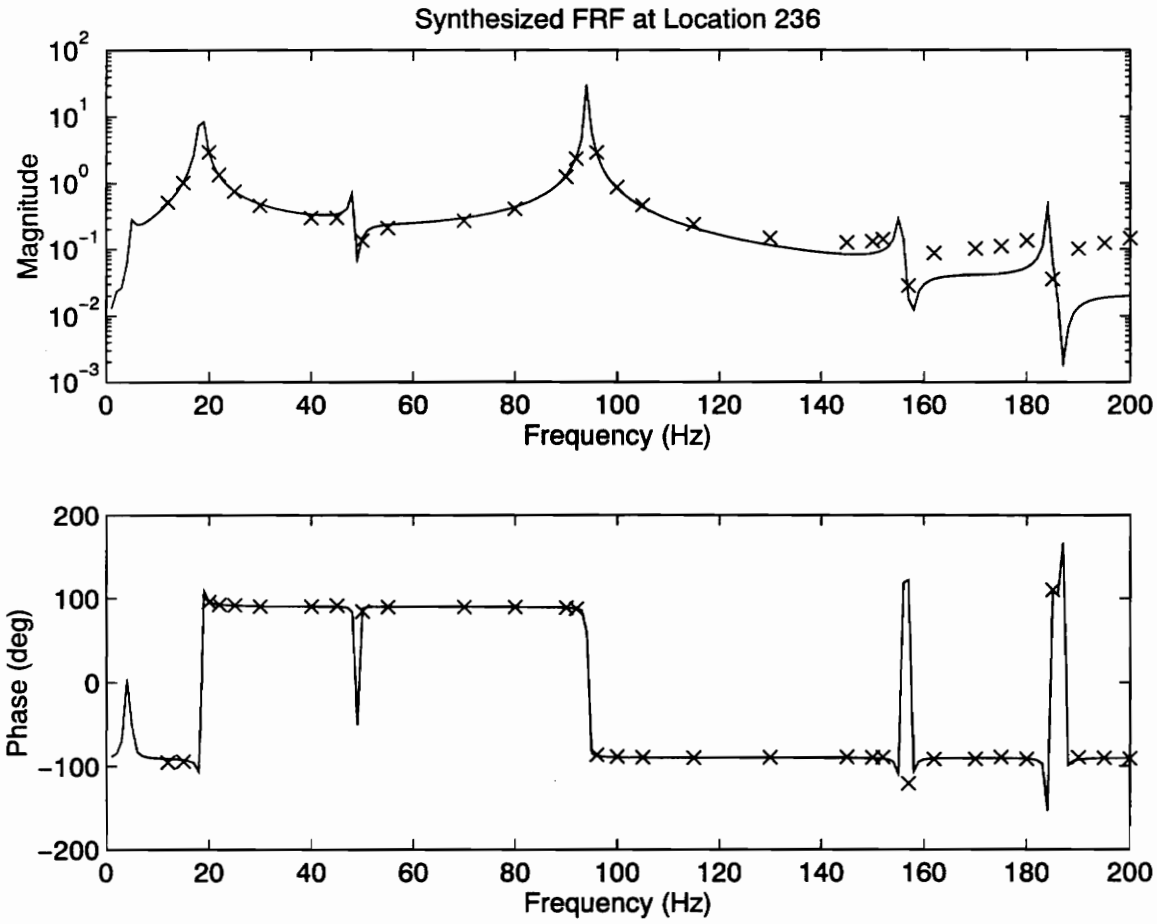

Figure 42: Synthesized FRF at location 236 using poles from FRF #5

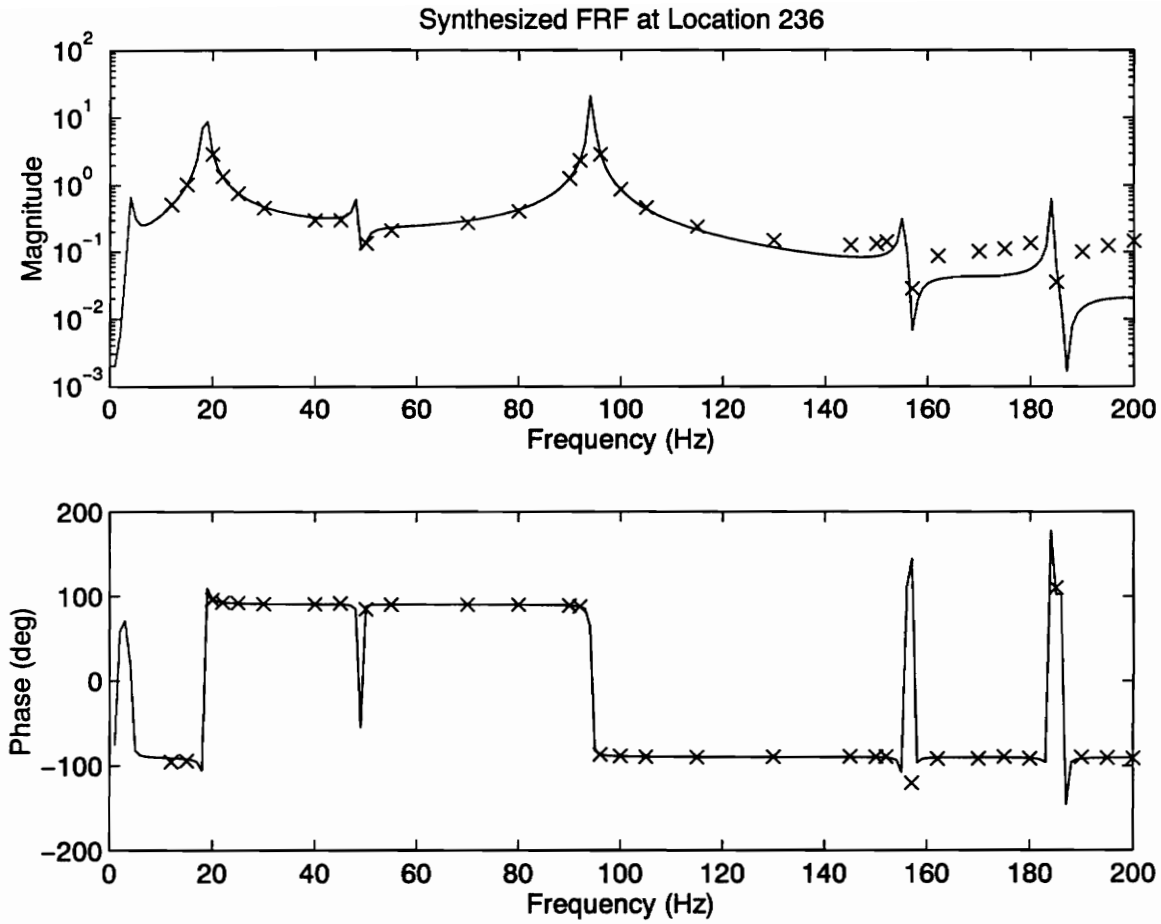

Figure 43: Synthesized FRF at location 236 using the Global Parameter Estimation Technique

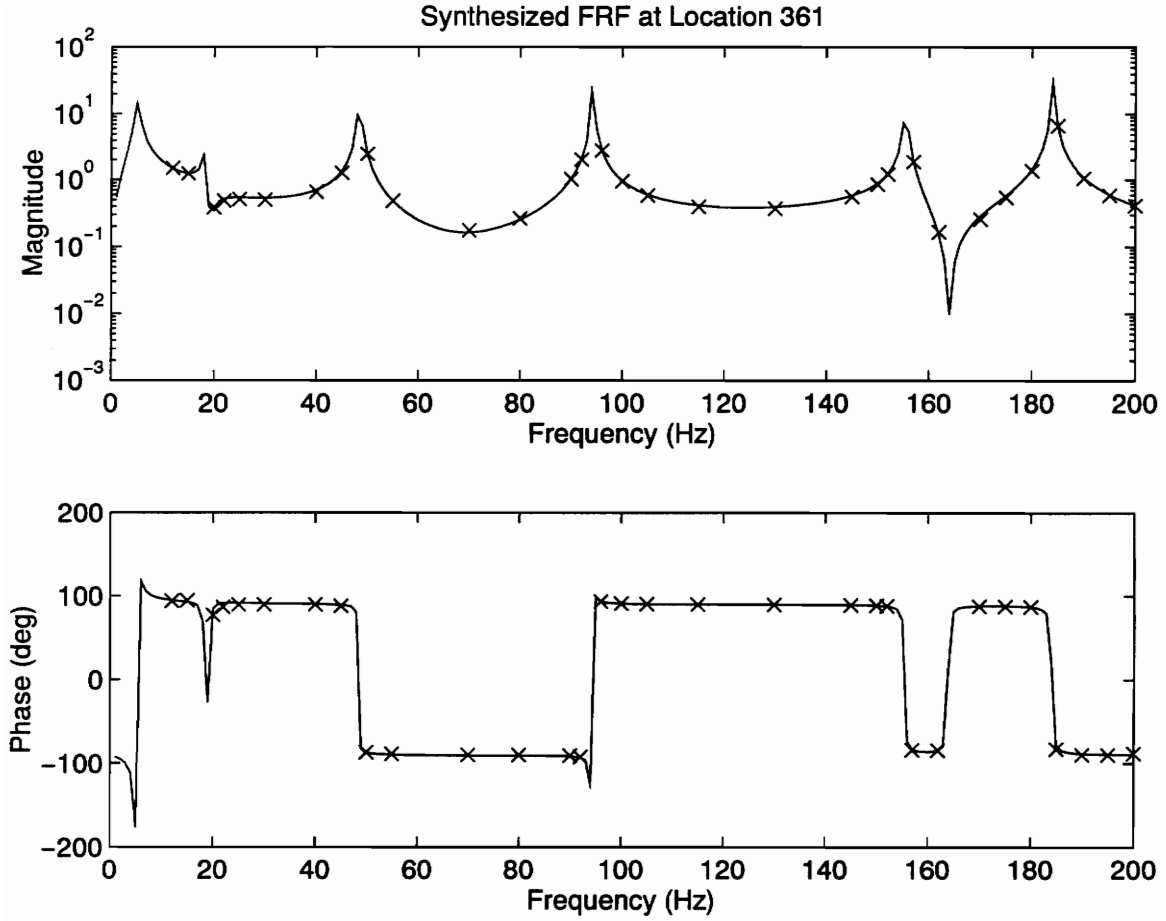

Figure 44: Synthesized FRF at location 361 using poles from FRF #4

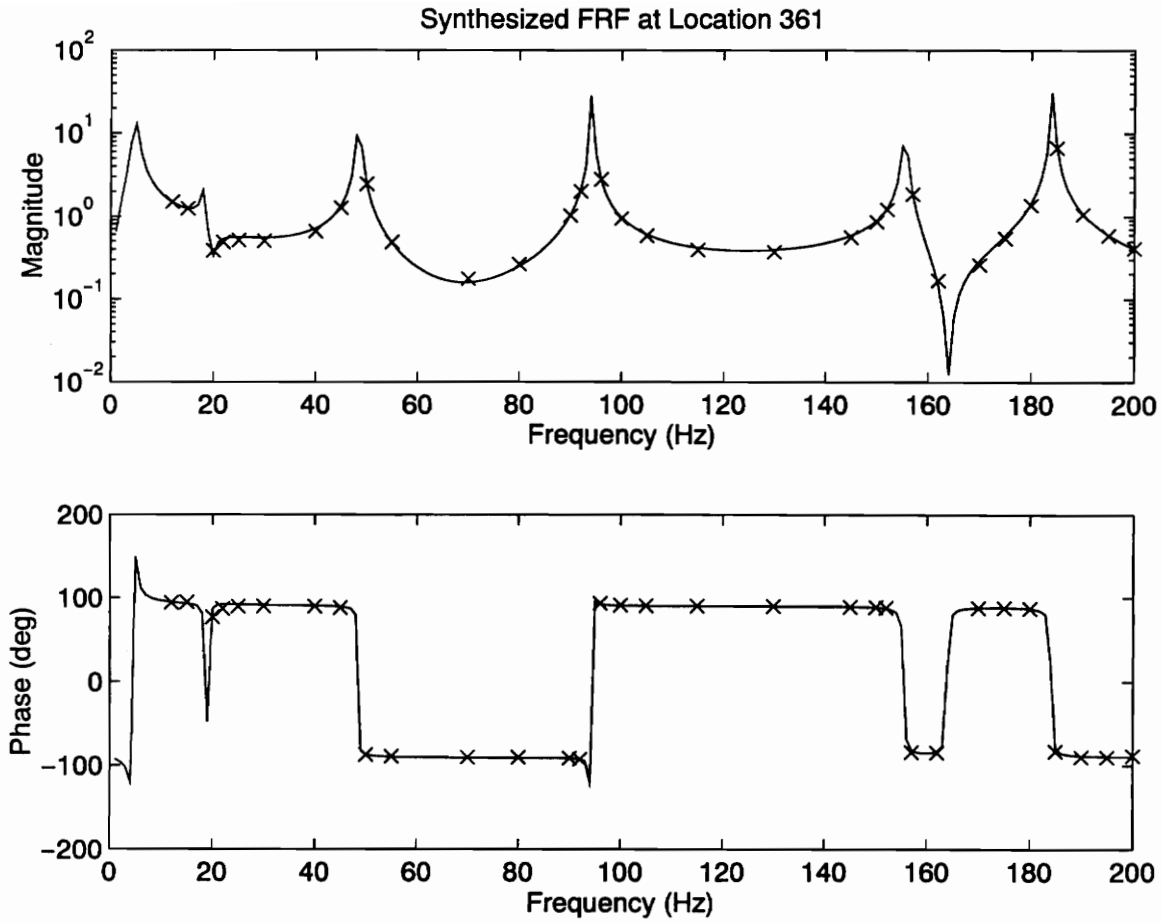

Figure 45: Synthesized FRF at location 361 using poles from FRF #5

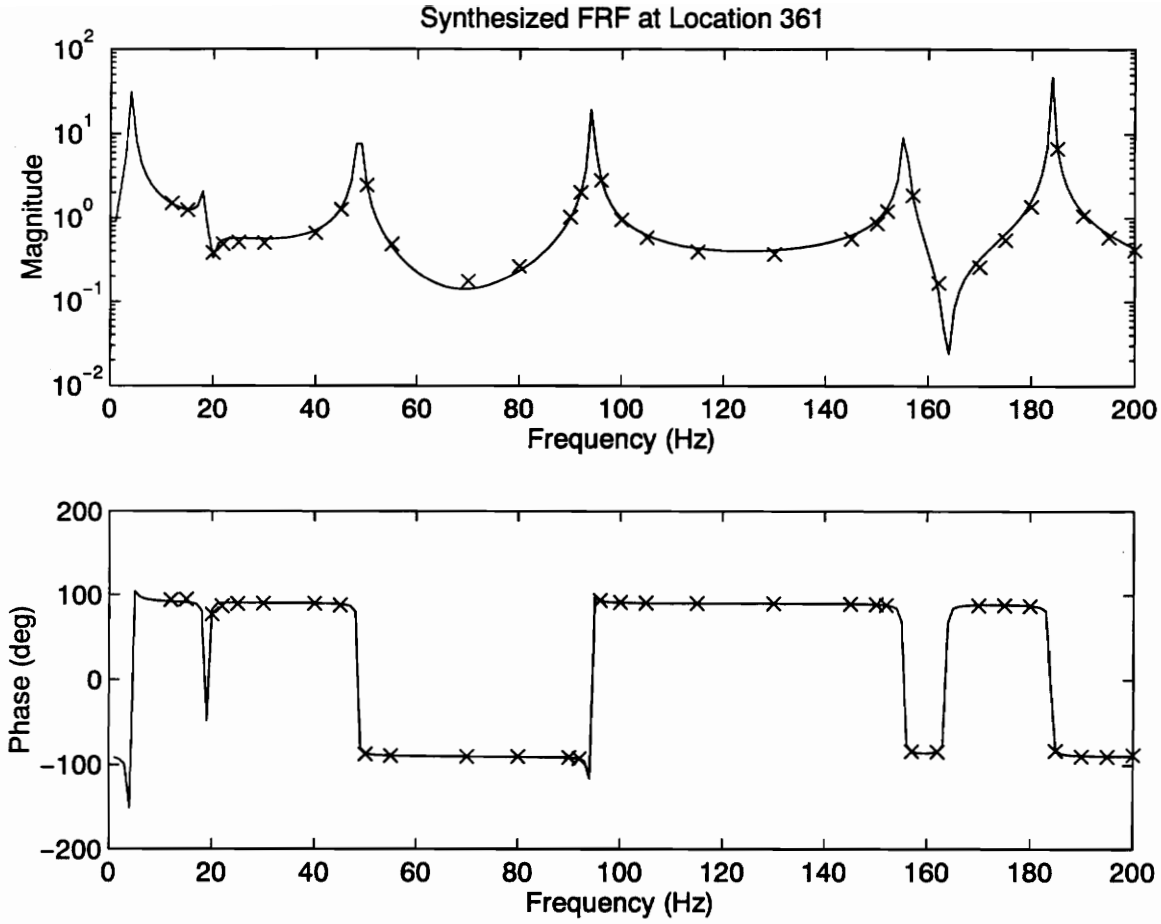

Figure 46: Synthesized FRF at location 361 using the Global Parameter Estimation Technique

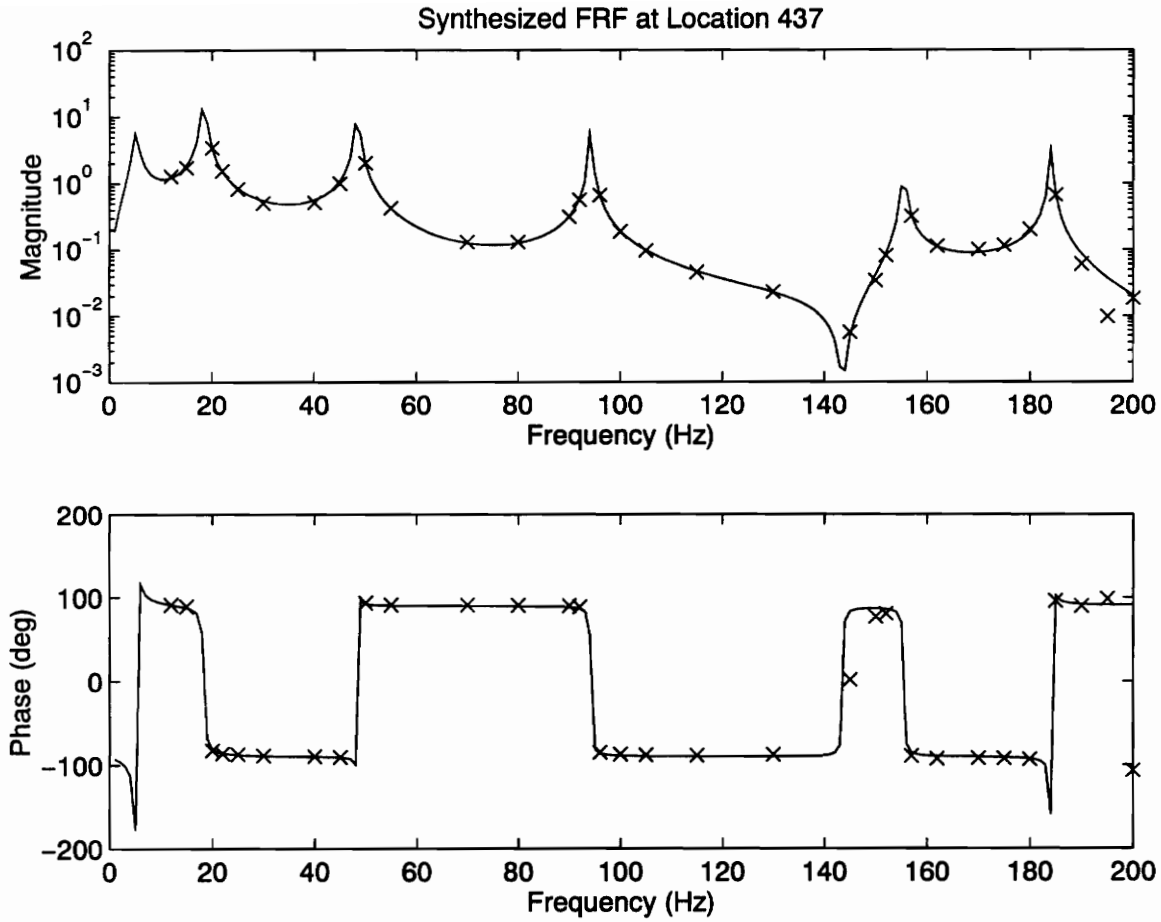

Figure 47: Synthesized FRF at location 437 using poles from FRF #4

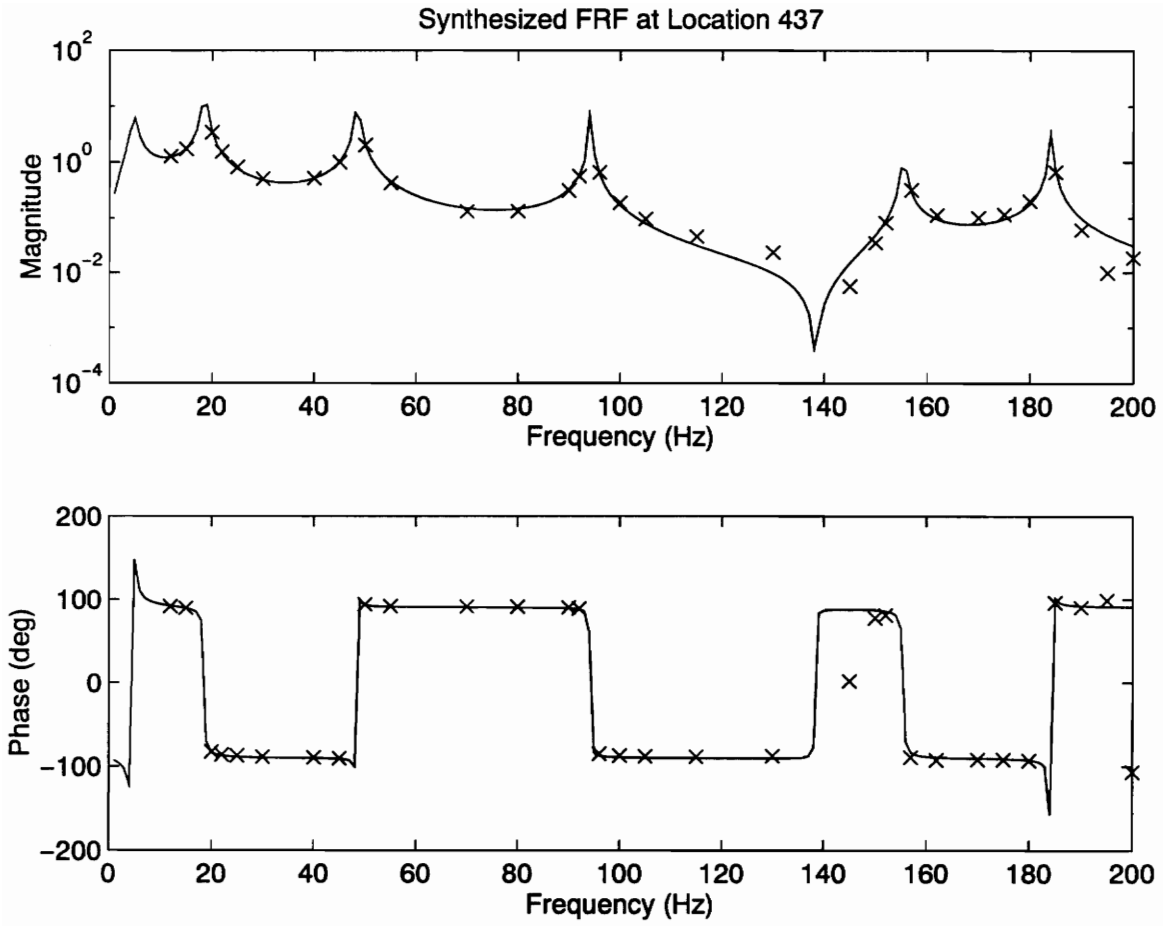

Figure 48: Synthesized FRF at location 437 using poles from FRF #5

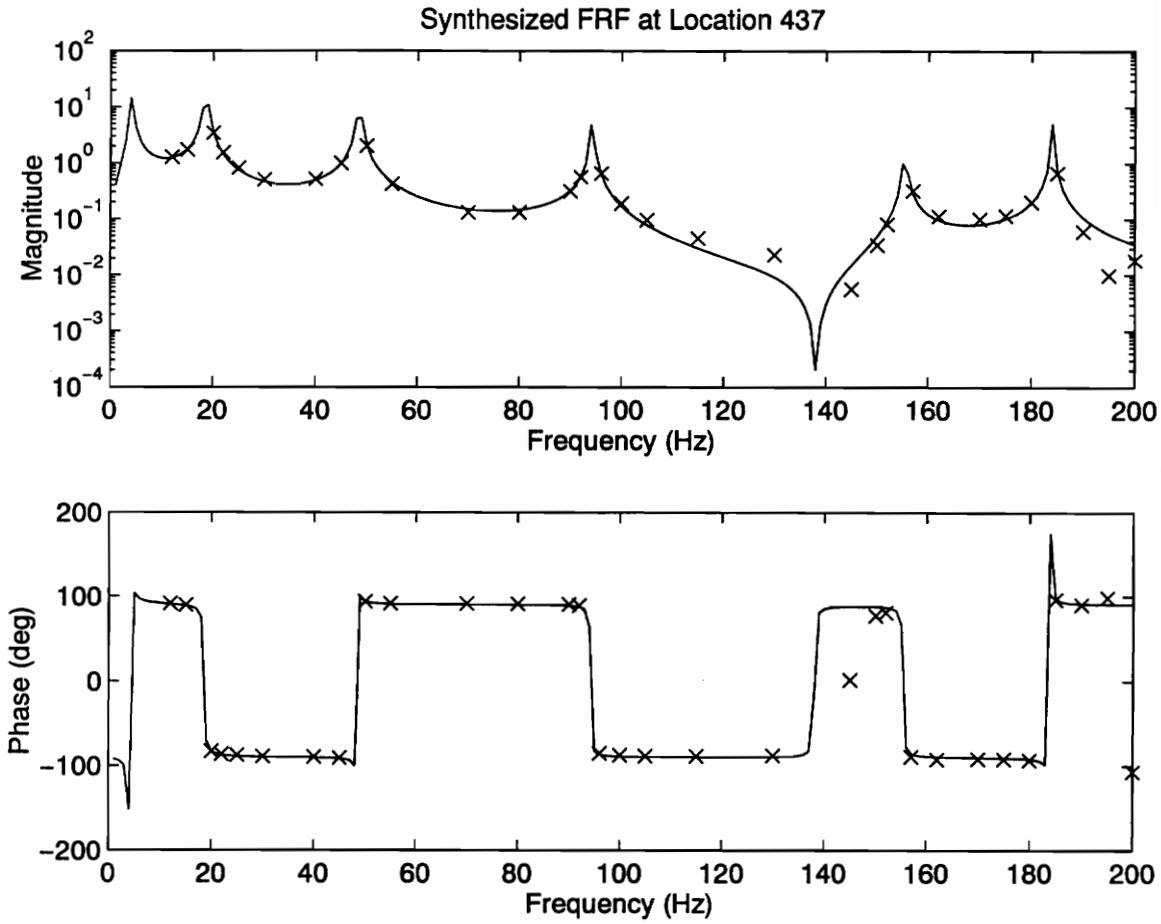

Figure 49: Synthesized FRF at location 437 using the Global Parameter Estimation Technique

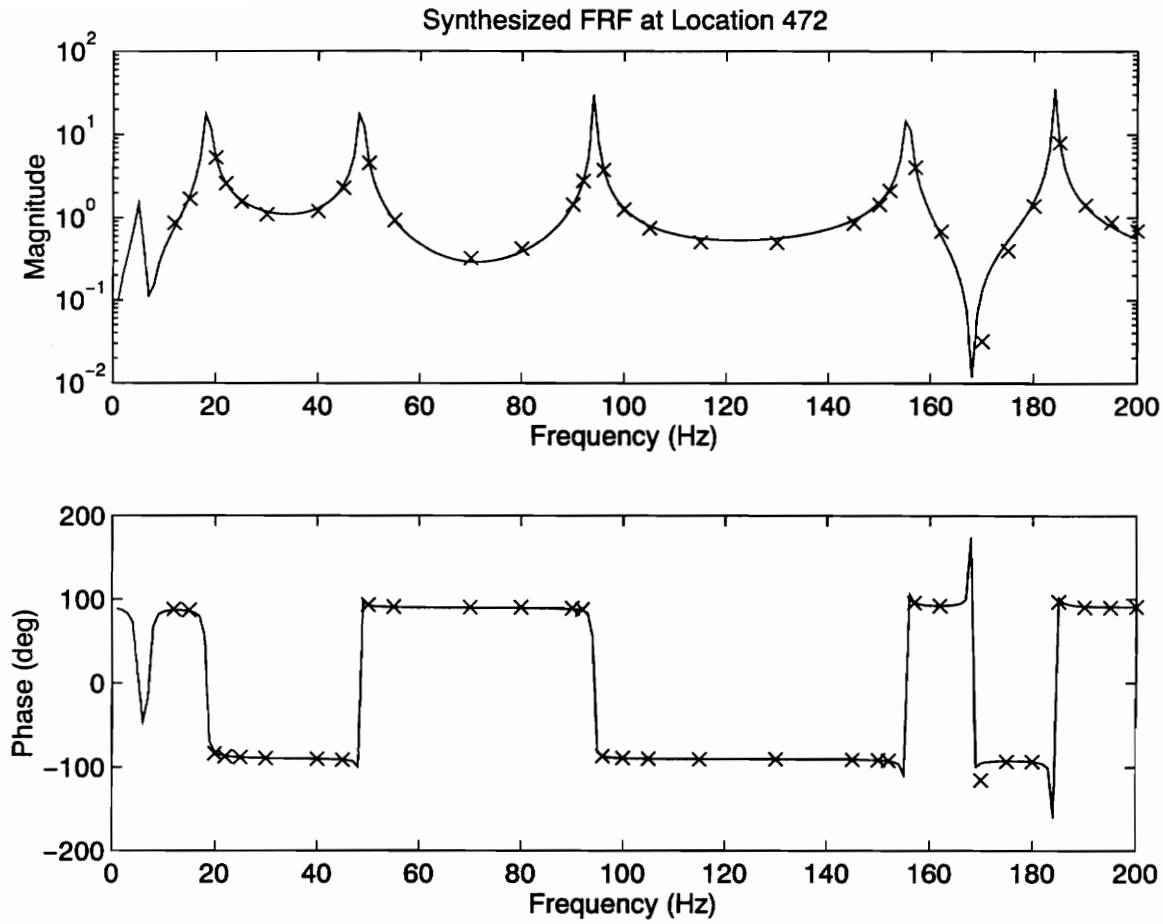

Figure 50: Synthesized FRF at location 472 using poles from FRF #4

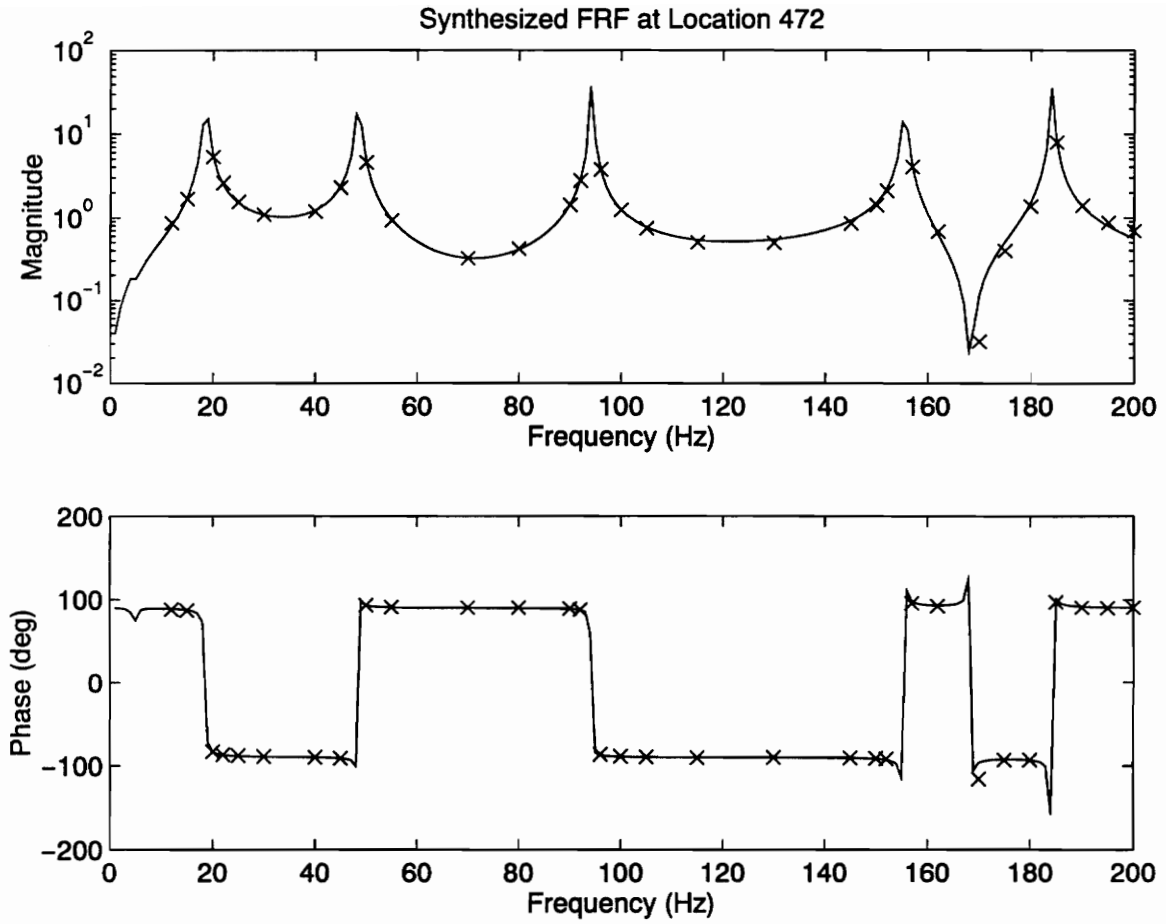

Figure 51: Synthesized FRF at location 472 using poles from FRF #5

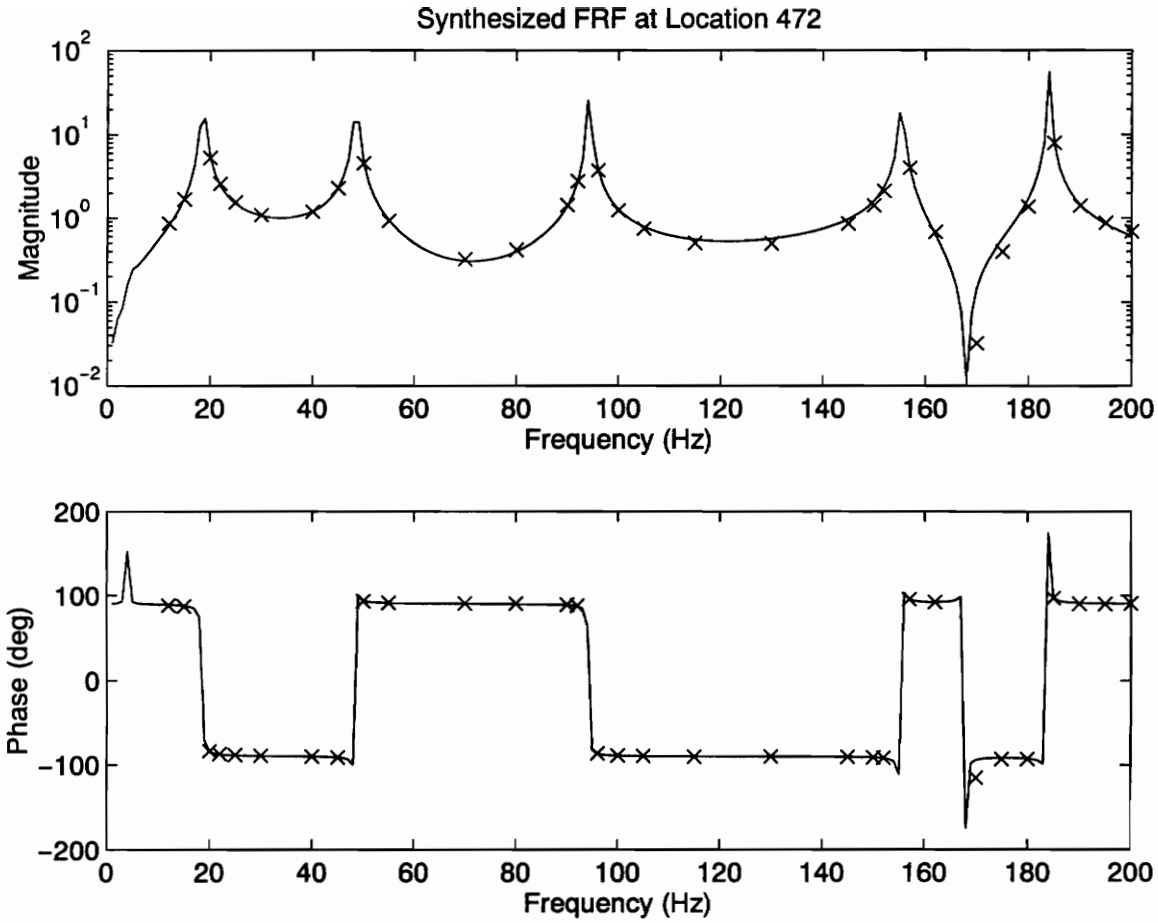

Figure 52: Synthesized FRF at location 472 using the Global Parameter Estimation Technique

4.5 Mac Tables

Table 2 shows MAC tables calculated from the results of a fixed-poles analysis using the poles estimated from driving point FRFs #1 through #5. Additionally, a MAC table derived from the results of the global parameter estimation analysis of the laser FRFs is included. Section 4.1.2 explains the modal assurance criterion (MAC) and the desired results.

Table 3 shows MAC tables calculated with mode vectors from Euler beam theory and mode vectors estimated from experimental data. Euler beam theory predicts only bending modes, so only experimentally determined bending modes are included in the MAC tables. Six tables are included, each showing the orthogonality of each of the experimentally determined bending modes of the beam with respect to the bending modes calculated from Euler beam theory.

Table 2: Modal Assurance Criterion Tables - Experimental Results

Fixed Poles Analysis Using Poles from FRF 1

	Mode 1	Mode 2	Mode 3	Mode 4	Mode 5	Mode 6
Mode 1	1.0000	0.0148	0.0001	0.0000	0.0001	0.0062
Mode 2	0.0148	1.0000	0.0000	0.0002	0.0002	0.0001
Mode 3	0.0001	0.0000	1.0000	0.0000	0.0006	0.0003
Mode 4	0.0000	0.0002	0.0000	1.0000	0.0000	0.0001
Mode 5	0.0001	0.0002	0.0006	0.0000	1.0000	0.0004
Mode 6	0.0062	0.0001	0.0003	0.0001	0.0004	1.0000

Fixed Poles Analysis Using Poles from FRF 2

	Mode 1	Mode 2	Mode 3	Mode 4	Mode 5	Mode 6
Mode 1	1.0000	0.0128	0.0001	0.0000	0.0001	0.0061
Mode 2	0.0128	1.0000	0.0000	0.0002	0.0003	0.0001
Mode 3	0.0001	0.0000	1.0000	0.0000	0.0006	0.0003
Mode 4	0.0000	0.0002	0.0000	1.0000	0.0000	0.0001
Mode 5	0.0001	0.0003	0.0006	0.0000	1.0000	0.0002
Mode 6	0.0061	0.0001	0.0003	0.0001	0.0002	1.0000

Fixed Poles Analysis Using Poles from FRF 3

	Mode 1	Mode 2	Mode 3	Mode 4	Mode 5	Mode 6
Mode 1	1.0000	0.0103	0.0001	0.0001	0.0001	0.0063
Mode 2	0.0103	1.0000	0.0000	0.0002	0.0003	0.0001
Mode 3	0.0001	0.0000	1.0000	0.0000	0.0006	0.0003
Mode 4	0.0001	0.0002	0.0000	1.0000	0.0000	0.0001
Mode 5	0.0001	0.0003	0.0006	0.0000	1.0000	0.0002
Mode 6	0.0063	0.0001	0.0003	0.0001	0.0002	1.0000

Fixed Poles Analysis Using Poles from FRF 4

	Mode 1	Mode 2	Mode 3	Mode 4	Mode 5	Mode 6
Mode 1	1.0000	0.0034	0.0002	0.0000	0.0001	0.0061
Mode 2	0.0034	1.0000	0.0000	0.0003	0.0002	0.0000
Mode 3	0.0002	0.0000	1.0000	0.0000	0.0005	0.0003
Mode 4	0.0000	0.0003	0.0000	1.0000	0.0000	0.0001
Mode 5	0.0001	0.0002	0.0005	0.0000	1.0000	0.0002
Mode 6	0.0061	0.0000	0.0003	0.0001	0.0002	1.0000

Table 2: Modal Assurance Criterion Tables (con.)

Fixed Poles Analysis Using Poles from FRF 5

	Mode 1	Mode 2	Mode 3	Mode 4	Mode 5	Mode 6
Mode 1	1.0000	0.0001	0.0001	0.0000	0.0001	0.0061
Mode 2	0.0001	1.0000	0.0000	0.0005	0.0001	0.0000
Mode 3	0.0001	0.0000	1.0000	0.0000	0.0005	0.0003
Mode 4	0.0000	0.0005	0.0000	1.0000	0.0000	0.0001
Mode 5	0.0001	0.0001	0.0005	0.0000	1.0000	0.0002
Mode 6	0.0061	0.0000	0.0003	0.0001	0.0002	1.0000

Global Parameter Analysis

	Mode 1	Mode 2	Mode 3	Mode 4	Mode 5	Mode 6
Mode 1	1.0000	0.0007	0.0002	0.0000	0.0001	0.0061
Mode 2	0.0007	1.0000	0.0001	0.0005	0.0001	0.0000
Mode 3	0.0002	0.0001	1.0000	0.0000	0.0004	0.0002
Mode 4	0.0000	0.0005	0.0000	1.0000	0.0000	0.0001
Mode 5	0.0001	0.0001	0.0004	0.0000	1.0000	0.0002
Mode 6	0.0061	0.0000	0.0002	0.0001	0.0002	1.0000

Table 3:
Modal Assurance Criterion - Theoretical vs. Experimental Results

Fixed Poles Analysis Using Poles From FRF #1 vs. Theoretical Beam Modes

	First Bending	Second Bending	Third Bending	Fourth Bending
First Bending	0.9908	0.0001	0.0089	0.0014
Second Bending	0.0007	0.9938	0.0004	0.0098
Third Bending	0.0002	0.0001	0.9843	0.0006
Fourth Bending	0.0002	0.0012	0.0000	0.9716

Fixed Poles Analysis Using Poles From FRF #2 vs. Theoretical Beam Modes

	First Bending	Second Bending	Third Bending	Fourth Bending
First Bending	0.9911	0.0001	0.0089	0.0013
Second Bending	0.0007	0.9937	0.0004	0.0099
Third Bending	0.0002	0.0001	0.9843	0.0005
Fourth Bending	0.0002	0.0012	0.0000	0.9711

Fixed Poles Analysis Using Poles From FRF #3 vs. Theoretical Beam Modes

	First Bending	Second Bending	Third Bending	Fourth Bending
First Bending	0.9921	0.0001	0.0089	0.0013
Second Bending	0.0007	0.9936	0.0004	0.0099
Third Bending	0.0002	0.0001	0.9841	0.0005
Fourth Bending	0.0002	0.0012	0.0000	0.9707

Fixed Poles Analysis Using Poles From FRF #4 vs. Theoretical Beam Modes

	First Bending	Second Bending	Third Bending	Fourth Bending
First Bending	0.9915	0.0001	0.0089	0.0013
Second Bending	0.0007	0.9937	0.0004	0.0099
Third Bending	0.0003	0.0001	0.9837	0.0005
Fourth Bending	0.0001	0.0012	0.0000	0.9714

Fixed Poles Analysis Using Poles From FRF #5 vs. Theoretical Beam Modes

	First Bending	Second Bending	Third Bending	Fourth Bending
First Bending	0.9912	0.0001	0.0089	0.0014
Second Bending	0.0007	0.9937	0.0004	0.0099
Third Bending	0.0005	0.0001	0.9826	0.0005
Fourth Bending	0.0001	0.0012	0.0000	0.9720

Global Parameter Analysis vs. Theoretical Beam Modes

	First Bending	Second Bending	Third Bending	Fourth Bending
First Bending	0.9904	0.0001	0.0089	0.0014
Second Bending	0.0007	0.9937	0.0004	0.0099
Third Bending	0.0005	0.0000	0.9824	0.0005
Fourth Bending	0.0000	0.0011	0.0000	0.9722

4.6 Frequency Placement Analyses

As described in section 3.2.2.3, two additional fixed-poles analysis of the laser data were performed. In one analysis, frequency measurements near resonances were used to determine the mode vectors of the beam. In the other analysis, frequency measurements away from resonances were chosen to use to determine the system's mode vectors. The locations of the frequencies used in each analysis relative to the beam's natural frequencies are shown in figure 10.

Figures 53-60 show FRFs synthesized from the mode vectors calculated during each analysis. The synthesized FRFs are shown as solid lines and measured data is marked with an 'x'. Table 4 includes a MAC table calculated from the mode vectors determined from each of the analyses. The significance of the entries in the MAC table are explained in section 4.1.2. The mode shapes estimated from each analysis are not included since the modes determined from these analyses are visibly no different than those in figures 18-23.

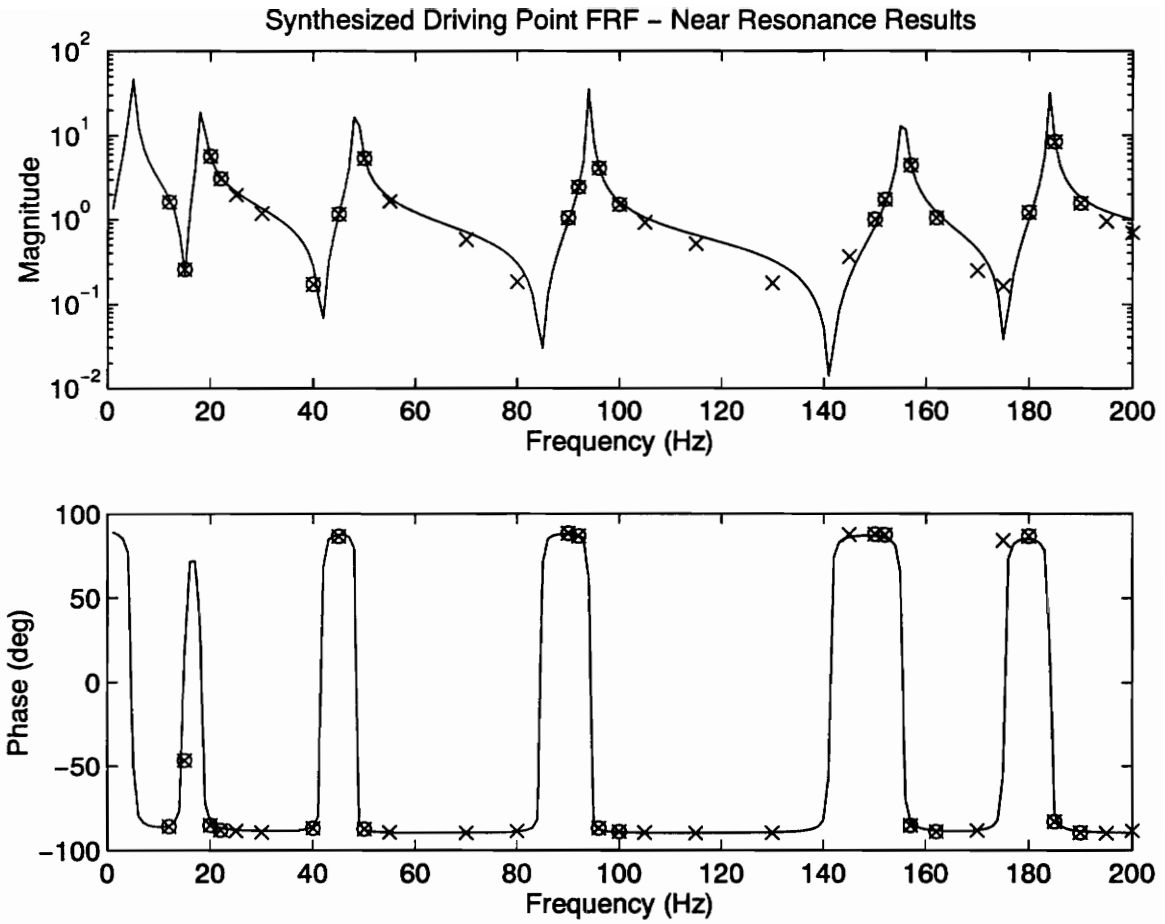

Figure 53: Synthesized FRF at Location 8 Using Data Points Near Resonance

Solid Line - Synthesized FRF
x - Measured Data
o - Data Used in Analysis

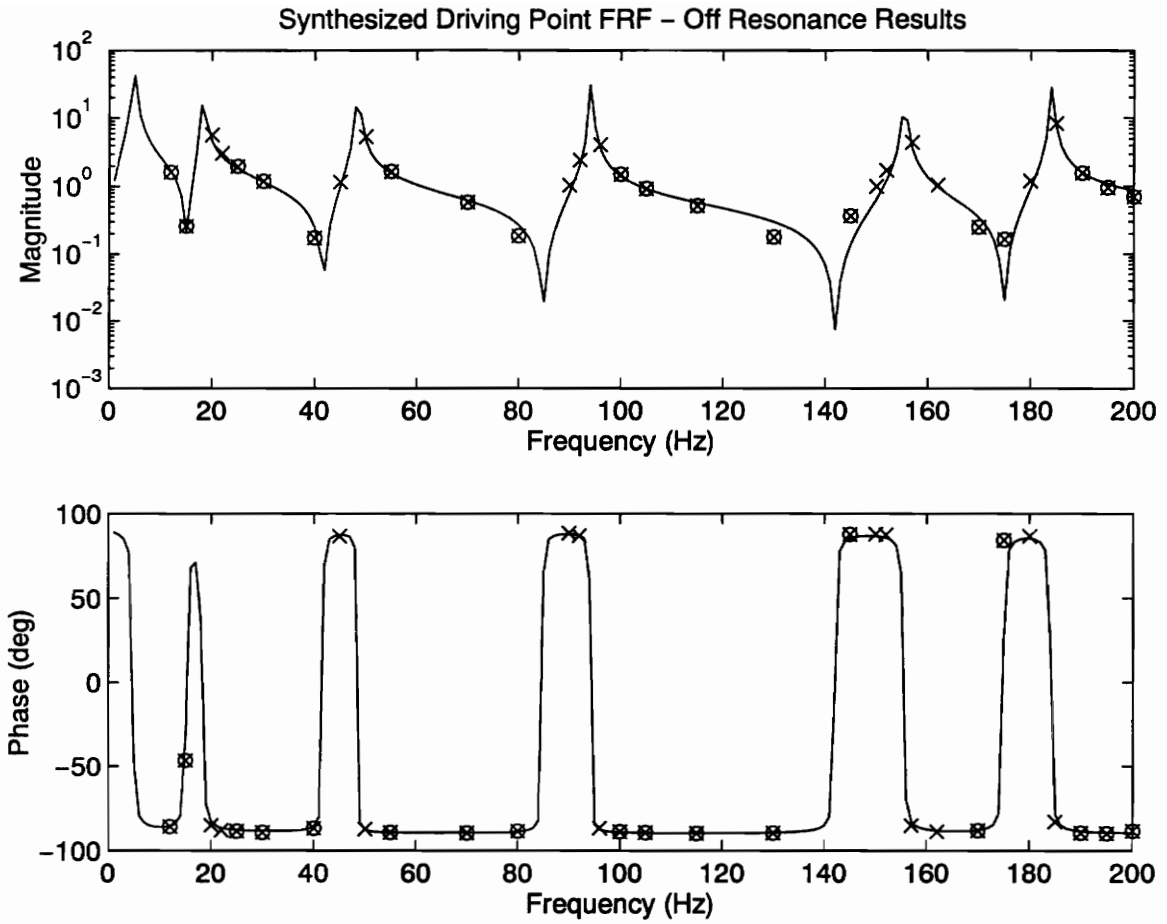

Figure 54: Synthesized FRF at Location 8 Using Data Points Off Resonance
Solid Line - Synthesized FRF
x - Measured Data
o - Data Used in Analysis

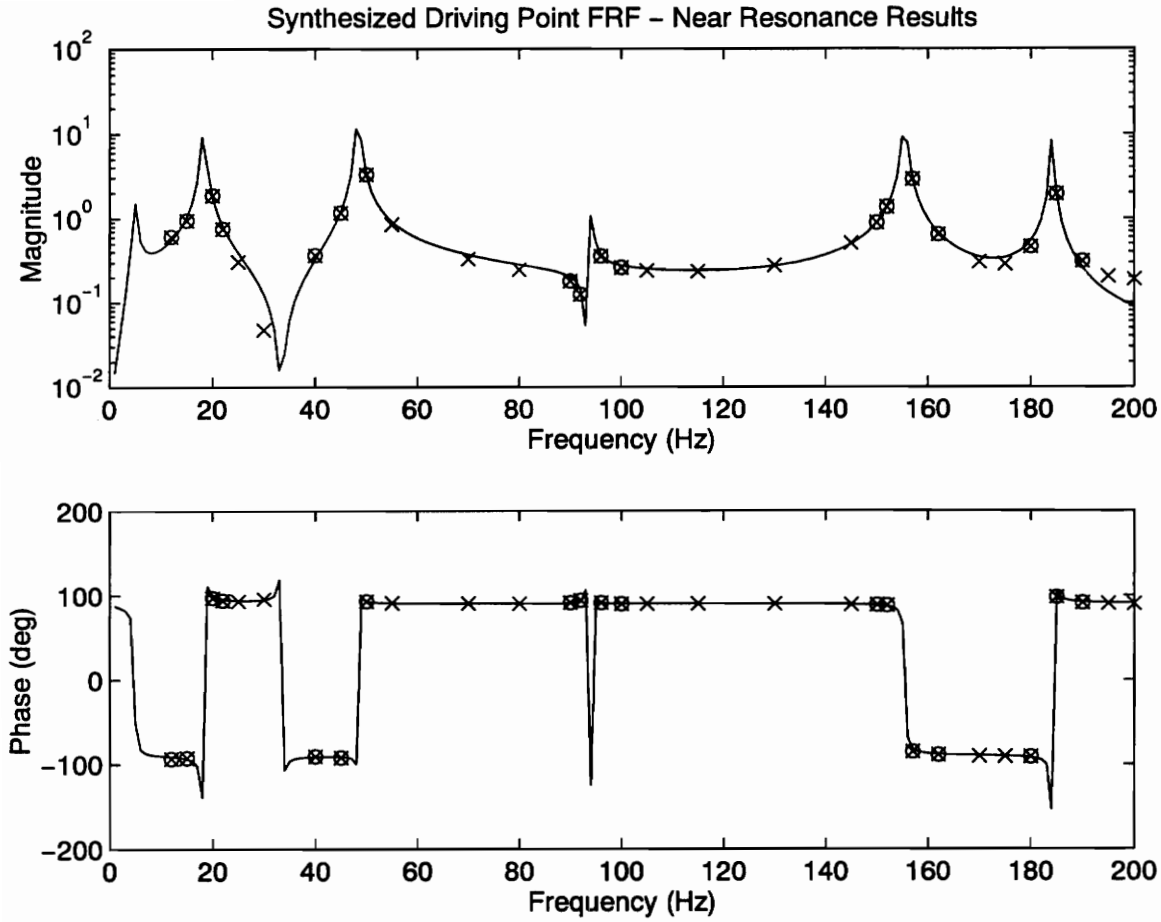

Figure 55: Synthesized FRF at Location 163 Using Data Points Near Resonance
Solid Line - Synthesized FRF
x - Measured Data
o - Data Used in Analysis

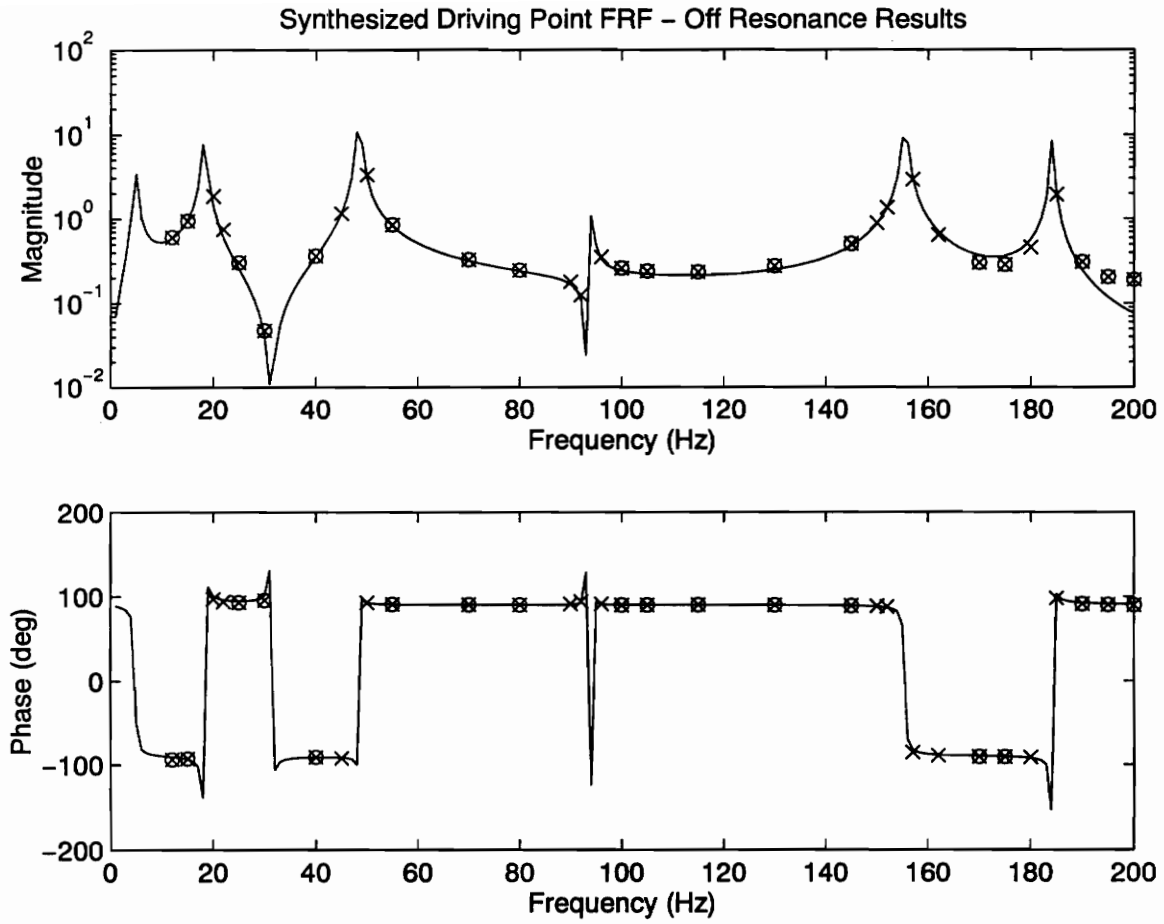

Figure 56: Synthesized FRF at Location 163 Using Data Points Off Resonance
Solid Line - Synthesized FRF
x - Measured Data
o - Data Used in Analysis

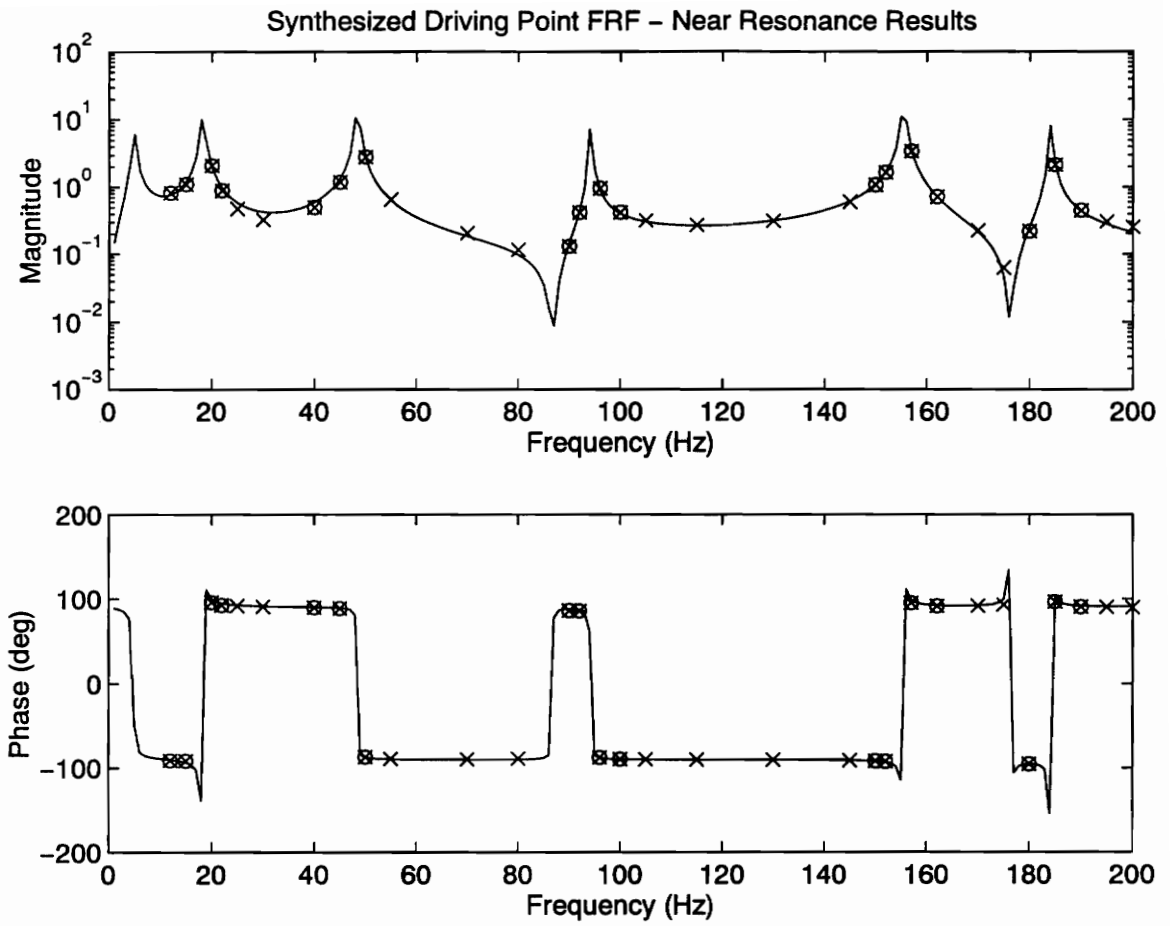

Figure 57: Synthesized FRF at Location 295 Using Data Points Near Resonance
Solid Line - Synthesized FRF
x - Measured Data
o - Data Used in Analysis

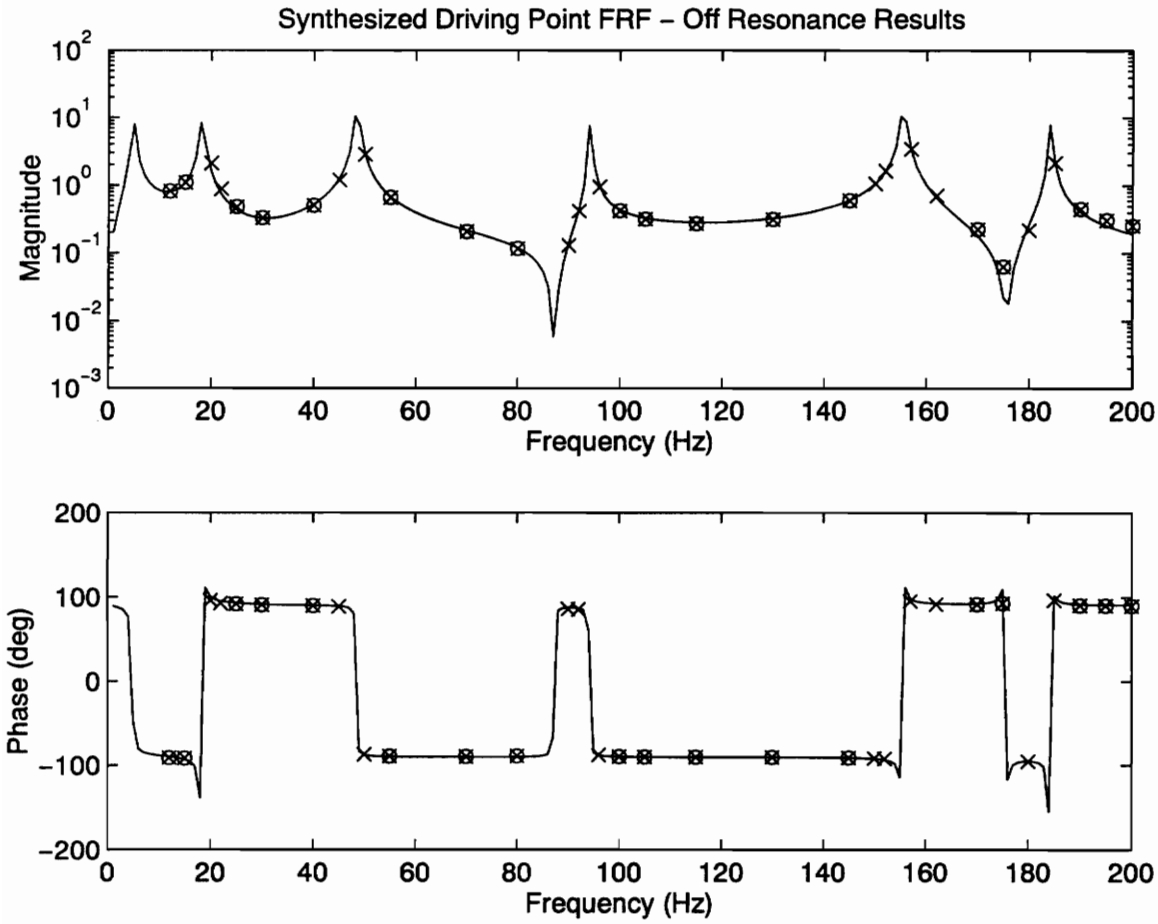

Figure 58: Synthesized FRF at Location 295 Using Data Points Off Resonance
Solid Line - Synthesized Data
x - Measured Data
o - Data Used in Analysis

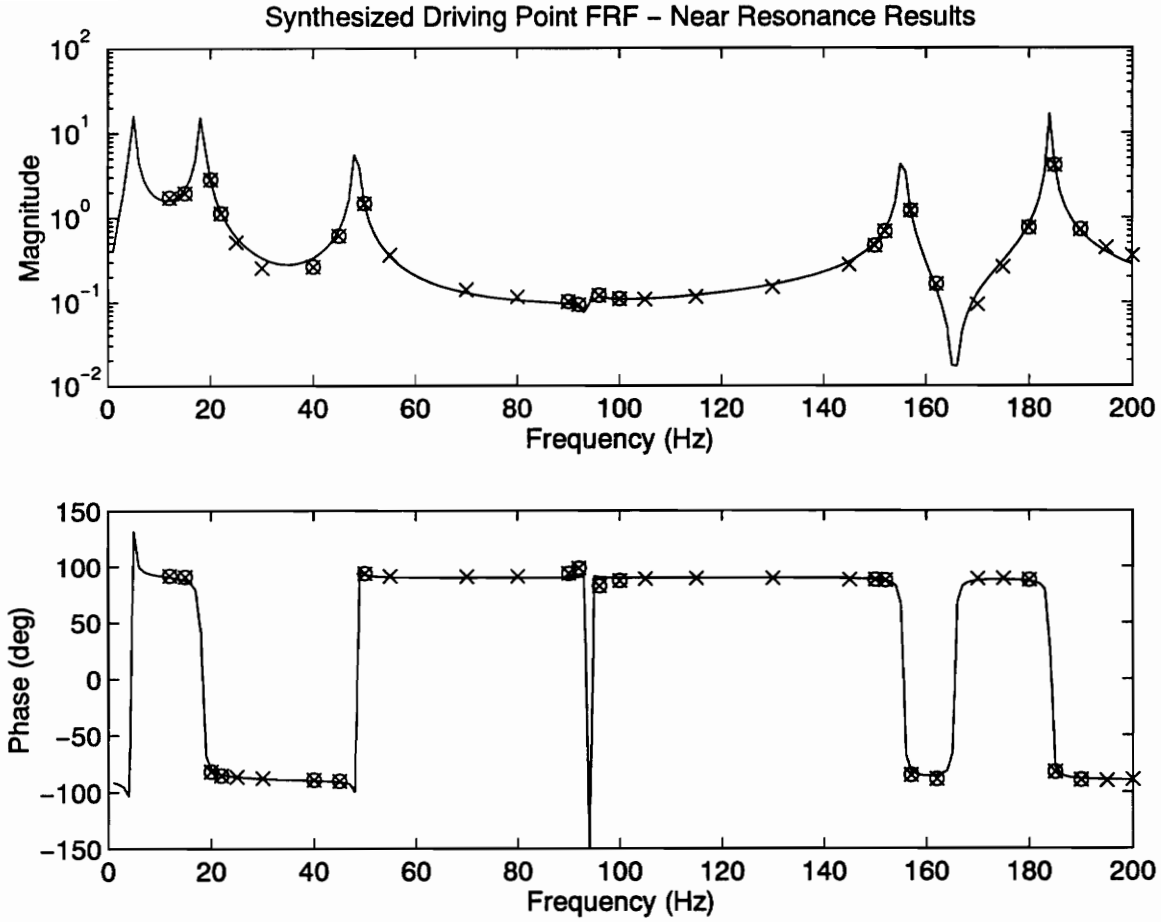

Figure 59: Synthesized FRF at Location 427 Using Data Points Near Resonance
Solid Line - Synthesized FRF
x - Measured Data Point
o - Data Used in Analysis

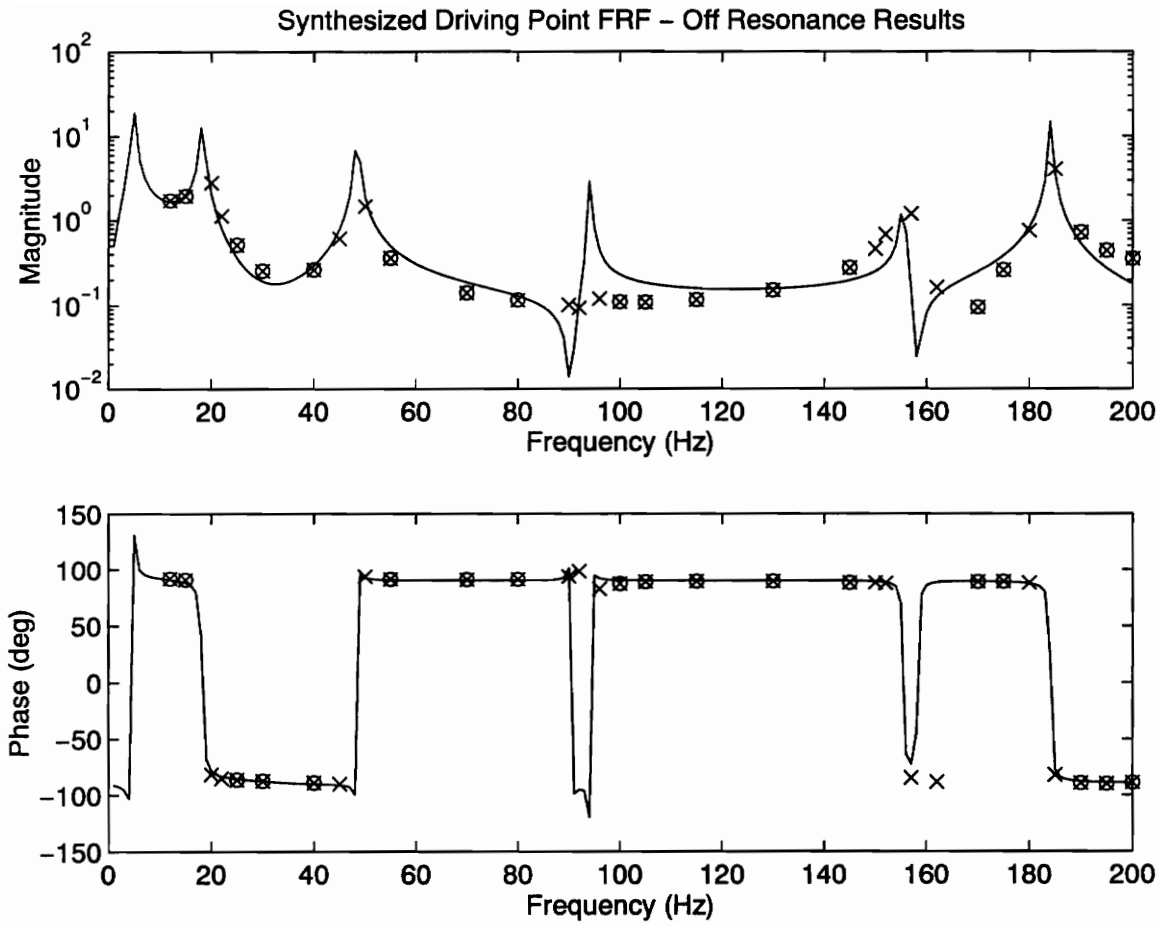

Figure 60: Synthesized FRF at Location 427 Using Data Off Resonance
Solid Line - Synthesized FRF
x - Measured Data
o - Data Used in Analysis

Table 4: MAC Tables Using Results from Varying Frequency Location Analysis

Fixed Poles Analysis Using Frequencies Near Resonance

	Mode 1	Mode 2	Mode 3	Mode 4	Mode 5	Mode 6
Mode 1	1.0000	0.0150	0.0001	0.0000	0.0001	0.0062
Mode 2	0.0150	1.0000	0.0000	0.0004	0.0001	0.0000
Mode 3	0.0001	0.0000	1.0000	0.0000	0.0006	0.0003
Mode 4	0.0000	0.0004	0.0000	1.0000	0.0000	0.0001
Mode 5	0.0001	0.0001	0.0006	0.0000	1.0000	0.0002
Mode 6	0.0062	0.0000	0.0003	0.0001	0.0002	1.0000

Fixed Poles Analysis Using Frequencies Between Resonances

	Mode 1	Mode 2	Mode 3	Mode 4	Mode 5	Mode 6
Mode 1	1.0000	0.0011	0.0001	0.0000	0.0001	0.0066
Mode 2	0.0011	1.0000	0.0074	0.0089	0.0290	0.0022
Mode 3	0.0001	0.0074	1.0000	0.0002	0.0000	0.0002
Mode 4	0.0000	0.0089	0.0002	1.0000	0.0006	0.0000
Mode 5	0.0001	0.0290	0.0000	0.0006	1.0000	0.0000
Mode 6	0.0066	0.0022	0.0002	0.0000	0.0000	1.0000

Chapter Five

Conclusions

The conclusions of this work are:

1. The fixed-poles procedure is a viable method of high resolution modal analysis.
2. The input signal used to measure the pole-determining FRF has little affect on the final results.
3. The fixed-poles procedure results in results that are comparable to a global parameter estimation technique.
4. In modal analyses with large numbers of FRFs, the fixed-poles method requires less computational time than a global parameter estimation approach with the time advantage dependent on the number of iterations required for a solution using the global approach.
5. SLV measurement frequencies near resonance frequencies yield superior results to measurement frequencies away from resonances when applying the fixed-poles algorithm.

5.1 General Method

The mode shapes, synthesized FRFs, and MAC tables given in Chapter 4 each give results to show that the fixed-poles algorithm is a viable procedure for modal analysis of frequency response data. The mode shapes illustrated in figures 18-23 agree with those determined from Euler beam theory. Figures 29-52 show that the analytical model of the beam (poles and residues) can be used to synthesize frequency response functions that agree well with measured data.

The off-diagonal entries in the MAC tables in table 2 are very close to zero, indicating orthogonality between the estimated mode shapes. Beam modes are known to be orthogonal with respect to each other (Rao 1990: 400), so the orthogonality of the modes indicates that each mode is decoupled from every other mode. Were the modes not decoupled, the resulting mode shapes would be combinations of various mode shapes, and the off-diagonal terms in the MAC tables would not be close to zero.

Table 3 shows the degree of orthogonality between the estimated bending modes and theoretical modes calculated using Euler beam theory. The diagonal entries are close to unity, indicating that the nth theoretical bending mode is approximately the same as the nth estimated bending mode. Additionally, the off-diagonal terms are approximately zero, indicating that the nth theoretical bending mode is orthogonal to the mth estimated bending mode.

Fixed-poles results agree well with the results from a standard global parameter estimation. The estimated mode shapes using both analysis techniques are visibly the

same and the estimated pole locations, shown in table 1, generally agree. The combination of good results in comparison to a standard method of data analysis and good results when compared to theory prove that the fixed-poles method can accurately be used to determine the modes of vibration of a structure.

5.2 Spatial Resolution

The purpose of the fixed-poles technique is to improve the resolution of modal analysis results. The fixed-poles method produces a high resolution modal analysis with no limit on the resolution of the results. Use of the scanning laser vibrometer allows tightly spaced frequency response function measurements, and the automatic nature of the scanning process allows the spatial resolution of the measurements to be increased by simply re-programming the scanning controller.

Using the fixed-poles technique, increasing the spatial resolution adds only a minimal amount of computational work to the analysis. Since the system's poles are set by a single FRF, the increased computation involved in adding more frequency response measurements is the calculation of mode vector estimates for each extra FRF.

5.3 Input Force Signal

The quality of the results of the fixed-poles analysis depend completely on the quality of the estimates of the system's poles. The poles are estimated from a single driving point FRF, and the quality of this lone FRF is paramount.

Various types of force input signals, as described and illustrated in section 3.1.2.3.1, are available for use in measuring the driving point FRF. Section 3.1.2.3.1 showed that the periodic chirp or burst chirp inputs should yield FRFs with the least corruption due to leakage. Results, however, showed that the driving point FRF measured using a burst random input (accelerometer FRF #5) provided the best estimates of the poles in comparison to global parameter estimates of the poles. The differences between the results using all five sets of estimate of the poles are minor, so the importance of the forcing input is not as significant as was initially assumed.

5.4 Comparison to a Global Parameter Estimation Algorithm

A global parameter estimation algorithm was used as the standard method to which to compare the results of the fixed-poles analysis of the beam. In the global parameter estimation, all measured SLV data was used to determine the system's poles, as opposed to using only the accelerometer measurement to determine the system's poles. The global parameter technique used is described in section 2.2.2.

5.4.1 Result Quality

An analysis of the data using the global parameter estimation algorithm produces results comparable to analysis using the fixed-poles method. Table 2 quantifies the orthogonality between the modes determined in the six analyses of the data. Every beam mode should be orthogonal with respect to every other as described in section 4.1.2, so the entries in Table 2 that indicate the orthogonality of one mode with respect to another mode (the off-diagonal entries) should be zero. The results from Table 2 are that the overall orthogonality of the mode shapes determined with the global parameter estimation is between the best and worst results obtained using from the five different fixed-poles analyses. Differences between the two methods stem, of course, from the different choice of poles. The manner in which the mode vectors are calculated is the same in both methods, as shown in section 2.2.

The differences in the results between different analyses of the data all relate to the estimation of the rigid body mode (mode 1). In many cases, the only large entries in the MAC tables occur when the MAC is calculated between a flexible mode and the rigid body mode. Ignoring results involving the rigid body mode, the MAC tables formed by the flexible body modes are all very similar with all off-diagonal entries ranging in the tens of thousandths.

Table 3 further supports the conclusion that the results of the fixed-poles analysis of the data are comparable to results obtained using a global estimation technique. Table 3 quantifies the similarity between the Euler beam theory mode shapes and those obtained

experimentally. Of course, Euler beam theory only predicts bending modes, so only bending modes are compared. If the experimentally determined mode shapes were exactly equal to those predicted by theory, the diagonal entries in table 3 would be one. Off diagonal terms would, ideally, be zero since every mode should be orthogonal with respect to every other mode. The global parameter analysis results lie, again, between the best and worst results of the five fixed-poles analyses.

5.4.2 Computational Time

One great advantage of the fixed-poles method is the reduction in computational resources required. The traditional algorithm requires iteration using all FRF data in order to estimate the poles and residues of a system. The time required to perform each iteration increases exponentially with the amount of data collected. In the test case of the steel beam, over 14500 (472x31) data points were used during the iteration process.

Only 800 data points were used in the iterative process to determine the poles of the steel beam. Since the estimation of the residues is the time consuming component of the traditional algorithm's iterations, the time required to determine the residues from the 472 SLV FRFs, once the system's poles were set, was approximately as long as one iteration using the global estimation algorithm. For this case, the global solution required three iterations, so that the fixed-poles analysis was nearly three times faster. Both increased spatial resolution (more SLV measurements) and an increase in the number of

iterations required for a global solution would cause the speed advantage of the fixed-poles algorithm to grow.

5.5 Frequency Placement

The frequency placement test, as described in section 3.2.2.3, showed that when using the fixed-poles algorithm, it is best to make scanning laser measurements near resonance frequencies. The MAC tables in table 4 show that the results of using near resonance frequencies in the analysis results in mode shapes that are more orthogonal with respect to each other than if off-resonance frequencies were used in the analysis.

Locations where a mode has no contribution are termed nodes, and nodes are best estimated using measurements at frequencies near resonance in the analysis. Synthesized FRFs at location 427 using off-resonance and near resonance data are shown in figures 59 and 60. Location 427 is very close to a node for the beam's third bending mode. Figure 59 shows that the synthesized FRF using near resonance data follows the measured data well to indicate a node. The off resonance analysis produces a synthesized FRF that does show a node at this location for the third bending mode. The off resonance analysis fails because the data used in the analysis does not contain sufficient information about the contribution of this mode at this location. Measurement frequencies closer to resonance contain more information about the strength of the mode and produce better results.

Chapter 6

Recommendations

Two recommendations are included to improve the implementation of the fixed-poles method. Including out-of-band modes would improve mode vector estimations by accounting for the contribution of higher modes in the measured data. Additionally, the speed at which data is collected from the SLV can be improved by making multi-frequency measurements.

6.1 Including Out-of-Band Modes

All of a system's modes make a contribution to the system's response at any frequency. Often, it is assumed that modes that are outside the frequency range of the measurements make little or no contribution. In many cases, a mode lies just outside measurement range and makes a significant contribution to the measurements, especially at high frequencies.

Out-of-band modes could be accounted for in a fixed-poles analysis by increasing the frequency span of the driving point FRF. Determining the poles of the driving point would give estimates of the locations of the out of band modes. During the process of

estimating the system's mode vectors, the higher modes mode vectors would be estimated as if it were within the measurement band. The estimates of the out-of-band mode's mode vectors might be poor because of its weak presence within the measured frequency band, but its contribution would be accounted for so to improve the estimates of the in-band modes.

As an example of including out-of-band modes, consider the steel beam used as the subject of the fixed-poles analysis. The driving point FRF could be measured from 0 to 400 Hz instead of measuring only 0 to 200 Hz. The SLV measurement frequency range would still reach only to 200 Hz. The two modes just beyond 200 Hz could be estimated from the driving point FRF, and mode vectors fit to these two poles. The estimates of the lower modes would benefit the overall solution of the modes in the 0 to 200 Hz range by accounting for the contribution of the higher modes during the mode vector estimation process.

6.2 Multiple Frequency Measurements

The reason for making measurments with the SLV at only one frequency was given in section 1.1.1: low dynamic range. Measuring each frequency individually is a time consuming task.

Multiple frequency measurements could be measured, so long as the amplitude of the system's response within the measured frequency range is not dramatic.

Measurements very close to a lightly damped mode, for instance, would be difficult because of the fast increase in the response of the structure near resonance. The response of the system could be calculated either by directly calculating a FRF from the Fourier transform of the output divided by the Fourier transform of the input, or through a least squares approach.

Assuming the input frequencies are known, a least squares problem can be formulated to estimate the phase and amplitude of the response at each of the input frequencies. The phase and amplitude of the input force at each of the input frequencies could also be determined through a least squares formulation. The approach of determining the input and output by a least squares approach is very much like that described in section 3.1.2. The difference between the approach described in section 3.1.2 and multi-frequency approach is simply the assumed analytical form that describes the input and response signals.

Bibiliography

Dominguez, J.C.L. 1994. "Reconstruction of 3-D Dynamic Response Fields: An Experimental, Laser-Based Approach with Statistical Emphasis," Ph.D. Dissertation, Department of Mechanical Engineering, Virginia Polytechnic Institute and State University, August 1994.

Drain, L.E. 1980. The Laser Doppler Technique. New York: John Wiley and Sons.

Han, M.C. 1991. "Improved Approaches to the Indirect Force Determination Problems via Experimental Modal Analysis," Ph.D. Dissertation, Department of Mechanical Engineering, Virginia Polytechnic Institute and State University, January 1991.

Rao, S.S. 1990. Mechanical Vibrations 2nd Edition. Reading, MA: Addison-Wesley Publishing Company.

Richardson, M.H., and D.L.Formenti. 1982. Parameter Estimation From Frequency Response Measurements Using Rational Fraction Polynomials. Proceedings of the First International Modal Analysis Conference. Society for Experimental Mechanics. Nov. 8-10, 1982.

Vita

John Fulton Porterfield was born on September 14, 1972 to John Robert and Katherine Barker Porterfield in Portsmouth, Virginia. Until coming to Virginia Polytechnic Institute and State University in August of 1990, he lived in Chesapeake, Virginia. He received both Bachelor of Science and Master of Science degrees in Mechanical Engineering from Virginia Tech in May 1994 and December 1995, respectively.

On July 29, 1995 he married Melissa Lynne Sitterson in Sandston, Virginia.

John plans to pursue a career with ITT Automotive Electrical in Dayton, Ohio as a design engineer.